Experimental Investigation of Volume Change Behavior of a Swelling Soil

by

Thamer Alyaqoub

B.S., Kuwait University, 2002

M.S., University of Colorado, 2007

A thesis submitted to the

Faculty of the Graduate School of the

University of Colorado in partial fulfillment

of the requirement for the degree of

Doctor of Philosophy

Department of Civil, Environmental, and Architectural Engineering

2011

This thesis entitled:
Experimental Investigation of Volume Change Behavior of a Swelling Soil
written by Thamer Alyaqoub
has been approved for the Department of Civil, Environmental and Architectural Engineering

_____

Professor Dobroslav Znidarcic, Committee Chair

_____

Professor Hon-Yim Ko

_____

Professor John McCartney

Date _____

The final copy of this thesis has been examined by the signatories, and we find that both the content and the form meet acceptable presentation standards of scholarly work in the above mentioned discipline.

Thamer Alyaqoub (Ph.D., Civil, Environmental and Architectural Engineering)

Experimental Investigation of Volume Change Behavior of a Swelling Soil

Thesis directed by Professor Dobroslav Znidarcic

This research presents experimental investigation of swelling mechanisms of a highly expansive soil. The amount and rate of volume change for highly expansive material was studied by considering several variables such as; relative humidity, liquid water, soil suction and wetting rate. The swelling pressure development was investigated by restricting lateral and axial deformations under oedometric conditions. The test results were analyzed in framework of several constitutive relationships and used to investigate time-dependent one-dimensional swelling in terms of coefficient of volume compressibility, coefficient of permeability and coefficient of hydraulic diffusivity. To achieve the research objectives, particular tasks included: (1) investigation free shrinkage-swelling behavior by controlling the aforementioned variables; (2) measuring the swelling pressure by performing constant volume oedometer test and one-dimensional swelling test; and (3) the experimental results were analyzed in order to determine the rate of swelling. Based on experimental results, the actual swelling was occurring at degree of saturation higher than 80%. Under 80% saturation, the volumetric expansion due to suction reduction was taking place. The soil suction change in the range higher than 1 MPa had minimal effect on the volume change due to the stiffness of the expansive soil as opposed to that in the range lower than 1 MPa. The constant volume swelling pressure test results indicated that the swelling pressure increased as the initial water content decreased due to the suction dissipation. The rate of swelling at higher void

ratio may not be only controlled by hydraulic conductivity but rather by the ability of the highly expansive clay material to absorb water.

Dedication

To my father, my mother and my whole family

ACKNOWLEDGMENTS

First and foremost, all praise to Allah the almighty.

I would like to express my deepest gratitude and appreciation to my academic advisor, Professor Dobroslav Znidarcic. His guidance and support were invaluable throughout my studies and in the completion of this research at the University of Colorado at Boulder. He is faithful friend and excellent teacher whom I shall ever respect and remember.

Thanks are also due to Professors Shideh Dashti, Hon-Yim Ko and John McCartney for serving on my committee. Their time and effort that they and the other geotechnical faculty have put into the coursework guided me towards becoming a critical thinker and an independent researcher. I would like to thank the external committee member, Dr. Howard Perko for providing his valuable assistance to strengthen my research.

My sincere gratitude to the Kuwait Institute for Scientific Research for providing the financial support that without it this research would not have been possible. The excellent support and cooperation from Advanced Terra Testing, Inc. in using the chilled-mirror dew point device should be acknowledged.

Finally, I must thank my parents, all of my family members and friends for their encouragement and endless love throughout my study. I am also grateful for many friends at the University of Colorado at Boulder, Anwar Alkandari, Majid Ghayoomi, Ali Khosravi and Joonyong Lee for their friendship, advice and discussion, which created such a motivating environment for research.

LIST OF CONTENTS

LIST OF FIGURES

LIST OF TABLES

CHAPTER 1

INTRODUCTION

1.1 Introduction

Classical soil mechanics deal primarily with saturated as well as completely dry soils where all procedures in geotechnical engineering have been developed assuming that these conditions apply; however, saturated or completely dry conditions do not always represent the actual field situations in most soils near the ground surface. The state of these soils is influenced by infiltration of rainfall or evaporation process and most of these soils are therefore, unsaturated. Many investigators and researchers have observed that unsaturated soil layers cover most of the land on earth and are above the ground water table. In other words, the majority of civil engineering works will deal with soil layers that are in an unsaturated state. In particular, the mechanics of unsaturated soils lead to highly nonlinear problems and involve more variables that make application of geotechnical engineering practices to unsaturated soil mechanics most challenging.

Many geotechnical engineering practices, whether conventional such as compaction to improve various designs of earth structures, or highly advanced, as in engineering barriers for nuclear waste disposal or as landfill isolations, demand firm knowledge of the performance and behavior of unsaturated soils under such applications. Regardless of the benefits of employing unsaturated soils in their projects, the

consequences of using or working with expansive types of soils are bothersome. Several reports, including that by Johns and Holtz (1973), have stated that expansive soils cause major destruction and defects of structures as well as pavement damage. This kind of problem will certainly cause tremendous cost for maintenance alone. Chen (1975), Nelson and Miller (1992), and Pusch and Yong (2006) have agreed that expansive soils are well known for non-uniform deformations and random movements caused by moisture content changes and, in turn, cause extensive damage.

In natural occurrence, unsaturated soil comprises two phases: solids (soil particles) and fluids (mostly water and air) (Lu and Likos, 2004). The presence of air in the fluid phase generates capillarity effects that create suction where the pore water pressure is going to be below the atmospheric pressure. Change in suction affects unsaturated soil's behavior, such as strength, and deformability phenomena, like collapsing and swelling. Generally, collapsing and swelling are responses by unsaturated soil to drying and wetting effects. Other factors contributing to these phenomena include soil structure, particle interactions (mineralogy), stress history and specific surface (e.g., see Scott, 1963; Chen, 1975; Nelson and Miller, 1992; Pusch and Yong, 2006; Murray, 2007). Many field and laboratory tests have been conducted in which soil properties, such as strength and permeability, were monitored and analyzed. While researchers have developed various testing techniques to evaluate swelling behavior, such as measuring swelling pressure, shrinkage-swelling relationships, and their characteristics in expansive soils according to the change of moisture content, relatively few studies have addressed issues over the rate of these changes when they are associated with hydraulic diffusivity and hydraulic conductivity. This research is limited to the study of mechanisms controlling the

swelling behavior of expansive soil and explores how the swelling behavior is affected by the rate of wetting, surcharge pressure, and lateral confinement. Thus, the collapsible soils are not included.

1.2 Expansive Soils

Expansive soils consist primarily of a high percentage of fine-grained clay particles. Briefly, the clay particles have minerals that contain two basic sheets of silica tetrahedrons (SiO_4) confining octahedral aluminum hydroxide [$AL(OH)_3$] and other ions like Li, Mg, and Fe (e.g., see Das, 1998; Pusch and Yong , 2006). The clay particles have predominantly negative electrical charges (ions) and are stacked according to certain stacking configurations that depend primarily on the strength of bonds controlled by interparticle forces and the spaces present between particles. In the case of expansive clays, two clay particles are combined within the pores in the presence of water and dissolved solutes in the interparticle space. The presence of adsorbed pore water and dissolved solutes maintains the stability of clay particle interactions since they provide essential positive electrical charges (cations) to balance negative electrical charges across the clay sheets. The change of moisture content and/or concentration of the solutes will definitely disturb the equilibrium of clay particles; therefore, the disturbed equilibrium will lead to a redistribution of the clay-water-air system (Nelson and Miller, 1992). The equilibrium results from the combination of attractive and repulsive forces that occur near the soil-water interface; their effects, in turn, depend on mineral composition and the actual spacing between the layers. If the attractive forces are greater than the repulsive forces, the expansive soil will shrink and vice versa.

Classifications have been developed to distinguish between the degree of swelling of non-expansive to highly-expansive soils according to their physical properties, chemical compositions, and mineral content, such as those provided by Pusch and Yong (2006) in terms of the thickness of interlayer hydrates, and by Chen (1975) in terms of the probability of volume changes for expansive soils. With this knowledge in hand, the clay mineral known as montmorillonite is the most active clay mineral and provides the highest degree of swelling; accordingly, it will be used in this research. Such classifications give a conceptual image of the behavior of expansive clays and might be useful for soil sciences but may be of limited use to the geotechnical engineering. For complete description and explanation of swelling behavior in addition to mineralogical components of expansive soil, one needs to know that the degree of swelling in expansive soils is affected by stresses, suction ranges and time (testing duration).

1.3 Research Objectives

The first objective of this research is to experimentally investigate the shrinkage-swelling behavior of unconstraint-unsaturated highly-expansive soil by controlling specified wetting rates. The results of this investigation will be used to evaluate the role of the wetting rates on the swelling potential in terms of deformation. Also, the latter approach covers the contribution of soil suction to the amount of shrinkage-swelling behavior. Part of this study will explore conditions under which significant swelling deformations are most likely to occur. This investigation covers the entire soil suction range for both shrinkage and swelling paths.

The second objective is to complement the significant activity of swelling deformation from the first objective with another favored measure of swelling potential

termed as swelling pressure. This requires applications of surcharge pressure as well as lateral confinement of specimens. The influence of such applications on the swelling pressure development is also investigated and the overall correlation between the swelling deformation and swelling pressure is evaluated. The experimental investigation of the second objective will cover the low to very low soil suction range for both shrinkage and swelling paths.

The third objective is to utilize the outcomes from the previous objective for quantifying compressibility coefficients in addition to hydraulic diffusivity and permeability coefficients.

1.4 Research Organization

This research is organized as follows:

- Chapter 2 consists of basic concepts and definitions especially used for describing types of clay minerals and interparticle forces within clay particles as well as soil suction, moisture retention, and diffusivity characteristics, and shrinkage-swelling mechanism of expansive clays;
- Chapter 3 comprises a literature review of past research work that is divided into main two categories; namely, micro-structural and macro-structural levels. An overview of approaches, results, and observations obtained by several researchers is briefly addressed;
- In Chapter 4, material selection, description of the experimental setup and experimental procedures are explained in detail. The methods that have been used for drying specimens in shrinkage test and for rewetting specimens in free swelling test are provided and explained in detail. The other swelling pressure

tests; namely, constant volume swelling pressure, one dimensional swelling pressure, and submergence tests are also provided and explained;

- Chapter 5 consists of results and primary observations of the experimental work provided in Chapter 4. Those observations are related to provide a conceptual image about the behavior of the expansive soil used in this research;
- The analyses and discussions of the results provided in Chapter 5 are included in Chapter 6. An in-depth analysis is provided that concerns the influence of hygroscopic absorption and reversible/irreversible components on the swelling behavior as well as the contribution of soil suction variation to swelling deformation and swelling pressure. The relationship between soil suction and swelling pressure variations is also described in this chapter;
- Chapter 7 comprises the determination of compressibility coefficient, coefficient of hydraulic diffusivity, and coefficient of permeability. A simple mathematical modification of the hydraulic diffusivity expression derived from the governing equation of transient water flow in unsaturated soil is proposed; and
- Chapter 8 is the final chapter, in which general conclusions and recommendations for future research are listed.

CHAPTER 2

DEFINITIONS AND BASIC CONCEPTS

2.1 Introduction

Before proceeding, it would be advisable to consider some definitions and basic concepts used in the literature review (Chapter 3) and in analyses of swelling soil behavior. In this chapter, some of the definitions and basic concepts regarding clay particles and types of minerals, interparticle forces, suction in unsaturated soil, moisture retention characteristics, diffusivity in unsaturated soil, and shrinkage and swelling mechanisms are briefly discussed.

2.2 Clay Particles and Types of Minerals

According to Scott (1963) the types of minerals occurring in soil influence the engineering properties and behavior of the soil. The effect of mineral increases as particle size decreases; hence, the effect of interparticle forces is consequently increasing. Considering smaller soil particles, types of minerals, and the effect of interparticle forces, it is likely that clay triggers changes in soil behavior and properties. Soil scientists and agricultural engineers are more focused on types of clay minerals and clay structures whereas civil engineers are more concerned about water seepage through soil and its effect on soil behavior. However, it is evident that the type of mineral has a dominant

effect on the degree of swelling; thus, classification is required as described by Nelson and Miller (1992), into three main groups as follows:

- Kaolinite group – generally nonexpansive.
- Mica-like group – includes illites and vermiculites, which have lower degree of expansion.
- Smectite group – includes montmorillonites, which are highly expansive clay mineral types.

2.3 Interparticle Forces

The nature of the bonds between clay particles is depending on the type of clay mineral, but the presence of water as an aqueous medium is also essential. In addition, the magnitude of swelling potential is related to water chemistry, as discussed in Chapter 3; therefore, interparticle bonds are categorized on the basis of bond strength that holds clay particles together or links the water molecules to clay particles. Pusch and Yong (2006) categorized the types of bonds as follows:

- Primary valence bonds: whether the bonds are ionic or covalent, they connect clay particles and are considered strong or high-energy bonds. These bonds have the strongest attractive forces and need high energy to be broken. For compacted smectites, this state requires greater energy. These types of bonds arise mostly from a solid-solid interface.
- London – van der Waals forces: They are relatively weak – attractive forces compared with primary valence bonds and occur between clay particles, which

are separated by water. London – van der Waals forces are functions of types of clay minerals and distance of separation.

- Hydrogen bonds: these bonds are weaker than primary valence bonds and form between water molecules (oxygen and hydrogen atoms). The attractive forces that bring water molecules together are called hydrogen bonds, are mostly concentrated around clay particles.
- Bonds by sorbed cations: They depend mainly on the dissolved solute in water. Thus, sorbed cations located in interparticle spaces have a role in swelling potential as discussed in Chapter 3.

2.4 Suctions in Unsaturated Soil

If moisture content remains unchanged, there will be no volume change (Chen, 1975). In other words, with no constraints, a clay whether saturated or partially saturated is in an internal equilibrium state when the moisture content of the soil remains unchanged. The consequent volume change (contractive or dilative) when moisture content varies, depends on type of clay mineral as mentioned in section 2.2. Capillary force is a significant means of water transfer (Chen, 1975); therefore, during the process of moisture content uptake or intake, a new equilibrium state is necessary to counterbalance the current condition of the soil.

The effect of capillary force, which results from the surface tension of the air-water interface, along with attractive forces (other than primary valence), are combined and termed *matric* suction (ψ_m) (e.g., see Lu and Likos, 2004). In the case of clay soils, Lu and Likos (2004) identified *osmotic* suction (ψ_o) resulting from the presence of

dissolved solute, whereas *total* suction (ψ_t) is the algebraic sum of (ψ_m) and (ψ_o). (ψ_m) is a common term used to describe the capillarity effect in unsaturated soil, which is the difference between pore air pressure (u_a) and pore water pressure (u_w) occurring in the air-water interface balanced by surface tension forces (e.g., see Nelson and Miller, 1992; Lu and Likos, 2004). On the other hand, (ψ_o) represents chemical activity in the water phase and the interaction of this activity with the solid phase. For example, the higher the solute concentration on the clay particle surface, the higher the osmotic suction. Therefore, more water molecules will be driven toward the clay particle surface during wetting process. In that regard, it is advisable to determine (ψ_t) in unsaturated clay soil if possible.

2.5 Moisture Retention Characteristic

The main controlling factor of unsaturated soils mechanics is a change in moisture content resulting from drying or wetting processes. The graphical view that describes the moisture content change of unsaturated soils is called the soil water retention curve (SWRC) or soil water characteristic curve (SWCC), as shown in Figure 2.1.

The SWRC illustrates the relationship between water content (volumetric water content, θ or gravimetric water content, ω or degree of saturation S) and suction (ψ_t or ψ_m or ψ_o). Various S shapes will be generated depending on material properties of unsaturated soils such as grain size distribution, pore size distribution, clay content, mineralogy, density and organic material (Lu and Likos, 2004); therefore, the constitutive relationship of SWRC depends on type of soil. The volume change of sand soil is most likely minimal because of the absence of active minerals unlike clay soil, where the

active minerals are present in sufficient quantities to affect the volume change of material. In addition, the specific surface of sand particles is smaller than that of clay particles; water adsorption is therefore lower around sand particles. However, the capillarity effect (ψ_m) of sand soil controls the suction mechanism. While the ψ_m and the ψ_o (depends on clay mineralogy) are contributing the suction mechanism of clay soil.

Thus, the SWRC for sand soil elucidates the constitutive relationship between ψ_m and w or *S* while, a constitutive relationship between ψ_t and θ is elucidated by SWRC for clay soil. The SWRC is hysteretic; Lu and Likos (2004) showed a typical hysteresis in SWRC as illustrated in Figure 2.2. Because of air bubble occlusion, it is hard to regain the same water content during a wetting process. The drying (desiccation) and wetting (infiltration) cycles of SWRC are a transient process and thus, have a great significance on flow and deformation behavior of unsaturated soil.

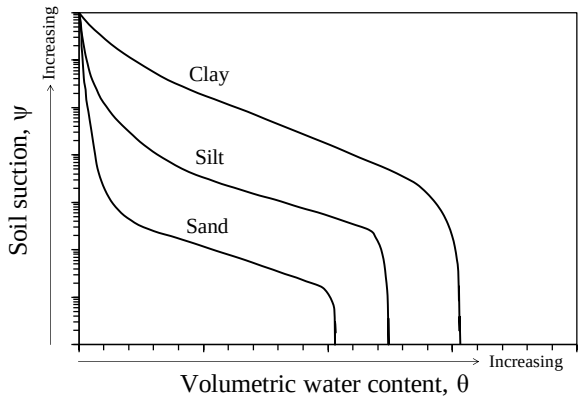

Figure 2.1. Representative soil-water characteristic curves for sand, silt, and clay (After Lu and Likos,2004).

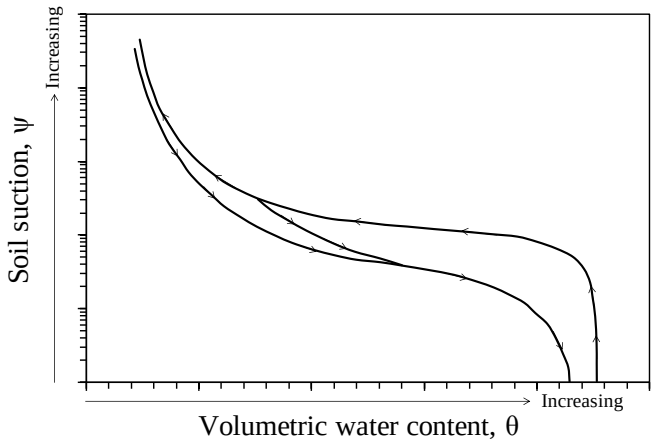

Figure 2.2. Conceptual illustration of hysteresis in soil-water characteristic curve (After, Lu and Likos, 2004).

2.6 Diffusivity in Unsaturated Soil

As shown in Figure 2.2, the air entry value for the clay soil is higher than for sand and silt soils. It is also most likely that the water transport changes from liquid to vapor flow at higher suction in clayey soils. This transmission is called diffusion due to a gradient of water vapor. This gradient describes the driving mechanism for water vapor transmission. Various types of gradients involve in such mechanism in unsaturated clay problems that are; chemical gradient, hydraulic gradient, and thermal gradient or a coupling of them depending on assumptions or conditions used to satisfy particular study. Therefore, diffusion coefficient can be expressed according to the type of driving mechanism.

For example, Fick's first law quantitatively expresses the diffusion process when the concentration of water solutes varies in porous medium of unsaturated soil (Cheery and Freeze ,1979). It is also used to express the vapor transport in unsaturated soil, as follows (e.g., Lu and Likos ,2004):

$$q_v = -D_v \nabla \rho_v \quad (2.1)$$

Where D_v, is the diffusion coefficient of water vapor in porous medium that depends on temperature, pressure, tortuosity of accessible flow path for vapor movement $\left({}^{L^2}/_{T}\right)$; ρ_v is the density of pore water vapor $\left({}^{M}/_{L^3}\right)$; $\nabla \rho_v$ is the gradient that describes the driving mechanism of pore water vapor at certain position and has negative quantity in the diffusion direction; and q_v is the rate of mass flux through pore spaces that is normally driven from high pore water vapor concentration to low pore water vapor concentration as indicated by the negative sign in the right hand side of the above equation $\left({}^{M}/_{TL^2}\right)$.

Equation 2.1 is similar to Darcy's law (1856) that describes the apparent rate of water flux q $\left({}^{L}/_{T}\right)$ through porous medium in terms of hydraulic conductivity k $\left({}^{L}/_{T}\right)$ and hydraulic gradient $\left({}^{dh}/_{dL}\right)$, which expresses the rate of change of the total head loss h per a given distance L of flow in a given direction as follows:

$$q = -k\, i \quad (2.2)$$

The transient process of water flow through any given soil volume is governed by principle of mass conservation where the net flux of water inflow and outflow through the soil element is equal to the storage capacity (Lu and Likos, 2004). The storage capacity is time-dependent term that describes the total mass of water stored in the soil whether this amount of water is lost or grained during the transient flow process. Lu and Likos (2004) termed the general expression for the governing equation of transient water flow in soil where Equation 2.2 is involved as follows (see Appendix-A):

$$-\rho_f\left(\frac{\partial q_x}{\partial x}+\frac{\partial q_y}{\partial y}+\frac{\partial q_z}{\partial z}\right)=\frac{\partial(\rho_f\theta)}{\partial t} \tag{2.3}$$

Where, ρ_f (M/L^3) is water density, θ (%) is the volumetric water content, t (sec) is time, and the rate of fluxes in x, y ,and z directions are q_x, q_y, and q_z, respectively. Equation 2.3 is applicable for simulating transient flow process and compressibility of expansive soil. Furthermore, a specific storage term (S_s) is introduced into the right hand side of Equation 2.3 as suggested by Freeze and Cherry (1979) if the soil is homogeneous and the transient flow is isotropic as follows (see Appendix-A):

$$\frac{\partial^2 h}{\partial x^2}+\frac{\partial^2 h}{\partial y^2}+\frac{\partial^2 h}{\partial z^2}=\frac{S_s}{k}\frac{\partial h}{\partial t} \tag{2.4}$$

Lu and Likos (2004) stated the term $\frac{k}{S_s}=D$ $\left({}^{L^2}/_{T}\right)$, which is the hydraulic diffusivity and thus, equation (2.4) is simplified as follows:

$$D\left(\frac{\partial^2 h}{\partial x^2}+\frac{\partial^2 h}{\partial y^2}+\frac{\partial^2 h}{\partial z^2}\right)=\frac{\partial h}{\partial t} \tag{2.5}$$

In case of unsaturated transient flow process, the governing equation (2.3) becomes more complicated for the reason that unsaturated k becomes a function of suction that is in most cases referred to ψ_m(or negative pressure head). Thus, Equation 2.3 is rewritten where the soil is assumed to be homogeneous as follows (see Appendix-A):

$$\frac{\partial}{\partial x}\left[k_x(\psi_m)\frac{\partial \psi_m}{\partial x}\right]+\frac{\partial}{\partial y}\left[k_y(\psi_m)\frac{\partial \psi_m}{\partial y}\right]+\frac{\partial}{\partial z}\left[k_z(\psi_m)\frac{\partial \psi_m}{\partial z}+1\right]=\frac{\partial \theta}{\partial \psi_m}\frac{\partial \psi_m}{\partial t} \tag{2.6}$$

Where, $\frac{\partial \theta}{\partial \psi_m} = C(\psi_m)$ is the specific moisture capacity that requires SWRC to be obtained as stated by Lu and Likos (2004).

The k function of unsaturated soil can also be a function of θ if the Darcy's law is rewritten as follows:

$$q = -k(\theta)\frac{\partial h}{\partial \theta}\frac{\partial \theta}{\partial l} = -D(\theta)\frac{\partial \theta}{\partial l} \tag{2.7}$$

Where, l is the a position (length) at specified flow directions $(x, y, or\ z\ (gravity\ direction))$, and $D(\theta) = {}^{k(\theta)}\big/_{C(\theta)}$ is the hydraulic diffusivity of unsaturated soil. By incorporating Equation 2.7 into Equation 2.3, the following Equation 2.8 can be expressed as follows:

$$\frac{\partial}{\partial x}\left[D_x(\theta)\frac{\partial \theta}{\partial x}\right] + \frac{\partial}{\partial y}\left[D_y(\theta)\frac{\partial \theta}{\partial y}\right] + \frac{\partial}{\partial z}\left[D_z(\theta)\frac{\partial \theta}{\partial z}\right] + \frac{\partial k_z(\theta)}{\partial z} = \frac{\partial \theta}{\partial t} \tag{2.8}$$

Two characteristic functions are plugged in the above equation, namely; unsaturated hydraulic conductivity function and hydraulic diffusivity function. Keep in mind that thermal and chemical effects in unsaturated transient flow process are not included in the above equation. The difficulties of measuring the hydraulic conductivity of unsaturated expansive soils motivate many researches to develop mathematical and empirical formulations to calculate the diffusivity coefficient in order to back calculate the unsaturated hydraulic conductivity as discussed in the next chapter.

2.7 Shrinkage and Swelling of Unsaturated Expansive Soils

A General description of the shrinkage phenomenon of expansive soils was described by Fredlund (1967) and Sharma (1998). In the case of highly expansive soil, both pore sizes and particle sizes are smaller, such that capillary tensions are higher and the relative particle movements are easier than in other types of soils. However, this phenomenon is similar to a reduction in overall saturated soil volume when subjected to an increase of effective overburden pressure. Except that, in cases of unsaturated expansive soils, the reduction in volume results from additional internal pressures that are caused by both capillarity and osmotic effects. In the contrary, a cumulative increase of moisture content of unsaturated expansive soil can result from both a reduction of soil suction and an increase in volumetric swelling. This is similar to an effect which occurs when the effective overburden pressure on saturated soil is unloaded.

CHAPTER 3

LITERATURE REVIEW

3. Introduction

It is acknowledged that loss or gain of moisture in expansive soils due to drying or wetting conditions is accompanied by a volumetric change phenomenon. In order to investigate this phenomenon, many studies have been implemented to research the behavior of expansive soils. Some of the researchers concentrated on the engineering point of view in their studies, while others dedicated their efforts in different directions such as from the mineralogical or statistical perspectives.

In this chapter, a brief review of the methodologies, techniques, and observations of some of the previous studies is addressed in order to provide comprehensive review of the existing research results. Preliminary understanding and comments about the factors that induced swelling and the features of expansive soils are summarized later in this chapter.

3.1 Mineralogical Studies

Microscale and macroscale studies facilitate the understanding of the swelling phenomenon since they provide a fundamental representation of the properties of expansive soils. Thus, incorporating mineralogical studies with geotechnical engineering one will provide a proper interpretation of such phenomenon.

Soil scientists are interested in mineralogical studies of different kinds of soils. The most complicated types of soils are those, that consist of clay minerals in a solid phase. Clay minerals influence the swelling behavior and strength of soils, through chemical, physical, or mechanical effects.

"The interlamellar hydrates largely determine the swelling potential, whereas the surface properties of the stacks of lamellae almost entirely determine their plasticity and rheological behaviour" (Pusch and Yong, 2006).

In addition to the previous statement, Figure 3.1 shows a representation of soil structure ranging from single discrete particle form to macrostructure form. The physico - chemical interactions are significant at the soil microstructure level whereas the mechanical effects are dominant in soil macrostuctural spaces.

In more general perspective, Ferber et al. (2009) explained the swelling development of high plasticity clays as a decrease in macropores void ratio associated to an increase of micropores void ratio.

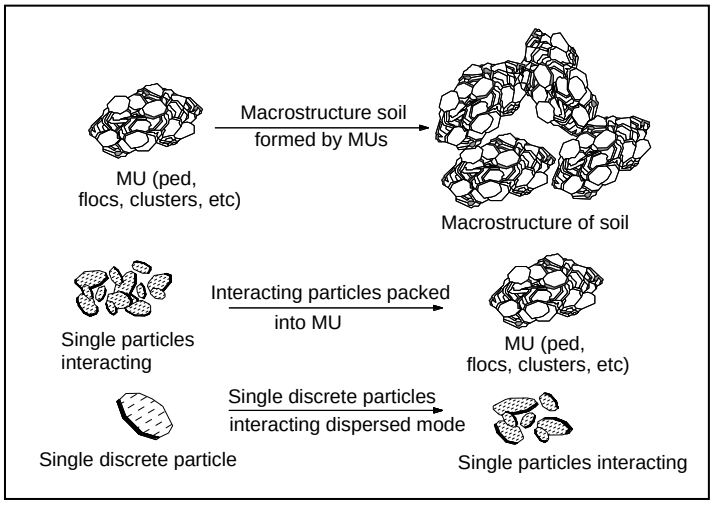

Figure 3.1. Hierarchic representation of soil structure beginning with interacting discrete particles and progressing onward to microstructural units and macrostructure of soil (after Pusch and Yong, 2006).

Davidson and Page (1956) were among the pioneers in studying the factors influencing the swelling-shrinking behavior of soils such as mineralogical composition, exchangeable cations, and other factors. This study was accomplished by measuring the swelling pressure as shown in Figure 3.2. As the sample swelled, it created a pressure on the piston that was transmitted by lever arm to push down the micro-switch. The micro-switch opened the solenoid valve and the water flowed into the flask. This process continued until no further swelling occurred, which was indicated by the built up back pressure that released the micro-switch. The collected water was thus, representing the swelling pressure. It was concluded that montmorillonite showed the significant swelling pressure compared to kaolinite and illite.

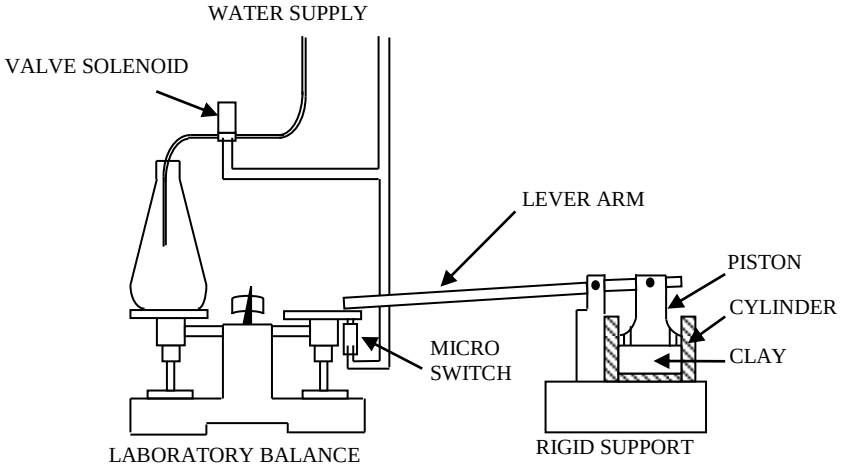

Figure 3.2. Apparatus developed to measure swelling pressure (after Davidson and Page, 1956).

Such approach motivated many researchers to conduct specific studies about the impact of those factors on swelling characteristics of expansive soils as explained in the following subsections.

3.1.1 X-Ray Diffraction Method

As mentioned in the previous chapter, some of the clay soils are expansive and the degree of expansivity ranges from non-expansive clays (e.g., Kaolinite) to highly expansive clays (e.g., Semectite) and is determined mainly by the mineralogical composition of clay particles and their atomic structure on one side, and the nature and water chemistry on the other side. Accordingly, many authors such as Scott (1963), Chen (1975), Mitchel and Soga (2005), and Nelson and Miller (1992) explained in details of types of clay minerals and water solutes that affect the degree of expansion. Some kinds of salts and minerals commonly form crystals. A crystal's structure is a bundle of atoms that are arranged repeatedly in a three-dimensional formation under conditions in which pressure magnitude and type of water chemistry play important roles of their formation (e.g., see Mitchel and Soga, 2005). Since the foundation of a crystal is atoms, x-ray diffraction is the method widely used in material science to characterize the crystal structure by determining the arrangement of atoms and, the angle and distance between bonded atoms. From them, one can observe the level of expandability of the tested material by determining the basal spacing.

Laird et al. (1995) used the x-ray diffraction method to study the hysteresis of crystalline swelling of smectite clays by measuring the basal spacing when the sample reached equilibrium state. After studying the hysteresis, they concluded that the crystalline swelling is an irreversible process and the hysteresis was associated with the change of salt concentration, relative humidity, and other factors.

In addition to x-ray diffraction method, Yitagesu et al. (2009) suggested a spectroscopy as the cost effective and time saving study, which can easily identify the

clay mineralogy. This research verified the collaboration with geotechnical investigation to quantify the engineering properties such as Atterberge limits, cation exchange capacity, and others.

3.1.2 The Influence of Water Chemistry on Swelling Potential of expansive Soils

Water chemistry induced swelling focused researchers' attentions to where they recognized the correlation of dissolved solute types in the interparticle spaces with swelling potential. Some of the researchers tried to improve the behavior of swelling soils by changing the physico-chemical properties such as exchanging the water chemistry with other dissolved solutes or increasing/decreasing the concentration of the same water chemistry. Consequently, the expandability and permeability of the swelling soils will definitely change. This approach is essential when dealing with the performance of swelling clays as hazardous waste (nuclear or radioactive waste) barriers, where the concentration of the dissolved solute in swelling soils is highly variable.

The dominant cation type of the dissolved solute is easily used for categorizing the swelling soils as shown in Table 3.1, which represents the classification of highly expansive soils.

Smectite clay	M[a]	1st hydrate	2nd hydrate	3rd hydrate
Montmoeillonite	Mg	3	3.03	3.05
	Ca	3.89	2.75	-
	Na	3.03	3.23	3.48
	K	2.42	3.73	-
Beidellite	Mg	2.69	2.69	-
	Ca	2.3	2.3	-
	Na	2.15	2.15	-
	K	2.54	-	-
Nontronite	Mg	2.92	3	-
	Ca	3.05	3.37	-
	Na	2.7	2.79	-
	K	2.6	-	-

Table 3.1. Number and thickness of interlamellar hydrates in (after Kehres, 1983).

The interaction between the pore water and the smectite clay influences the physico-chemical state of the pore water as actively studied by Pusch and Carlsson (1985). This physico-chemical alteration of pore water within the interlamellar space of Na bentonite was observed to induce major impact on many physical properties of such smectite, namely; swelling pressure, diffusivity of dissolved solutes, and hydraulic conductivity.

In addition to the correlation of adsorbed cations and water molecules to the hydration of the interlamellar space, which was discussed by Yong (1999), bond strengths and diffuse double layer are important factors that will be explained later in this chapter.

Castellanos et al. (2006) studied the swelling capacity of high-density bentonite clay by soaking the compacted specimen under oedometric conditions using three different solutions namely; distilled water, sodium chloride (NaCl), and calcium chloride ($CaCl_2$). The samples were then loaded and unloaded under saturated conditions to study the effects of compressibility on soil expansion. It was concluded that at the same molar concentration of these solutions, the value of liquid limit (LL) determined from the samples saturated with $CaCl_2$ was smaller than those values determined from samples saturated with NaCl. Moreover, the ionic strength of $CaCl_2$ is higher than NaCl at the same concentration that lowered the LL value and consequently, the double layer thickness and the repulsive forces should be further reduced.

The previous argument is comparable with Pusch and Yong (2006), who claimed that the coupling of water molecules and sodium (Na) in the interparticle spaces of Na-

montmorillonite is probably weak and the cations are relatively free to move as compared to Ca-smectite, which leads to significantly higher diffusion coefficient.

Stabilizing agents such as calcium (Ca^{+2}) and potassium (K^{+}) ions were used to improve the highly expansive soil properties by using electrokinetic method (Abdulla and Al-Abadi, 2010). Their device consists of electrokinetic cell with anode and cathode compartments by which the well-distributed agents through the sample could be obtained. The sample was then, taken and divided into several identical specimens to perform Atterberg limit, swelling potential, and shear strength tests. The Atterberg limit tests showed that the K^{+} agent significantly decreased the plasticity index as compared to unstabilized soils. The swelling potential tests provided similar results, which confirmed a uniformity of the agent concentration in all specimens. Moreover, the K^{+} agent reduced the swelling potential from 14.0 % to 0.4 %, where the Ca^{+2} agent reduced the swelling potential from 14.0% to 3.0%.

To simplify the discussion of the influence of water chemistry on swelling potential of expansive soils, the effect of cation exchange capacity (CEC) and diffuse double layer (DDL) is explained in a separate section.

3.1.2.1 Cation Exchange Capacity (CEC) and Diffuse Double Layer (DDL)

The clay minerals have the ability to absorb ions. As the negative charges (anions) are predominantly on the clay surface, the positive charges (cations) of water solute in pore spaces are considerably more absorptive near the clay surface, more than anions of the same water solute. This is the reason this chemical phenomenon is called CEC and has been discussed by several authors including Scott (1963), Chen (1975), Mitchel and Soga (2005), and Nelson and Miller (1992). The CEC is a quantitative measurement

performed by calculating the amount of salt cations required to equilibrate the predominant anions on the clay surface in milliequivalent per 100 grams of dry soil. Chen (1975) tabulated the CECs of various clay minerals as illustrated in Table 3.2, and; these results prove that a higher value of the specific surface leads to higher CECs.

	Kaolinite	Illite	Montmorillonite
Particle thickness	0.5 - 2 microns	0.000 - 0.1 microns	less than 9.5 A
Particle diameter	0.5 - 4 microns	0.5 - 10 microns	0.5 - 10 microns
Specific surface (sq. meter/gram)	10 - 20	65 - 180	50 - 840
Cation exchange capacity (milliequivalents per 100g)	3 - 15	10 - 40	70 - 80

Table 3.2. Ranges of cation exchange capacity of various clay minerals (after Chen, 1975).

The most exchangeable cations in clay minerals, according to Chen (1975) are as follows:

Ca^{2+}, Mg^{2+}, H^{+}, K^{+}, NH_4^{+}, and Na^{+}

The concentration of cations on the clay surface is dependent upon the activity of the exchangeable cations of water chemistry in the interparticle spaces. As cations start to accumulate over the clay surface under certain conditions such as moisture content change, degree of saturation change, change in relative humidity, or change of external pressure, diffuse double layer (DDL) will form.

The thickness of DDL relies primarily on the bonds strength in which the distribution of cations on clay particles is influenced by the balance of attractive and repulsive forces (e.g., Scott, 1963 and Nelson and Miller, 1992). As noted in Section

3.1.3, the swelling soil that contains Na^{+} as a prime salt cation of water chemical composition tends to form a DDL greater than the swelling soil that contains Ca^{2+} as a prime salt cation of water chemical composition.

Komine (2004) studied the relationships between swelling-pressure and swelling-deformation characteristics in terms of physicochemical properties of several types of bentonite clays. The results showed that the content of clay's mineral, such as montmorillonite, had a strong influence on the maximum swelling pressure of the samples tested rather than the exchangeable-cation composition. Conversely, the maximum swelling strain was influenced strongly by the exchangeable-cation composition rather than the content of clay's mineral. Therefore, Na-bentonite has a larger maximum swelling strain than Ca-bentonite.

Laird (2006) excluded the free anions in the interlayer pores and considered the cations as a major component in balancing the negative clay surface charges which in turn, controlled the crystalline swelling. He referred to an additional chemical activity in which two types of cations presented in an aqueous smectite system (e.g., Ca^{2+} and Na^{+}), namely Cation Exchange Selectivity (CES), to the point that the selectivity of cations preference to balance the anions spread over the clay surface controls the extent of crystalline swelling.

3.2 Statistical Approach to Identify the Expansive Soil Characterization

This approach requires tremendous efforts and repetitions to obtain reasonable results, which concisely express the common characteristics of expansive soils. These tests are actually branched by standard geotechnical engineering tests, microscopic tests, and mineralogical tests. Nelson and Miller (1992) provide some of the particular tests

used for this approach, such as the Atterberge limits tests, clay content test, x-ray diffraction, and cation exchange capacity test, among others, in which most are international standards such as ASTM standards. The statistical study performed by Komorink and David (1969) demonstrated a correlation between *combined* data of density, water content and liquid limit and swelling pressure. They concluded that the swelling pressure increases with the increase of initial density and liquid limit and with the decrease in moisture content. Moreover, it was confirmed that even most "plastic" clay may be non-expansive under certain dry density, water content and structure. In 2004, Kariuki and Van der Meer (2004) accomplished a similar study by correlating the swelling indices to establish a unified Expansive Soil Index (ESI).

Excluding the mineralogical studies, the geometrical studies (size and shape of particles), and water chemistry; the interparticle forces and the moisture content variation between the soil macrostructures are rather important in this research. Particularly, the interparticle forces (such as capillary forces) of fluid-air interface that form weaker bonds are one of the factors responsible for the swelling phenomenon. However, the interparticle forces also affect the strength behavior of the soils but the focus of this research is primarily on the volumetric strain behavior, and therefore, only these related research papers are reviewed as discussed in the following subsections.

3.3 Total, Matric, and Osmotic Suctions Measurements

Total suction ψ_t is the key to understanding the behaviors and properties of unsaturated soils. The effect of total suction on soil behavior is studied by subjecting samples to cycles of wetting and drying and relating the volumetric or gravemetric water content to the suction values. From it, one can develop hydraulic hysteresis of the

laboratory tests to replicate the environmental conditions in unsaturated soils. Many geotechnical engineers assumed that the change of osmotic suction ψ_o component was negligible due to the insignificant change in the water chemistry of unsaturated soil and thus, it can be considered that the change in ψ_t is equal to the change in matric suction ψ_m. However, when dealing with clay soils, the dissolved solute in pore spaces makes it important to account for ψ_o. Yong (1999) agreed with the requirement that both ψ_m and ψ_o govern the swelling performance of expansive clays. Furthermore, it was concluded that other component potentials might be as important as ψ_m and ψ_o such as gravitational potential ψ_g, pneumatric (air) pressure ψ_a and external pressure potential ψ_p.

Several techniques as illustrated in Figure 3.3, have been developed to measure the total suction of clay soils. Relative humidity technique or non-contact filter paper methods are the most common tests used to measure the total suction of clay soils. While the axis translation or contact filter paper techniques have the best control over measuring the ψ_m especially for unsaturated soils other than clays in which the change of ψ_o can be negligible and normally having lower air entry values.

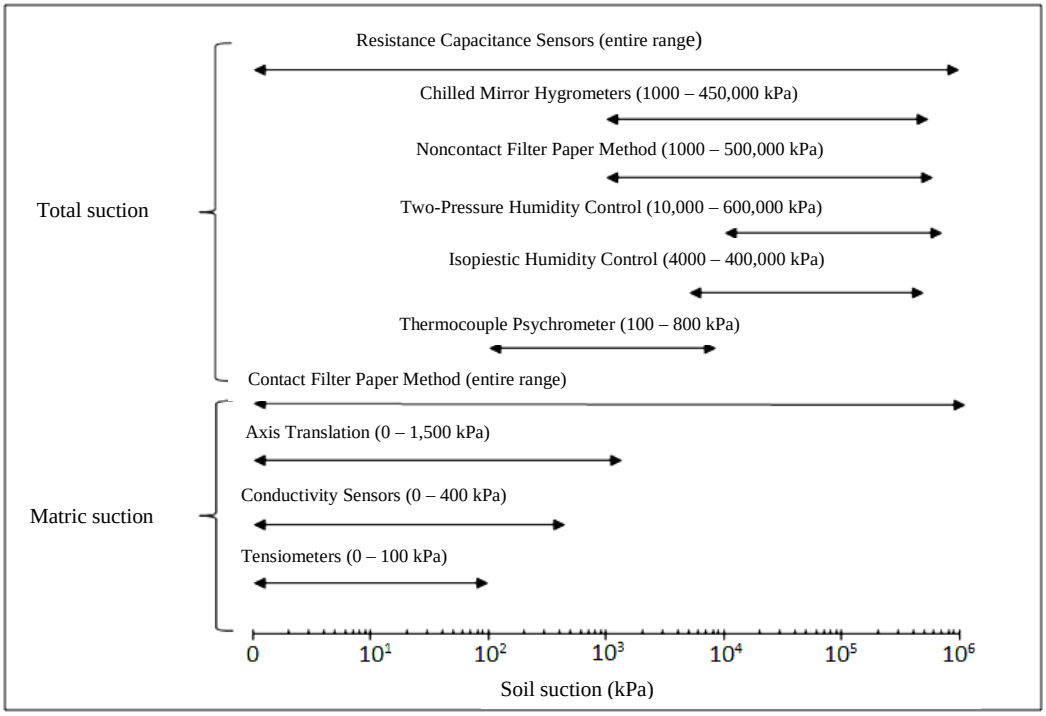

Figure 3.3. Approximate measurement ranges for various suction measurement techniques (after Lu and Likos, 2004).

Filter paper technique became a standard test because of its ability to indirectly measure the osmotic suction by calculating matric suction and total suction (e.g., see Fredlund and Rahardjo ,1993). Lu and Likos (2004) stated that the initially dry filter paper in direct contact with unsaturated soil that is placed in enclosed container, is called "contact" filter paper and used for matric suction measurement. The initially dry filter paper that is placed in the same enclosed container without contacting unsaturated soil is called "noncontact" filter paper and used for measuring the total suction. After placing the "contact" or "noncontact" filter paper in the sealed container partially filled with unsaturated soil specimen as shown in Figure 3.4, the moisture from the unsaturated soil will be absorbed by the initially dry filter paper. The transmission of moisture content from the soil specimen to the filter paper is in the form of liquid or vapor; but, the

transmission process must last for at least seven to ten days to assure that the suction value of the filter paper is at equilibrium with respect to the suction value of the soil specimen (Likos and Lu, 2003). The American Society for Testing and Materials (ASTM D5298 – 03) provide a calibration in terms of water content of the filter paper vs. total suction in semi-logarithmic scale as well as by the type of filter paper required for this type of test.

Madsen and Müller-Vonmoos (1989) performed micro-scale studies in order to make a distinction between two categories namely; the innercrystalline swelling and the osmotic swelling. It was found that during water uptake in completely dry clay, the hydration mechanism (the innercrystalline swelling) was mainly caused by exchangeable cations located in the interparticle spaces. Subsequently, the osmosis mechanism (the osmotic swelling) was driven by a substantial difference in cation concentration on the clay sheets which was responsible for creating the DDL. Therefore, the innercrystalline swelling occurred in the first place followed by the osmotic swelling during the progression of the swelling phenomena.

The filter paper method, the Electrical Conductivity (EC) test and the oedometer tests are performed by Rao and Shivananda (2005) to examine the osmotic suction, pore water salinity and swelling potential of salt – amended clays, respectively. The aim of the study was to investigate osmotic suction influences on swelling potential by changing the pore water salt concentration. The salinity concentration in pore water was measured by EC based on ASTM D4542 – 07 in which the salinity value obtained increased with the dissolved solute in pore water. They concluded that the dry density and water content

determine the swelling potential of salt – amended clays more than the pore water salinity whereas the osmotic suction, significantly affects the rate of swelling.

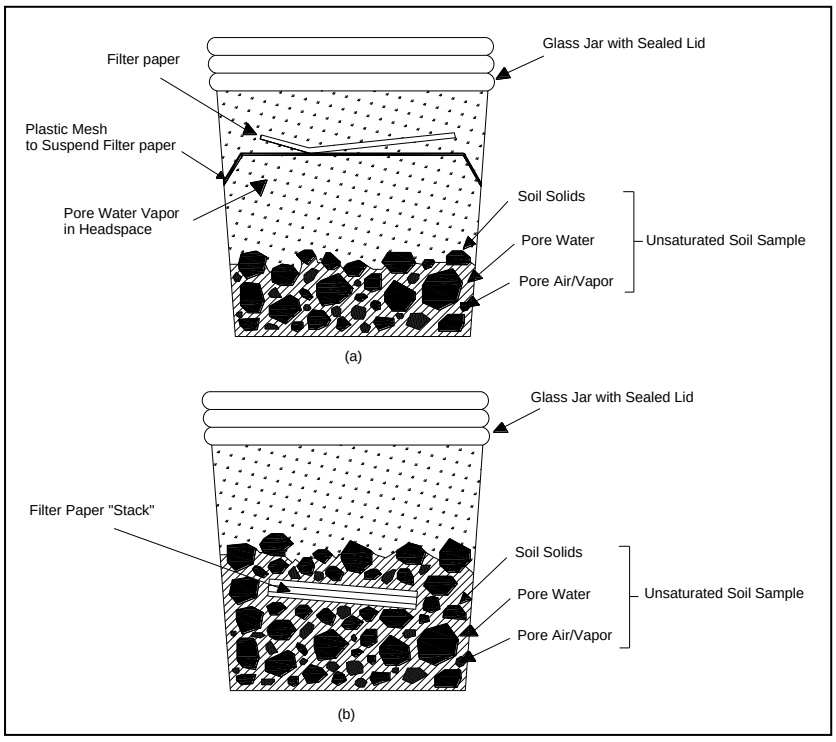

Figure 3.4. General testing configurations for filter paper testing: (a) "noncontact" method for total suction measurement, and (b) "contact" method for matric suction measurement (after Lu and Likos, 2004).

Sreedeep and Singh (2006) proposed other methodologies such as a dewpoint potentiometer (WP4) and pressure membrane extractor (PME) to quantify both matric and total suctions instead of using the filter paper method. Their results indicated that the total suction was higher than matric suction due to the dissolved solute presence in the tested soil that generated the osmotic suction. Figure 3.5 indicates that the osmotic suction continuously changes as water content changes. Moreover, the researchers noticed higher solute concentration at lower water content or at higher osmotic suction.

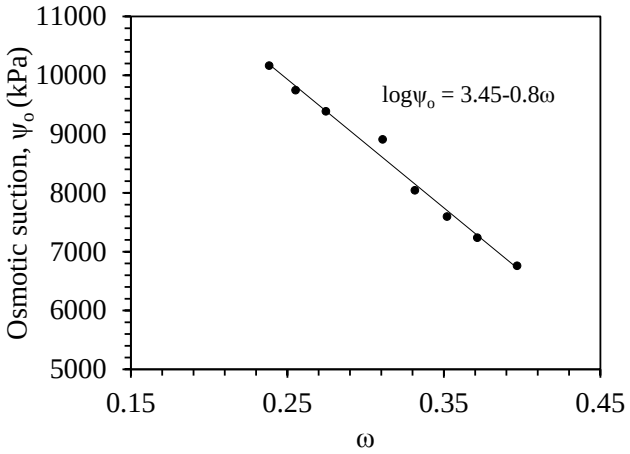

Figure 3.5. Variation of the osmotic suction with water content (after Sreedeep and Singh , 2006).

Miller and Nelson (2006) came to the same conclusion as Sreedeep and Singh (2006) regarding the significant effect of osmotic suction on total suction measurement. In spite of their agreement, Miller and Nelson (2006) observed that the concentration of salt had insignificant impact on volume change of the soil during desiccation process, which means that the shrinkage of the soil is a response of matric suction changes. Patrick et al. (2007) compared measurements between filter paper technique and chilled-mirror dew point technique where similarities and discrepancies of measuring total suction performed by some researchers were addressed. The study showed that major inconsistencies of the total suction measurements obtained from both techniques were probably because of incomplete equilibration in WP4-T (chilled-mirror device model) sealed test chamber. This problem could be avoided by allowing more time for specimen to fully reach equilibrium state, which is far shorter than that by using filter paper technique. The chilled-mirror dew point technique is faster, simpler and several total suction values can be acquired on one specimen by changing its moisture content.

In 2008, mathematical models proposed by Abedi-Koupai and Mehdizadeh (2008) were used to simplify the complexity of interrelations between soil moisture, ionic strength of soil solution, chemical composition of the solute, and the exchangeable ions residing on the solids surface of the soil particles. It was observed that the transfer of salt ions was stopped once the equilibrium between the filter paper and soil attained a specific suction.

Relative humidity (RH) is a term used to express the quantity of water vapor that exists in a gas phase (e.g., air), which usually ranges between 0% (dry state) to 100% (saturated state). In the case of unsaturated clay soils, RH depends not only on temperature, pressure and water availability but also on dissolved solute effects (Lu and Likos, 2004). Likos and Lu (2003) utilized their computer-automated system to examine expansive and non-expansive soils. The system was capable of controlling relative humidity to determine the total suction characteristic curve under higher suction ranges (7 to 700 MPa). Furthermore, Likos (2004) modified the same system by incorporating the axial strain measurement of expansive soil due to relative humidity changes by using a Linear Variable Differential Transformer (LVDT). It was observed that during the drying-wetting cycle, the cumulative axial stain occurred for each increment of relative humidity or total suction.

Along with the previous techniques, the osmosis principles were adopted to measure the soil suction as performed by Nowamooz and Masrouri (2009). This study was focused on describing the suction limits between micro-macro structure and between nano-microstructure. Since the suction limits depend strongly on soil fabric and density of the soil, the osmotic oedometer technique (as briefly explained in section 3.6) was

used on loose and dense samples. The results in Figure 3.6 (a) demonstrate the suction limits as a function of void ratio which are the intersection points of two slopes. In addition, the role of compaction energies on the convergence of the loading collapse yield surface (LC) (i.e., the preconsolidation pressure as a function of suction) and saturation curve yield surface (SC) (i.e., saturation pressure as a function of suction) is evident in Figures 3.6 (b) and (c). The saturated pressure was identified as an intersection point between the virgin compression line and normally consolidated curve that was produced by several compressibility curves at different suction values.

A comprehensive evaluation of common techniques used to measure soil suction as a function of gravimetric water content of compacted bentonite-sand mixtures, was performed by Agus et al. (2010). It was found that regardless of different ratios of bentonite to sand mixtures, the chilled mirror hygrometer technique presented more precise results of total suction measurements than filter paper, psychrometer, and dew point sensor (polymer capacitance sensor normally used in meteorology) techniques due to its most ability of maintaining the isothermal equilibrium between the soil and vapor space in the closed chamber.

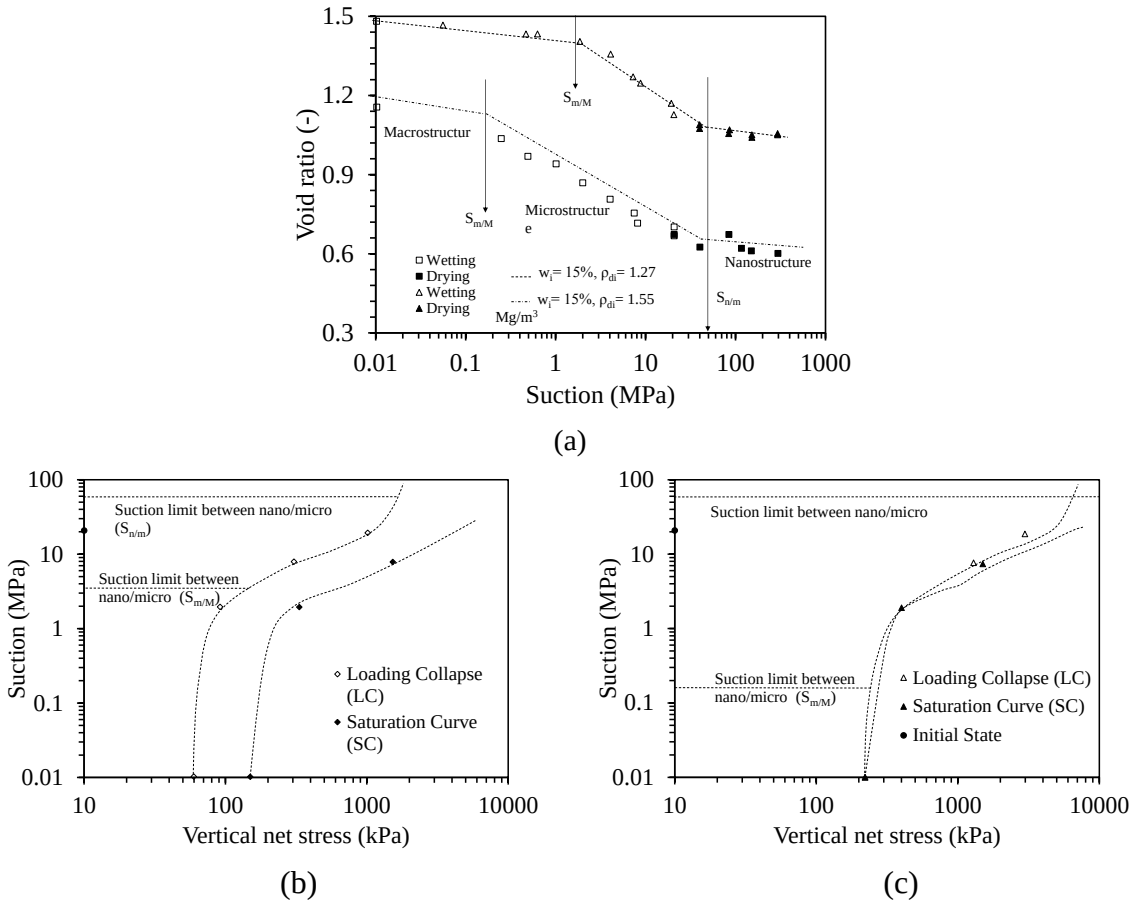

Figure 3.6. (a) Variation of void ratio on function of suction for loose and dense studied samples, (b) estimated yield surfaces for the loose compacted soil with an initial dry density of 1.27 Mg m^{-3}, and (c) estimated yield surfaces for the dense compacted soil with an initial dry density of 1.55 Mg m^{-3} (after Nowamooz and Masrouri , 2009).

3.4 Free Swell Measurements

Free swell is another index used to identify the expansive soil characteristics. ASTM D 4546 - 08 is a standard usually used to determine the free swell of dry expansive soil by submerging the soil in water without external constraint. Free swell index, also known as differential free swell, is performed by measuring the percentage of volume change after attaining an equilibrium state (no less than 24 hours of soil

submergence) to initial volume. Nelson and Miller (1992) stated that the combination of climatic conditions and the expansion characteristics of the soil play an important role in the value of free swell percentage. For example, free swell values between 1200 % to 2000 % were obtained by testing commercial bentonite while Dawson (1953) concluded that 50% of free swell value was enough for Texas clays to cause considerable expansion. Ashayeri and Yasrebi (2008) found that the high plasticity clays consisting of montmorillonite showed the most swelling potential. Furthermore, it was confirmed that moisture content and dry density affect the degree of free swelling after compaction. This means that a compacted sample at optimum moisture content may not signify the greatest swelling potential.

3.5 Swelling Pressure Measurements

Holtz and Gibbs (1954) and Jenning and Knight (1957) were pioneers in adopting the conventional oedometer (consolidation apparatus) to evaluate the swelling pressure of expansive soil. The swelling pressure is defined as the applied pressure that prevents the soil specimen from any further swelling caused by the wetting process. This test also is referred to as the Zero Swell Test (ZST) (Basma et al.; 1995 and Fattom and Barakat, 2000), while the Consolidation Swell Test (CST) has opposite procedures (Basma et al., 1995). The soil specimen used for CST is allowed to completely swell under a token load and upon wetting with water then, the soil specimen is recompressed to its original volume by gradually applying the pressure. Thus, the value of the applied pressure that ceases the swelling process is defined as swelling pressure. Moreover, Jenning and Knight (1957) first proposed a Double Oedometer Test (DOT), which was capable of predicting the settlement rate or total heave. The philosophy of DOT based on void ratio

versus log applied effective pressure relationship of two normally consolidated and identical samples. The dotted curve in Figure 3.7 (a) refers to a sample that has natural moisture content (unsaturated), while the solid curve refers to a fully saturated sample and thus, a heave due to wetting can be predicted at certain applied effective pressure.

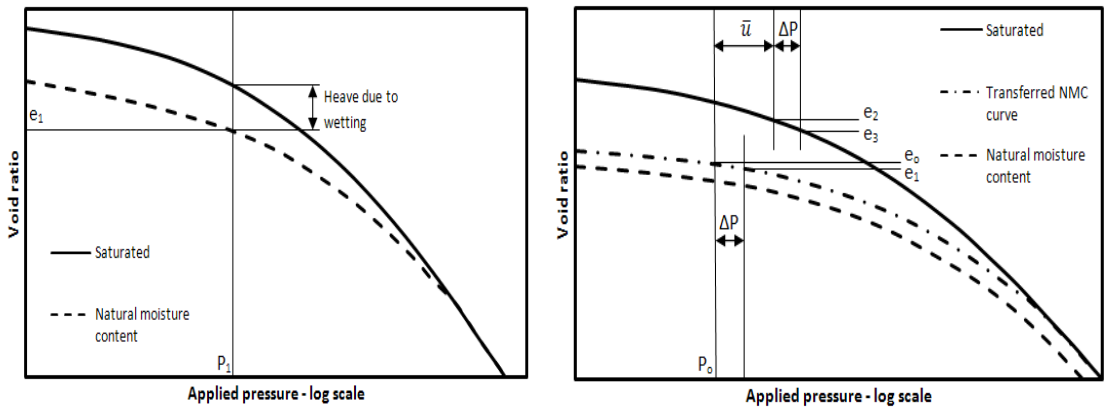

(a) (b)

Figure 3.7. (a) log p curves showing release of capillary pressure and (b) log P curves showing adjustment to bring straight line portion coincident (after, Jenning and Knight ,1957)

The hypothesis relies on coincident straight-line portions at higher applied effective pressure. That is at least acceptable to adjust vertically the dotted curve of natural moisture content sample and be coinciding with the curve of fully saturated sample as shown in Figure 3.7 (b) and thus, the settlement and heave can be predicted. Measurements of the dotted curve were less accurate due to the local variations in moisture content of the adjacent samples (Jenning and Knight ,1957). Figure 3.7 (b) illustrates an example of soil that endures an initial applied pressure (p_o) at certain depth and if a surface loading is applied (e.g., foundation), an additional pressure will increase the applied pressure $(p_o + \Delta p)$ as shown in the transferred curve. If the sample is

saturated at the same depth, an additional water pressure must be added to the applied pressure ($p_o + \Delta p + \bar{u}$) as shown on the solid curve.

A comparison between the swelling pressure of undisturbed and remolded specimen of the same kind was investigated by Shanker et al. (1982). Two approaches have been used to identify the swelling pressure namely; Constant Volume Method (CVM) (same as ZST), and Free Swell Method (FSM) (same as CST). At the same initial conditions, the swelling potential of undisturbed samples was found to be higher than those for remolded samples. In addition, the swelling pressure resulted from the FSM was found greater than that determined by the CVM for both kinds of soils.

It was observed that the development of the swelling pressure is proportional to dry unit weight and clay content percentage while inversely proportional to initial water content and initial applied pressure (Yevnin and Zaslavsky, 1970; El-Sohby and El-Sayed, 1981; Basma et al., 1995). This observation was obtained by performing the previous techniques (ZST, CST and DOT) and another technique called Restrained Swelling Test (RST) as performed by Basma et al. (1995). The RST is a technique where a sample was compacted by incremental applied pressure until it attained equilibrium deformation. The sample was submerged in water until full swelling was approached. The ratio of maximum expansion to initial height is defined as swelling potential whereas swelling pressure is defined as the pressure resulting in no expansion.

Although the above observation was consistent with the ones observed Komine and Ogata (1994), and Villar and Lloret (2008), the minor influence of the initial water content on the swelling pressure development was the only contradiction.

Shuai (1996) did an extensive study of the standard and modified oedometer tests. The study went even further by formulating a theoretical model to simulate the experimental results. The lateral swelling pressure was difficult to investigate by using oedometer test; therefore, the study was limited to one-dimensional framework. However, it was concluded that the coefficient of permeability is one of the important parameters required for the theoretical simulation, and recommended further research of the coefficient of permeability for swelling soils due to its influence on volume change and pore pressure behaviors during the test.

A robust computer system was developed by Thompson et al. (2006) in order to precisely control the increments of applied pressure during the constant volume swelling pressure tests on specimens obtained from several field sites. The results of these tests were compared with Load-Back Swelling Test (LBST is similar to CST) results and found that the swelling pressures resulted from the LBSTs overestimated the uplift skin friction. Whereas the swelling pressures obtained from the constant volume swelling pressure tests were comparable with those reported in the literature. Moreover, it is claimed that their computer-automated device is inexpensive and cost-effective for many geotechnical engineering projects and applications.

Baille et al. (2010) studied the compressibility behavior of initially saturated and compacted then, saturated swelling soils subjected to vertical high pressures under confined conditions using modified oedometer device in one-dimensional perspective. The research confirmed the knowledge about the swelling pressure test outputs which were achieved by many researchers as mentioned earlier. Furthermore, the values of coefficient of permeability were found extremely small for both type of soils produced in

this research (10^{-10} m/s to 10^{-14} m/s for initially saturated soils and 10^{-11} m/s to 10^{-14} m/s for compacted saturated soils).

3.6 Drying – Wetting Cycles Effect on Expansive Soils

The principal constitutive relationships that describe time – dependent engineering properties can be presented from testing expansive soils subjected to drying and wetting cycles in the form of (1) SWRC in terms of suction changes caused by moisture content changes, (2) soil deformation characteristic curve (SDCC) by which the drying process induces shrinkage deformation and wetting process induces swelling deformation , and (3) during water infiltration into the unsaturated expansive soils, the unsaturated hydraulic conductivity is as important property as the previous ones that is usually represented as a function of suction variable.

Miao et al. (2002) studied the hysteretic nature of SWRC by preparing two specimen sets: the first set of saturated specimens was allowed to volumetrically change without any pre-load applied and the second set of saturated specimens was subjected to pre-load to preserve the constant volume. They conclude that unlike the first set, the hysteresis potential of the second set was more stable. Thus, the second set was recommended in order to generate better SWRC; and from it, the unsaturated soil parameters, such as residual or saturated volumetric water contents, as well as predicting the properties of expansive soil can be obtained more accurately.

Alonso et al. (2005) utilized the elastoplastic model that was proposed earlier by Alonso et al. (1999) to evaluate the experimental data obtained by performing oedometric vapor equilibrium technique. The application of wetting and drying showed that the deformation of the expansive soil behaved elastically as number of cycles increased

which explained by the minimal difference between shrinkage and swelling accumulations during cyclic process.

Some researchers including Puppala et al. (2006) are concerned with expansive soils improvement by adding stabilizer products such as fly ash, lime, or other materials. They treated the expansive soils with different types of additives to reduce the swelling pressure and measure the SWRC using pressure plate apparatus to explicate the expansive soil behaviors, such as flow, strength, and volume change. Moreover, the possibilities of different volume changes of different soils that have the same Atterberg limits were noticed. Guney et al. (2007) observed that the swelling potential after each subsequent cycle increased with the increase of lime additive. In the case of non-treated soil samples, the maximum swelling potential was observed at the first cycle, followed by a gradual reduction of swelling potential as the number of cycles increased until the equilibrium was reached. The previous conclusion also was supported by Al-Homoud et al. (1995). They called this behavior a fatigue after each drying and wetting cycle and observed a reduction in plasticity as well as clay content, which led to a reduction in swelling characteristics.

Romero et al. (2006) investigated the accumulation of irreversible swelling or shrinkage strains of expansive soils during drying and wetting cycles. The applied suctions were controlled by relative humidity (vapor equilibrium technique), and the soils were tested under oedometer conditions. Miao et al. (2006) suggested using the volumetric water content, θ_v when testing the behavior of expansive soils subjecting to hysteresis of drying and wetting. The θ_v combines the effect of water content, degree of saturation, and void ratio, which in turn, affects the shape of SWRC that depends strongly

on the distribution of pore sizes. In that regard, Chao et al. (2008) used both the Fredlund SWCC device and filter paper method in order to determine the total, osmotic and matric suctions and construct the SWRCs in terms of the corresponding volumetric water contents. The experimental data produced almost identical trends in which they well-matched with the already published curve fitting equations.

Since the SWRC is an essential constitutive relationship in the unsaturated soil mechanics, it is important to establish a more reliable and credible method to be used for developing SWRC. A study published by Olsen et al. (2008) evaluated the reliability of chilled-mirror dew point devices (WP4 and WP4-T). The advantages of using the chilled-mirror devices are similar to those concluded by Sreedeep and Singh (2006). However, Chilled-mirror dew point devices are incapable of measuring the volumetric water content and thus, Olsen et al. (2008) developed the SWRC by using the constitutive relationship between soil suction and gravimetric water content.

The principles of osmotic system was used in soil science by Zur (1966), and Peck and Rabbidge (1966). This system was then adopted as an alternative technique in geotechnical engineering for studying the soil-water characteristics of expansive soils. For example, Kassiff and Ben Shalom (1971) were first who combined it with the conventional oedometer setup. Whereas Delage et al. (1998) improved this technique in order to control the soil suction up to 10.0 MPa. This technique mainly requires a semi-permeable membrane and a solution of polyethylene glycol (PEG). The semi-permeable membrane is only permeable to water molecules in the sample to drain through it depending on the concentration of PEG. Therefore, the higher the solution concentration,

the higher the water drainage and thus, the higher the soil suction (Delage et al., 1998; Cuisinier and Masrouri, 2005).

Bentonite/silt mixture was selected by Nowamooz and Masrouri (2008) to experimentally study the influence of hydraulic hysteresis on the mechanical behavior of the expansive soil. Cyclic of wetting and drying were implemented by controlling suction at different values using osmotic oedometer device. The sensitivity of the swelling and shrinkage accumulations to the imposed suction ranges was examined. In other words, insignificant void ratio variations were observed for suction cycles ranging between 3 to 8 MPa (this range was considered to be applied to soil microstructure). Whereas, significant shrinkage accumulation occurred as the initial vertical stress was increased within the suction range between 0 and 8 MPa (this range was considered to be applied to both soil micro- and macrostructures). Moreover, compression tests were performed with and without hydraulic cycles to determine the mechanical parameters such as virgin compression index, elastic compression index and preconsolidation pressure which were dependant on the stress paths.

Since the osmotic technique of the modified oedometer was only capable to measure suctions less than 8.5 MPa, Nowamooz and Masrouri (2010) applied the vapor equilibrium technique for measuring suctions up to 288 MPa. This approach led to cover a wide range of suction measurements in order to determine the soil-water retention curves of dense and loose compacted natural swelling soils. One purpose of this research was to confirm the existence of suction limits as discussed earlier. The main conclusion was that the cyclic of wetting and drying caused shrinkage accumulations for loose

samples, and swelling accumulations for dense samples until the equilibrium states were reached with number of cycles.

3.7 Swelling-Shrinkage Deformation of Expansive Soils

Swelling and shrinkage behaviors of expansive soils depend mainly on the external stress applied, the stress history, the water movement through the soil during drying and wetting cycles, environmental conditions, and mineralogical effects, as mentioned earlier. Due to different levels of expandability and shrinkage between soils or even for the same kind of soil, efforts have been made by many researchers toward better understanding of this phenomenon on the subject of innovative experimental works as well as theoretical frameworks.

Shanker et al. (1987) studied experimentally the swelling deformation of cubic soil specimens in three dimensional perspective. This exceptional study contained many approaches by means of the number of directions where the water was allowed to flow, and the number of directions where the swelling deformation was permitted. The overall observations signified the importance of the swelling deformation dimensionality as oppose to the drainage dimensionality as far as the degree of volumetric expansion is concerned. That is to say, the volumetric expansion increased with the number of directions where the specimen was permitted to swell.

Komine and Ogata (1994) used an improved oedometer apparatus to test the axial swelling deformation with time of compacted soils at different initial dry densities and initial water contents. It was concluded that the maximum swelling rate was independent on the initial moisture content but proportional to the initial dry density at constant vertical pressure. Moreover, the swelling deformation process was independent on the

initial water content for soils of low initial dry density and dependent on the initial water content for those of high dry density. Similar knowledge was verified by Villar and Lloret (2008), who interpreted the influence of water content and dry density on the swelling properties of a heavily compacted bentonite. Their results obtained by conventional oedometer tests demonstrated that the dry density had a major effect on swelling deformation. While at the same dry density and constant vertical pressure, the swelling deformation decreased with the initial water content.

Basma and Al-Homoud (1996) studied the influence of partial shrinkage – fully swelling cycles and fully shrinkage – fully swelling cycles on the shrinkage-swelling behavior. In case of the first approach, the swelling potential decreased with number of cycles until the equilibrium state was attained, as opposed to the second approach. In addition, the second approach contributed to gradual reduction of shrinkage potential as number of cycles increased towards equilibrium state. The latter observations suggested that in microstuctural point of view, the bond strength between the interparticle spaces, the structure of clay particles and their orientation, were influenced by the cyclic process. Similar approach had been carried out by Tripathy et al. (2002) who observed a reversible shrinkage-swelling path which was generally observed after performing the fourth shrinkage-swelling cycle.

Windal and Shahrour (2002) proposed flexible oedometer to account for both lateral and axial swelling strain. They provided experimental data that showed a reduction in swelling strain when using a flexible ring oedometer as compared to the conventional stiff ring oedometer.

Allen and Gilbert (2006) modified oedometer apparatus to incorporate the drying-wetting cycles and then, used it to generate a relationship between the vertical deformation and water content. The main advantage of their modified oedometer apparatus was the ability to accelerate the wetting and drying processes (less than a week) and replicate the field conditions.

In terms of a mathematical approach, researchers such as Gens and Alonso (1992) proposed a conceptual framework that describes primarily the mechanical characteristics of unsaturated expansive clays. The main feature of this framework was the coupling effects of soil structure in terms of a microstructural and macrostructural levels on the swelling behavior. Several basic assumptions had been considered such as the complete reversible deformation in the microstructural level during the hydration process, the possibility of the microstructural level to remain saturated, and the independency of the microstructural level deformation on that of the macrostructural level. Regardless of these assumptions, the model was capable of simulating many experimental evidences, which are, the irreversibility of the swelling deformations, the dependency of swelling pressure on void ratio change and testing methods. In the end, this conceptual model has motivated many researchers to improve their mathematical models. Alonso et al. (1999) proposed a mathematical model that describes the volumetric behavior of expansive clays. Their mathematical formulation is able to capture the experimental observations, such as irreversible dilation and contraction of expansive soils during suction cycles. Since the conceptual model proposed by Gens and Alonso (1992) was not developed for heavily compacted clays, another model was proposed by Cui et al. (2002) to overcome such a

limitation. This model was developed to predict the volumetric behavior of heavily compacted clays subjected to wetting-drying cycles.

Kim et al. (1999) simulated the one-dimensional deformation by extending the soil water continuity equation based on Lagrangian and Eulerian descriptions. It was found that the model using the Eulerian description could capture the experimental data slightly better than the model obtained by using the Lagrangian description. In 2006, Cornelis et al. used many mathematical models performed by different researchers to generate a Soil Shrinkage Characteristic Curve (SSCC) that describes the relationship between void ratio and moisture content. A year later, a microstructural fabric model proposed by Wayllace1 and Likos (2007) was capable of anticipating the bulk volume change as a function of RH, by which the interlayer and interparticle pores were influenced.

3.8 Hydraulic Conductivity Measurements

Gardner and Hsieh (1956) performed one of the earliest attempts for measuring moisture velocity in unsaturated soils. The study focused on experimental works for determining the f-function that has been plugged in Equation 3.1 similar to Darcy's law and used before by Gardner and Gardner (1951) because of the fact that both moisture content and flow channel size are continually changing during drying-wetting cycles.

$$v_{macro.} = -kf\ \nabla\phi \tag{3.1}$$

Where, k is the saturated flow permeability constant; $\nabla\phi$ is the gradient of moisture potential; f is dimensionless factor to account for unsaturated voids ranges from 0 to 1; and $v_{macro.} = v_c\theta$ is the macroscopic velocity in flow channel multiplied by volumetric water content. In spite of difficulties in explicitly measuring k at that time,

variation of k during drying-wetting cycles in unsaturated soils was confirmed, expanding many researchers' motivations in developing new methods for measuring unsaturated k.

Several techniques were developed for measuring hydraulic conductivity of saturated and unsaturated soils by considering constant pore spaces during the test, which is not the case when dealing with expansive soils. The hydraulic conductivity depends on the pore spaces, density of water, water viscosity and duration of water infiltration. The porous media in unsaturated expansive soil is variable and makes the nonlinear unsaturated hydraulic conductivity measurement even more difficult. Nakano et al. (1986) suggested using the space coordinate system adopted from Philip (1968) for developing equations based on the movement of water relative to movement of clay particles and the continuity equations for solid and water. They also introduced diffusivity coefficients (i.e., the apparent clay particle diffusivity and the apparent water diffusivity) in their governing equations, and from them, the hydraulic conductivity coefficient can be back calculated. Their experimental results (Figure 3.8 (a)) and theory were satisfactorily validated by using material coordinate system.

The methodology of determining the $D(\theta)$ in the material coordinate system was explained by several researchers including Smiles and Rosenthal (1968), Philip (1969), and De Veaux and Steele (1989). A one dimensional diffusion equation in a horizontal coordinate was used and Boltzman variable $\left(\lambda = x/\sqrt{t}\right)$ was introduced to convert the diffusion equation into simplified ordinary equation as follows:

$$D(\theta) = -\frac{1}{2}\frac{d\lambda}{d\theta}\int_{\theta_0}^{\theta}\lambda(\theta)d\theta \qquad (3.2)$$

For example, relationship between λ and θ (or void ratio) is calculated from a profile of volumetric water content and volumetric clay content (σ) versus depth during water infiltration as shown in Figure 3.8 (a) and from material coordinate system (m) as shown in equation (3.3) that leads to (Nakano et al., 1986):

$$\frac{dm}{dz} = \sigma \Rightarrow \lambda = m/\sqrt{t} \tag{3.3}$$

The slope $\frac{d\lambda}{d\theta}$ and area under the curve are determined graphically from Figure 3.8 (b). The hydraulic diffusivity in material coordinate system is thus, graphically presented in Figure 3.8 (c) as a function of θ. Therefore, unsaturated hydraulic conductivity can be calculated as a function of volumetric water content as follows:

$$k(\theta) = D(\theta)C(\theta) \tag{3.4}$$

Kim et al. (1999) carried on the previous approach to develop two models of unsaturated hydraulic conductivity function by using Eulerian and Lagrangian coordinate systems. A comparison of the two systems led to slightly higher values of unsaturated hydraulic conductivity simulation by using Eulerian coordinate because it over predicted the water content profile that was used to describe water flow during infiltration .

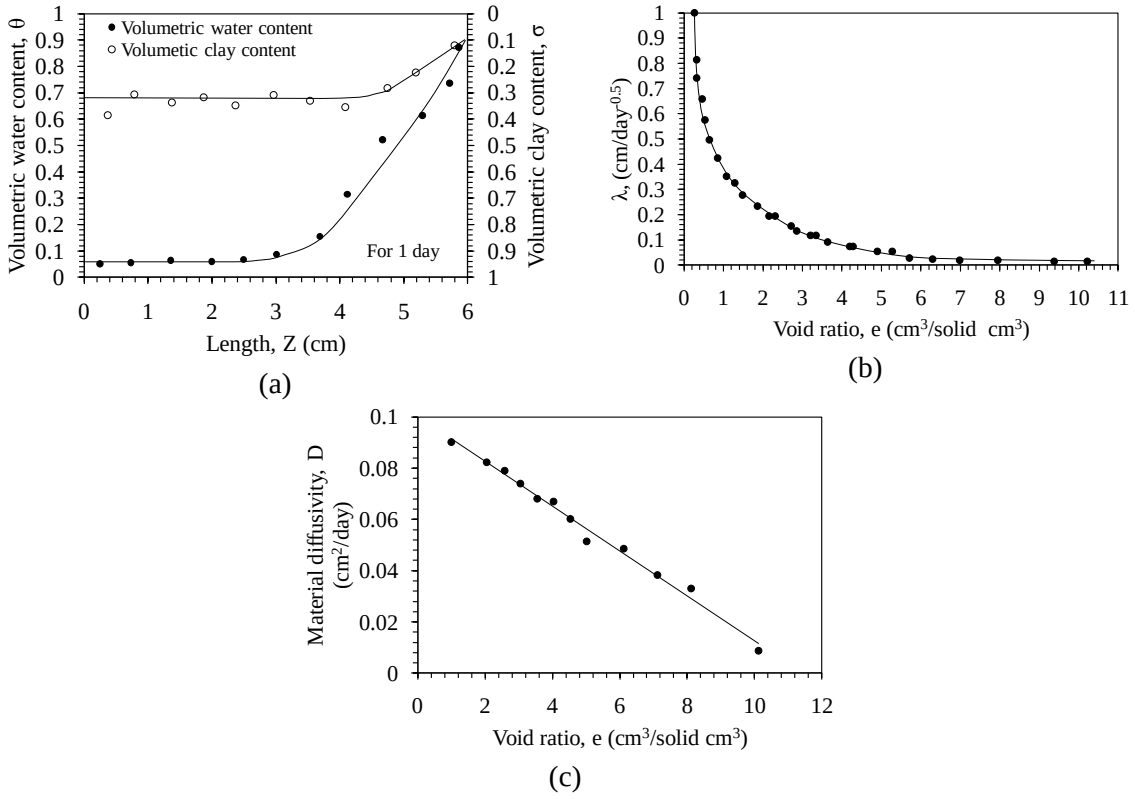

Figure 3.8. (a) An example of volumetric water and clay content profile for day 1, (b) relationship between λ and volumetric water content, and (c) material diffusivity as a function of volumetric water content (after Nakano et al., 1986).

Cui et al. (2008) measured the unsaturated hydraulic conductivity of compacted sand/bentonite mixture by using the instantaneous profile method under constant volume and free swell conditions during the infiltration process. Although the instantaneous profile method may suffer problems when examining highly expansive soils (Fredlund and Rahardjo 1993), Cui et al. (2008) observed a reduction of permeability of soils tested under constant volume conditions due to a simultaneous reduction of macropores. In the case where the free swell condition was applied, the higher values of unsaturated hydraulic conductivity were observed during infiltration because of the consequent increase in macropores. Masrouri et al. (2008) summarized the most common techniques

of measuring the unsaturated hydraulic conductivity for both swelling and non-swelling soils. This research paper provided a broad knowledge of these techniques and some of their assumptions and limitations to be considered in order to correctly understand the characteristics of unsaturated soil.

The theoretical equations proposed by Komine (2008) to predict the hydraulic conductivity of bentonite based backfill for underground disposal of radioactive wastes, were experimentally validated (Komine, 2010). When the sand-bentonite mixture had 20%, 30%, and 50% of bentonite contents, the hydraulic conductivity did not change significantly with swelling strains. However, in the case of the mixture with 10 % of bentonite content, the 1.0 % swelling strain caused the change in hydraulic conductivity values from 10^{-10} m/s to the range of 10^{-4} - 10^{-6} m/s. Therefore, it was suggested that the theoretical equations were applicable for backfills containing bentonite of 20%, 30%, and 50%.

3.9 Conclusion

- The previous literature review emphasizes the importance of studying the physical, chemical, and mechanical behaviors of expansive soils as a material primarily involved in various projects, which require a careful understanding of swelling soils' characteristics that govern the soil's quality and workability. Although the mineralogical and agricultural studies provided indications of the clay soil expandability, they are lacking the ability to characterize the essential property of soils in geotechnical engineering, which is the permeability during liquid (e.g., water) infiltration. Moreover, the wealth of information resulting from these studies regarding the swelling phenomena may or may not represent the bulk

volume change of clay specimens. Determining the degree of swellings was conducted under the main assumption of a perfectly flat structure of individual clay particles where the flow of water and dissolve solutes are taking place in between the particles. Nevertheless, no study was able to demonstrate if the swelling levels were the same for all individual particles of clay specimens. However, the knowledge behind the mineralogical and microstructural studies of swelling soils is useful to facilitate the experimental, theoretical and numerical studies from the geotechnical engineering perspective.

- The geotechnical engineering viewpoints of the factors that induced swelling of unsaturated clay soils commonly include the following: stress history; void ratio or porosity; initial water content; degree of saturation; initial dry density; infiltration rate; and total suction. Most of the stated factors are relevant for studying unsaturated soils, but for clayey soils the void ratio and osmotic suction are particularly important even if a clay soil is non-expansive.
- Regardless of the methodologies utilized, the relationship between the suction (total suction or matric suction) versus volume change and suction versus unsaturated hydraulic conductivity were nonlinear. The acquired nonlinearity trends were similar; for example, volumetric strain and unsaturated hydraulic conductivity decrease with the increase of suction and vise versa.
- When the hydraulic hysteresis control the behavior of unsaturated soils, SWCC must be developed first to accurately replicate the soil characteristics (Zhou and Yu 2005). In the case of expansive soils, the consequent soil characteristic is the volume change.

- Microstructural and mineralogy complexity of the swelling phenomena are reflected in the SWRC and therefore, adequate methodologies must be developed to measure volume change associated with moisture content variation.
- The oedometer, whether conventional or modified, is the one-dimensional consolidation device commonly used to perform swelling pressure and swelling deformation tests on expansive soils. Typically, the compacted sample is inundated with distilled water (from either top or bottom, or both) until the equilibrium of the swelling pressure and the corresponding swelling deformation is reached. If the degree of saturation is unity at the end of the test, it is possible to determine the compressibility coefficients by performing compression tests.
- Whether saturated or unsaturated, quantifying the swelling behavior of expansive soils by controlling specific water infiltration is lacking and demanding more investigation.
- The filter paper method is another common approach normally used to measure the total suction of deformable soils, and from it, the osmotic suction can be measured. This technique is simple, low cost, and effective, and can apply to a wide range of suction. On the other hand, it lacks accuracy and offers inadequate suction measurements. Leong et al. (2002) addressed the factors affecting filter paper method for suction measurement. They performed extensive assessments of the calibration curves based on the filter paper quality used in the literature. In addition, Likos and Lu (2003) proved that, although the filter paper method is applicable to a wide suction range, it may be insufficient for highly expansive soils.

- Since the air entry value of clay soils occurs at higher suction as compared to sand and silt soils, a partial transition during water movement from liquid phase to gas phase (e.g., water to water vapor) occurs at higher suction levels. That means the relative humidity must be quantified.
- Because the water movement in expansive soils is relative to the soil particles movements, implementing Darcy's law in the continuity equation is questionable. Darcy's law is widely used to describe the flow of water through unsaturated stationary or non-deformable soil particles. Therefore, it is advisable to use the hydraulic diffusivity as a function of suction in describing the flow of water in conjunction with soil particles movement or deformation instead of hydraulic conductivity function.
- Most of the constitutive models focused on simulating the nonlinear deformation of expansive soils during drying-wetting cycles. Sharma (1998) outlined some of the proposed mathematical models from different researchers and addressed his unified constitutive model to be used for both unsaturated non-expansive and expansive soils. Only limited efforts intended to simulate the unsaturated hydraulic conductivity are found in the literature.

CHAPTER 4

SOIL SELECTION, EXPERIMENTAL EQUIPMENT AND PROCEDURES

4.1 Introduction

As revealed in Chapter 3, studying the swelling mechanism of highly expansive clays is a challenging problem. The main reason for this complexity is that the process of the transient flow is accompanied by significant volumetric change. This means that the changes of the soil suction, the void ratio, and the hydraulic conductivity are greatly influenced by this phenomenon. Generally, the low permeability and very high air entry value of soil suction (where the soil starts to desaturate) are the fundamental properties of clays. Specifically, the permeability of highly expansive clays as a function of soil suction becomes significantly smaller with the decrease of void ratio. In addition, the high affinity of expansive clays to retain the moisture during the process of desiccation is also affecting the clay behavior in the saturated zone (where the clay remains saturated with the increase in soil suction). Therefore, to achieve the unsaturated conditions of highly expansive soils, a much greater soil suction value is required as opposed to the other clays.

Considering the above common observations, the focal point of the experimental work of this research led to:

- Selecting the appropriate materials proportions (silt and bentonite) in order to create the highly expansive soil that either simulates the field condition or can be used in geotechnical engineering design.
- Selecting materials proportions to provide a reasonable testing duration together with showing evidence of a significant volumetric change.
- The development of appropriate testing methodologies to attain satisfactory results and analyses.

In this chapter, the selection of materials, the determination of the geotechnical engineering properties, and soil preparation method are firstly described. Afterward, the apparatus used in this research and the testing procedures are addressed in detail. The influence of the mineralogical and physico-chemical characteristics on swelling behavior of the selected materials might be interpreted from the observations reported in the literature, but not investigated in this study.

4.2 Materials Selection and Soil Property Tests

Most of the soil samples used for experimental research as revealed in Chapter 3 were artificially prepared. It was preferable to test the mechanical behavior of such expansive soil than the natural ones (or undisturbed samples) for the reason of eliminating the possible variability between samples such as heterogeneity, and inconsistency of chemical or mineral composition (Sharma, 1998).

In that consideration, two materials have been selected in order to create artificial highly expansive soil, namely, Bonny silt and Black Hills bentonite. The Bonny silt is a material obtained from a sedimentary formation located at Bonny Dam, in eastern

Colorado State (Bicalho ,1999). It has the classification properties of LL = 25%, PL = 21%, Casagrande classification CL-ML and Specific Gravity (G_s) = 2.63. The grain size distribution of Bonny silt is shown in Figure 4.1. As the Bonny silt has particles of sand size, number 40 sieve (0.425 mm opening) is used to retain those particles and the remaining of Bonny silt material is mixed with Black Hills bentonite.

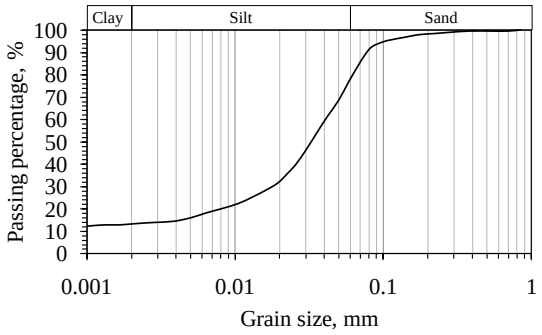

Figure 4.1. Grain size distribution of Bonny silt (After Hwang, 2002)

The Black Hills bentonite is a material obtained from commercial vendors (Mile hi Ceramics Inc.). This particular sodium bentonite has predominant smectite mineral, which is montmorillonite. The sodium bentonite is known as clay of high swelling potential and exhibiting viscous, and thixotropic characteristics. Those characteristics give bentonite exceptional uses for various geotechnical engineering applications that were explained in detail by Murray (2007).

Three sets of soil mixture proportions are preliminary tested based on free swelling and shrinkage tests (as explained later in this chapter). It is found that the slowest swelling process is observed when using a mixture of 20% bentonite to 80% Bonny silt ratio, which is not applicable in this study. Conversely, a mixture of 60% bentonite to 40 % Bonny silt ratio shows the quickest swelling process but causes cracks

problems that are widening as the moisture content of the specimen is reducing during shrinkage tests. Therefore, the mixture of 40% bentonite to 60% Bonny silt ratio is found suitable in this research in order to maintain a balance between avoiding the cracking issues and having the specimens ready to the forthcoming swelling tests within a more feasible duration of time.

Two geotechnical engineering tests have been performed to determine the selected soil properties:

- A specific gravity (G_s) test (e.g. see ASTM D854 – 06 e1), in which 2.53 is determined as the G_s of the selected soil mixture.
- A liquid limit test (LL) (e.g. see ASTM D4318 - 05), the LL of the selected soil is 126.4 % which gives an indication of considerably large volume changes as moisture content of the soil changes.

A laboratory mixer is used to thoroughly mix two quantities of the soil and 300 % of water content is added to form a slurry. The total mass of the sample is approximately 19 kg. This amount is sufficient to produce a big sample of approximately 10 mm in thickness after consolidation and 610 mm in diameter, so that multiple specimens can be obtained simultaneously for various testing, as explained in the next section.

4.3 Double Drainage Consolidation

The expansive soil samples that are produced in this test can be considered as remolded samples that have uniform pore size distribution (e.g., see Fityus and Buzzi, 2009). The role of the double drainage consolidation preparation is to produce big samples that have as small a thickness (the targeted thickness is 10 mm) as possible to

maintain the subsequent tests' durations at a reasonable length, convenient for the experimental program period of this research.

4.3.1 Experimental Equipment

The equipments, which is utilized for sample preparation consists of an aluminum container that has an inner diameter of approximately 610 mm and an inner height of 537 mm, a top aluminum platen that has four holes to allow the excess water in sample pores to expel from the top surface, two porous stone disks, two fine filter papers, a top aluminum ring, a bottom aluminum plate, a rubber O-ring, and connection rods that connect the top ring with the bottom plate. A schematic assemblage of the container is shown in Figure 4.2.

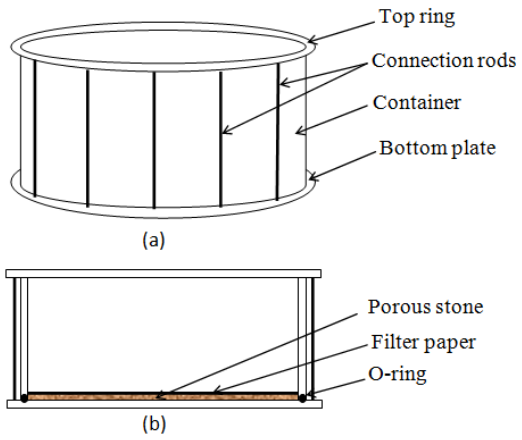

Figure 4.2. Schematic illustration of the container from (a) three dimensional view and (b) cross-sectional view.

The Material Testing System (MTS) is the machine used for the sample preparation. Its model is 661.23A-02 with the load cell capacity of 500 kN. It can be operated in two modes, namely, displacement-control mode and load-control mode.

4.3.2 Experimental Procedure

After carefully pouring the slurry in the assembled container, it is left uncovered for one day to allow for self-weight consolidation and solidifying the upper portion of the slurry. This strategy is found effective to support the additional weights of the top porous stone, the top platen, the wooden pieces, and the steel plate, respectively (Figure 4.3). The time interval between each additional weight is approximately one day. The slurry under the aforementioned weights is left for one more day.

The MTS machine is used to continue the consolidation process under displacement-control mode with a constant displacement rate of $1.2x10^{-5.0}$ m/min. The displacement rate is controlled by the base of the MTS machine and the gradual increase of the load is recorded onto the personal computer. The consolidation process lasts for about nine to ten days to reach the load capacity and designated thickness of the sample. The preconsolidation pressure is determined to be approximately 1448 kPa. After that, the displacement-control mode is switched to load-control mode to maintain the preconsolidation pressure until the consolidation is minimal.

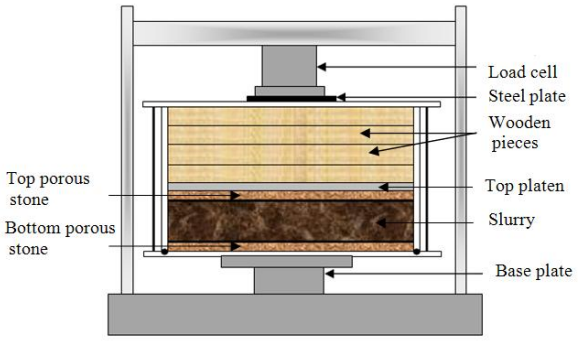

Figure 4.3. The installation of the contained in the MTS machine.

The container is disassembled and the sample is cut into several big pieces and preserved in sealed plastic bags. Those bags are placed in a closed plastic container and stored in the humidity room in which the relative humidity (RH) is fluctuating between 91.0 % and 93 %. Additional wet paper towels are set at the bottom of the closed plastic container to provide a RH of approximately 97.0 % (measured in the container) as illustrated in Figure 4.4.

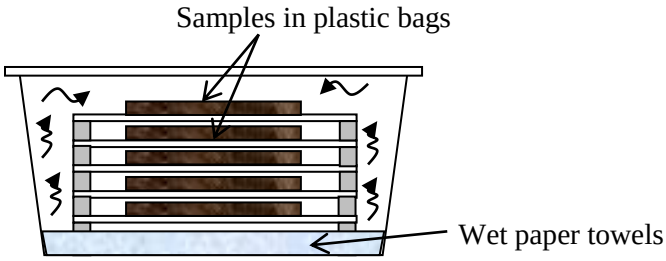

Figure 4.4. The plastic contained used to conserve the moisture content of the prepared samples by increasing the relative humidity in a closed environment.

4.4 Shrinkage Test

The primary objective of this test is to produce specimens at various reduced moisture contents and use them as a baseline for swelling tests. The relationship between the void ratio and moisture content during the desiccation process is examined as well.

Shrinkage is a response of soil particles movement caused by initial moisture content reduction and by the associated introduction of pore air into a soil mass over time. The soil particles movements are conceptually due to capillary tension development in water-air interface, which has a tendency to pull adjacent soil particles together until the shrinkage limit is reached. At shrinkage limit, the process of moisture content reduction continues without any further significant reduction in overall soil volume. In the field,

this behavior is caused by elevated temperatures (evaporation), transpiration, and lowering the groundwater table. In this test, instead of elevating the temperature, the specimens are permitted to dry under different values of RH where the temperature is held fairly constant.

On the basis of the theoretical relationship between RH and soil suction as shown in Figure 4.5, it is obvious that at the region of very high RH and very low soil suction, the slight change in RH greatly influences the soil suction variation. For example, at temperature of 22 ℃ and RH = 0.999, the corresponding total suction is 135.9 kPa. While at the same temperature and RH = 0.99, the corresponding total suction is 1365.2 kPa. Therefore, the RH may have a significant influence on soil suction variation if it is considered as one of the state variables (effective stress, water content, temperature, external pressure, hydraulic gradient, and others) that is governing the soil system (pore size distribution, hydraulic conductivity, and other soil properties).

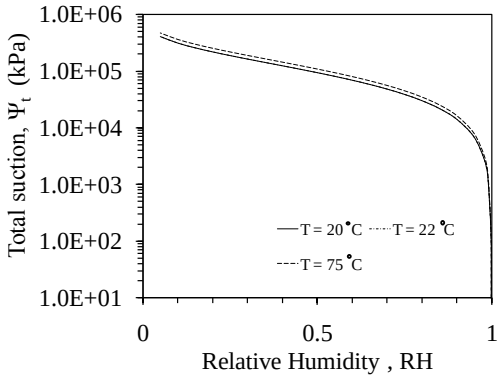

Figure 4.5. Theoretical relationship between relative humidity and soil suction based on Kelvin's equation.

The shrinkage process is observed at room temperature where the RH is considerably lower than in the humidity room is much faster. Since the specimens have

very low hydraulic conductivity, the desiccation process is non-uniform and leads to the desiccation-induced cracking due to a rapid moisture content reduction if the specimens are allowed to dry at room temperature. In order to avoid this problem and have a good control over the shrinkage process, all the specimens required for this test are placed in small plastic containers, as explained in the following section.

4.4.1 Experimental Equipment and Procedure

Firstly**,** an aluminum cutting tool (the inner diameter is 30.5 mm) is used to cut specimens from the samples prepared, as discussed earlier. The specimens are then placed in small plastic containers and quickly closed to preserve the initial moisture contents.

Secondly, the digital camera is installed in such a way that the distance between the stationary digital camera and the specimen is fixed when the images of the specimens are taken periodically during the test as illustrated in Figure 4.6. The pixel ruler is utilized to measure the specimen dimensions in pixels and converted to metric units after collecting the images onto a personal computer.

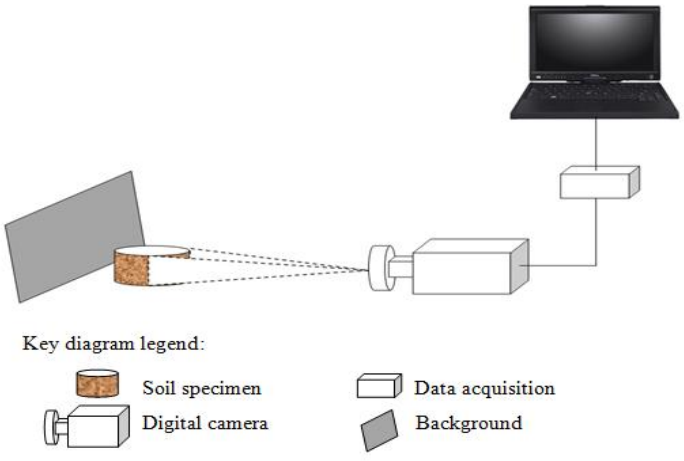

Figure 4.6. Schematic diagram of digital camera setup.

The shrinkage tests are then, initiated according to the following scheme (Figure 4.7):

- Shrinkage process #1: Some specimens (point #1 in Figure 4.7) are allowed to desiccate at room temperature where the RH is about 30.0%. These samples reach the shrinkage limit and the lowest moisture content in the testing program.
- Shrinkage process #2: Some specimens (point #2 in Figure 4.7) are permitted to dry in the humidity room where the fluctuation of the RH is between 91.0% and 93.0%. The test is stopped once the specimens have lost approximately 2.0 gm of water and the moisture distribution in the specimen is equilibrated.
- Shrinkage process #3: Some specimens (point #3a in Figure 4.7) are permitted to dry in the humidity room where the fluctuation of the RH is between 91.0% and 93.0%. The shrinkage test is stopped when no further reduction in water content and bulk volume is observed. Out of those specimens (point #3b in Figure 4.7), some are further dried at room temperature until the moisture content is equilibrated.
- Shrinkage process #4: Some specimens (point #4 in Figure 4.7) are allowed to dry in the dessicator container that has the RH of 99.0%. The shrinkage test is stopped once the reduction in moisture content and bulk volume are insignificant.

In the end, duplicate specimens are produced at similar moisture contents to be carried out for the free swell tests as explained in the next section.

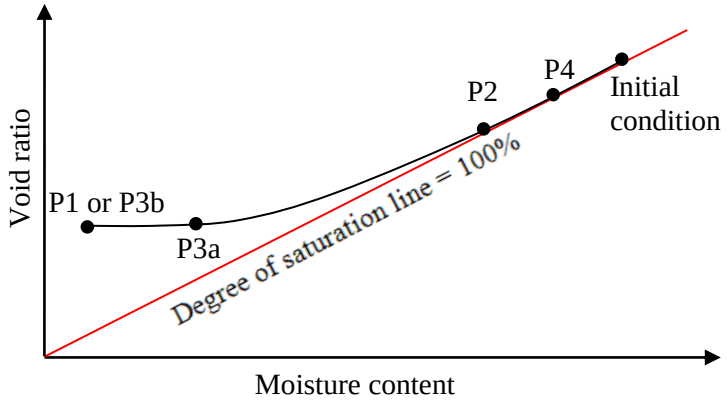

Figure 4.7. Conceptual illustration of the shrinkage processes.

4.5 Free Swelling Test

Since the deformation phenomenon of the soil is always of a three dimensional nature, the objective of this test is to periodically monitor the behavior of the swelling deformation as the unconstraint specimens are permitted to swell in all directions when subjected to both different specified wetting rates and hygroscopical wetting.

4.5.1 Experimental Equipment and Procedure

This is a straightforward test and yet, essential to quantitatively understand what factors will have major influences on the swelling deformability of the particular expansive soil used in this program. The selection of wetting rates (less than or equal to 1.0 gm/day) are based on the ability of the specimen to absorb additional water. The wetting rate beyond 1.0 gm/day requires a period more than one day for the specimen to absorb water and equilibrate its moisture content. However, the measurements of volume change during the wetting process (by using the same digital camera setup as in Section

4.1.1) are taken before adding the new amount of water (by using a plastic syringe) in order to allow the moisture content to equilibrate.

The free swelling tests are performed according to the following scheme:

- Wetting process #1: Some specimens are tested directly at their initial states by imposing different wetting rates of 0.2 gm/d, 0.5 gm/d, and 1.0 gm/d. It is found that the water should be added gradually during a day because of the very low permeability of the specimens relative to the specified wetting rates mentioned above.
- Wetting process #2: Some of the specimens that are dried at room temperature and the humidity room, are rewetted by increasing their moisture content hygroscopically in the desiccator until the equilibrium state is reached. Out of those specimens, some are further rewetted by applying similar wetting rates as in the wetting process #1.
- Wetting process #3: Some of the specimens that are dried at room temperature, are rewetted by increasing their moisture content hygroscopically in the humidity room until the equilibrium state is reached. Out of those specimens, some are further rewetted by applying similar wetting rates as in the wetting process #1.
- Approach #4: Some of the specimens that are dried in desiccator, are rewetted by applying similar wetting rates as in the wetting process #1.

4.6 Soil Suction Measurements

Having prepared the specimens being tested as explained in Section 4.4 and Section 4.5, the soil suction measurements at the end of each test are determined by using the chilled-mirror dew point meter device (WP4-T) and a tensiometer sensor. The results

of these tests will describe the correlation of soil suction variation with the mechanism of swelling behavior, which is the main objective of these tests.

4.6.1 Chilled – Mirror Dew Point Meter Device

Chilled-mirror dew point meter is becoming a common technique used in agricultural science. It is based on measuring the relative humidity by determining the dew point for the air in a closed chamber that has equilibrated with water potential of the specimen. Figure 4.8 shows the WP4-T model of chilled-mirror dew point device, which is manufactured by Decagon Devices. This device was connected to a personal computer where elapsed time, soil suction and temperature measurements were recorded.

Figure 4.8. The chilled-mirror dew point device model WP4-T.

4.6.1.1 Principles of Chilled-Mirror Dew Point Technique

Once the condensation is created by the chilled-mirror in the closed chamber, the dew point sensor starts measuring the dew point temperature of the air in the closed chamber. At this moment, the water vapor in the closed chamber is considered as

saturated vapor pressure. Then, the infrared thermometer measures the temperature of the sample. It is essential that the sample and closed chamber temperatures be at equilibrium (the fan in WP4-T accelerates the equilibration process). At this point the WP4-T equilibrates the liquid phase of pore water with the water vapor phase of the closed chamber such that the vapor pressure of the headspace in the closed chamber is equal to the partial pressure of the pore water vapor of the sample. Therefore, the RH can be measured in 13 to 15 minutes and from it, the total suction under isothermal condition can be computed by using the Kelvin's equation.

4.6.1.2 Experimental Procedure and Specimen Preparation

4.6.1.2.1 Experimental Procedure

The experimental procedure is described in the Advanced Terra Testing (ATT) manual (Appendix-D). The ATT is a company (performs soil, rock, and geosynthetic tests) where the chilled-mirror dew point tests were performed. The WP4-T is the temperature sensitive device and any temperature fluctuation may result in inaccurate total suction measurements. In addition to placing WP4-T in fairly constant temperature room, some preliminary preparations were performed prior to testing, as explained in the following subsection.

4.6.1.2.3 Specimen Preparation

Figure 4.9 shows stainless steel specimen cups that have a size of inside diameter of approximately 37 mm and inside depth of approximately 10 mm. The restriction of using some of the swollen specimens that have bigger sizes relative to the size of the steel cup and the chamber door requires the specimens to be trimmed. It is very important to

assure that the heights of all the specimens are somewhat less than 10.0 mm for moisture equilibrium purposes. Moreover, it is more critical to avoid the direct contact between the specimen and the chilled mirror in order to protect the device. It should be noted that after each test, the trimmed specimens are kept with their remnants in plastic containers for measuring the final moisture contents.

The purpose of using the WP4-T device is to determine the moderate to high range of total suction values and the corresponding moisture contents. The observations regarding the WP4-T limitations to measure total suction at very high moisture content in this study, is already confirmed by Leong, et al (2003), and Baille, et al (2010). Therefore, the tensiometer device is used to cover the range of very low soil suction values of specimens whose moisture contents are relatively high.

4.6.2 Tensiometer Sensor

The objective of using the tensiometer sensor (model T5 obtained from UMS) is to measure the matric suction in the wet range between saturation to 100 kPa of matric suction.

4.6.2.1 Experimental Equipment and Procedure

The schematic setup used for measuring the matric suction of the specimen is shown in Figure 4.9. The specimens at very low suction have a soft to gel-like texture that facilitates the insertion of the tensiometer. The stand is used to support the tensiometer to keep it in place during the test. Once the steady state of the suction records (obtained by personal computer) is reached (where the increase in suction records is stabilized), the tensiometer is removed, and the porous ceramic tip is cleaned to be

ready for the next test. The average value of matric suction records at the steady state is then, representing the soil matric suction of the specimen.

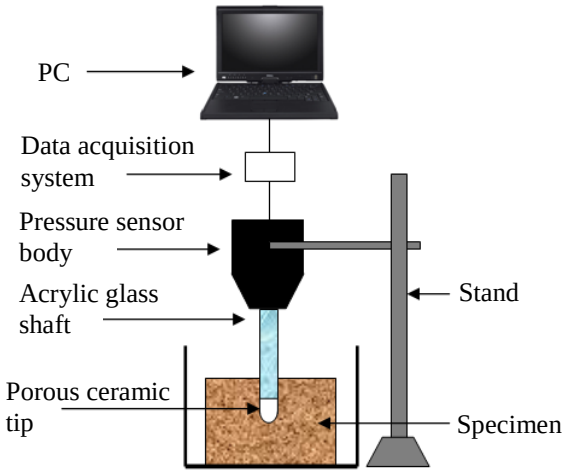

Figure 4.9. Schematic setup used for measuring the soil matric suction by using tensiometer sensor.

4.7 Constant Volume Oedometer Test and One dimensional Swelling Test

Several methodologies were proposed for predicting the swelling pressure of expansive soil (referred to Shuai, 1996) and the best practical ones that fit the testing program herein are the constant volume oedometer test (CVOT) and the one dimensional swelling test (1DST).

4.7.1 Specimen Preparation

The specimen preparation is the same as explained in Section 4.3, but the specimens are cut slightly bigger than the inner diameter of a rigid oedemeter ring (approximately 63 mm) by using a metal cutting tool. The specimens are then dried unrestrictedly in the humidity room to several targeted moisture contents and stored in plastic bags.

4.7.2 The CVOT

The CVOT is commonly used to predict the swelling pressure of a specimen where its volume change is completely restricted during the water uptake. In order to do this, the metal oedometer ring together with a load frame is used as described in the following subsection.

4.7.2.1 Experimental Equipment and Procedure

Figure 4.10 shows the schematic assembly of the setup that consists of: a conventional triaxial acrylic cell, a triaxial cell base pedestal with a fixed porous stone, a stainless steel oedometer ring, a top stainless steel platen with embedded porous stone, a loading frame with a load cell, water reservoir, a personal computer with a data acquisition system, a top cap, a loading ram, tie rods, and two filter papers.

When the desired reduced moisture content is attained, the specimen is cut by a cylindrical cutting tool that has the same inner diameter of the oedometer ring. Next, the specimen is inserted into the oedometer ring and the specimen surfaces are slightly trimmed. Then, the weight of the specimen and total volume are measured and the specimen is sandwiched with filter papers. Once the entire assembly of the triaxial cell is placed on the base plate, a constant setting load of 0.15 kN is applied to provide a good contact between the top platen and the top surface of the specimen. At this point, the position of the apparatus is fixed and the triaxial cell is filled with water. In order to decrease the test duration, the specimen is permitted to absorb the water from top and bottom.

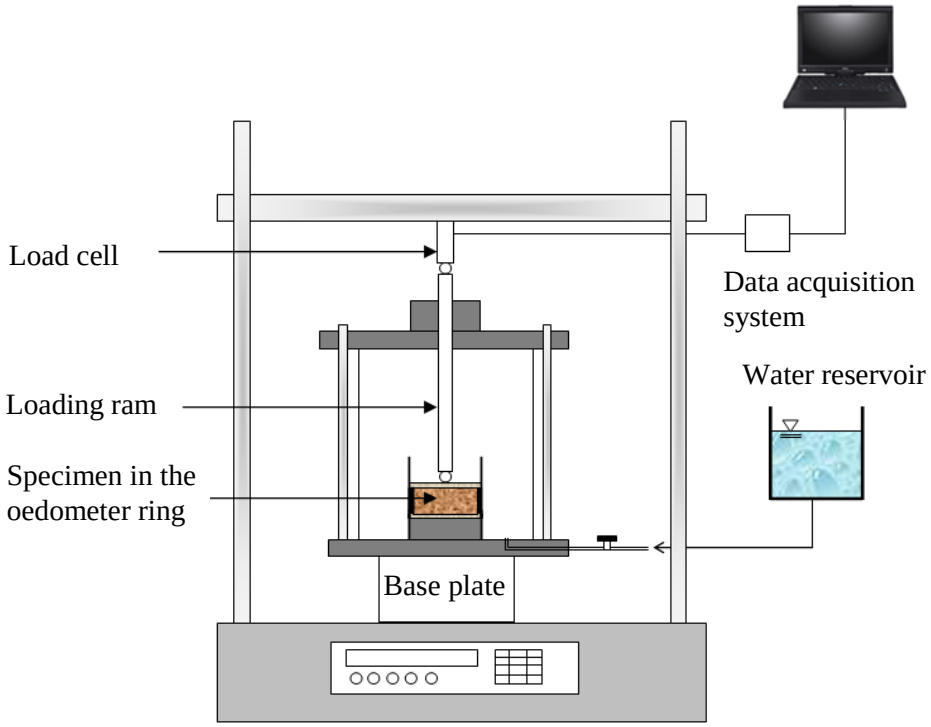

Figure 4.10. Schematic illustration of the CVOT setup.

After the steady state of the swelling pressure is reached, the base plate is slowly lowered (by using the speed of 0.1 mm/min) until the swelling pressure is in equivalent to the setting load. If the swelling pressure begins to regenerate up to the steady state, the specimen is once more unloaded back to the setting load value. This procedure may take several stages until the regenerated swelling pressure is minimized. Afterward, the specimen is completely unloaded and quickly placed into another testing setup to perform the 1DST.

4.7.3 The 1DST

The objective of this test is to investigate the additional axial swelling deformation for the specimens under nominal pressure of approximately 5 kPa. This test is set immediately after the accomplishment of the CVOT.

4.7.3.1 Experimental Equipment and Procedure

The experimental setup in this test is similar to the previous test as shown in Subsection 4.7.2.1. An additional LVDT system is installed to measure the axial swelling as schematically shown in Figure 4.11. The instrumentation of electro-pneumatic regulator and a diaphragm air cylinder are not utilized in this study and only the mentioned nominal pressure is regulated during the 1DST.

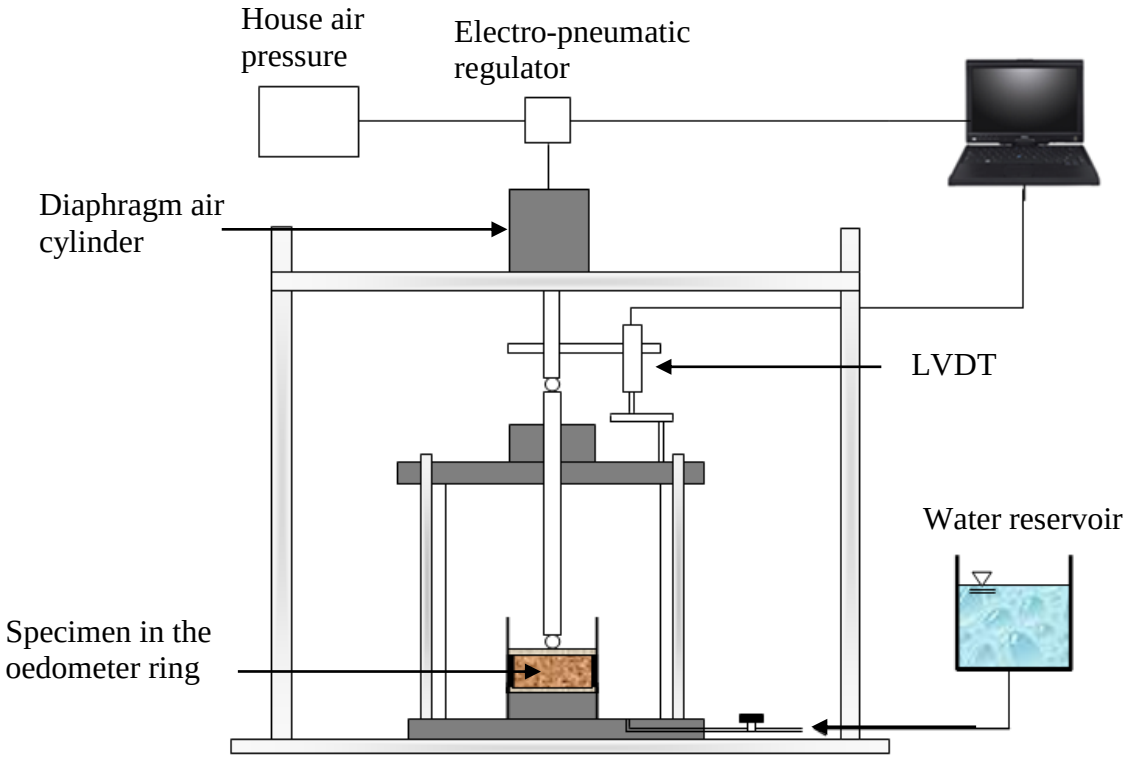

Figure 4.11. Schematic illustration of the 1DST setup.

The axial swelling deformation is ceased when the equilibrium state of the axial swelling deformation as a function of time is reached. The maximum value of axial swelling deformation will be used to determine the final void ratio of the swollen specimen.

4.8 Observations and Remarks.

Some observations and remarks are provided for some of the tests that are performed in this research:

- After preparing the specimens for chilled-mirror dew point test, change of moisture contents of the specimens were observed because the specimens are exposed to the air while quickly trimmed. However, the difference between the targeted moisture contents and the moisture contents after trimming is minimal and thus, assumed to be negligible.
- The shrinkage deformations during the free swelling test are observed to be isotropic. Therefore, the geometry of the specimen volume is always cylindrical.
- The non-uniform volume changes throughout some of the specimens during the process of free swell test are observed. This problem causes the volume of the specimen to have a truncated cone geometry as illustrated in Figure 4.12 (the upper portion has absorbed much more of the added water than the lower portion). Several diameters are measured from top to bottom of the specimen and their averaged value (d_{avg}) is used for calculating the volume of cylinder. Accordingly, the maximum error of diameter measurements is approximately ± 4 pixels (or ± 0.22 mm) which corresponds to percentage error of ± 0.17%.

Figure 4.12. An exaggerated figure of a truncated cone specimen showing the points where the volume of the specimen is assumed cylindrical.

CHAPTER 5

RESULTS AND OBSERVATIONS

5.1 Introduction

An overview of the experimental results is presented in this chapter. A summary of the specimens' preparation is provided in the first section that presents the initial conditions of the specimens (i.e., initial moisture content and initial void ratio) in order to establish a baseline for the subsequent experiments. The following section describes the free swelling test results and includes information about the time rate of water absorption and the corresponding volume change. Those results will give qualitative sense of the effect of the water infiltration rate on the swelling deformation of the selected expansive soil. Subsequently, the soil suction results are presented and correlated with those from the free swelling tests. The previous section offers a clear picture of how the zone of interest (i. e., the determination of the range of moisture content and the associated range of soil suction) is selected to perform the constant volume test and the one-dimensional free swelling test under oedometric conditions.

In that regard, the results of the constant volume oedometer tests are presented in the following section, in addition to the results of unloading stages that are performed as functions of time. Then, the results of one-dimensional swelling tests are provided to investigate any additional swelling potential under a very low soil suction range and

nominal applied load. The final phase of experimental work is the submergence of the unrestraint specimen take from the one-dimensional free swelling test to further examine, any additional potential for water absorption.

Brief observations and interpretations of the aforementioned test results are included in each section of this chapter.

5.2 A Summary of the Specimens' Preparation

Sufficient number of specimens was produced as explained in sections 4.3 and 4.4. The summary of the preparation procedure for the free swelling test is included in Table 5.3. The categorization of the specimens is based on the performance of the shrinkage processes as described in section 4.4.2. For greater simplification, the shrinkage processes were designated based on the shrinkage history as formulated in Tables 5.1 and 5.2 and illustrated in Figure 5.1.

Letter	Description
A	The specimen at its initial condition.
B	The specimen has lost approximately 2.0 gm of water in the humidity room at RH of 91.0 % to 93.0 %.
C	The specimen is permitted to dry in the humidity room at RH of 91.0 % to 93.0 %
D	The specimen is permitted to dry at the room temperature (RH = 30 %).
E	The specimen is permitted to dry in the desiccators under RH = 99.0 %.

Table 5.1. Legend key showing the description of shrinkage processes.

Shrinkage process	Shrinkage history
SH1	AB
SH2	ACD
SH3	AE
SH4	AD
SH5	AC

Table 5.2. The expressions of the shrinkage processes according to the shrinkage history.

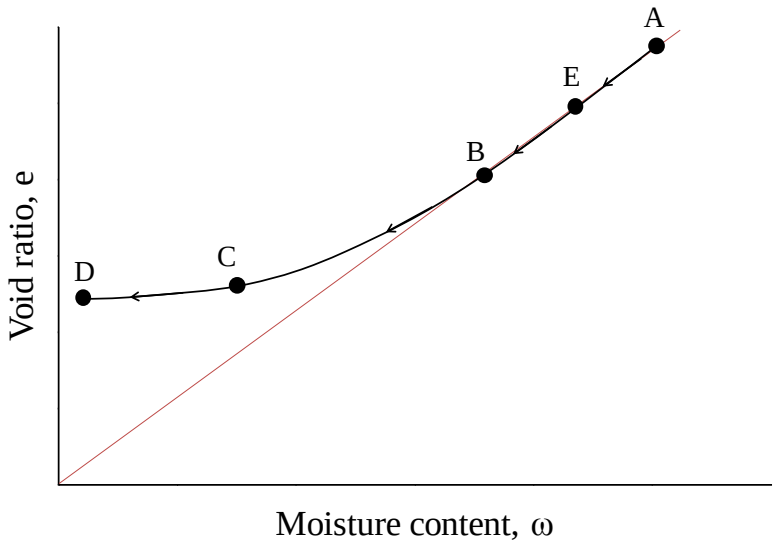

Figure 5.1. Graphical representation of the legend key used to describe the shrinkage processes.

Specimen #	Shrinkage Process	Initial moisture content, ω_i (%)	Initial void ratio, e
1	NO	48.47	1.23
2		52.19	1.32
3		47.06	1.19
4		43.79	1.11
5		43.71	1.11
6		45.12	1.14
7		49.77	1.26
8		49.53	1.25
9		53.49	1.35
10		43.77	1.11
11		40.78	1.03
12	SH1	44.73	1.13
13		47.74	1.21
14		49.69	1.26
15		49.59	1.25
16		46.03	1.16
17		48.28	1.22
18	SH2	39.50	0.99
19		41.77	1.06
20		42.71	1.08
21		41.28	1.04
22		46.92	1.19
23	SH3	45.79	1.16
24		44.68	1.13
25		49.01	1.24
26		50.55	1.28
27		52.55	1.33
28		54.39	1.38
29		49.73	1.26
30	SH4	48.10	1.22
31		47.24	1.19
32		48.91	1.24
33		54.70	1.38
34		47.00	1.19
35		54.95	1.39
36		44.95	1.14
37		50.85	1.29
38		46.63	1.17
39		47.28	1.19
40		45.06	1.14
41		49.89	1.26
42	SH5	43.92	1.11
43		51.11	1.29
44		47.53	1.21
45		49.72	1.26
46		52.55	1.33
47		45.15	1.14

Table 5.3. The summary of the specimens' preparation for the free swelling test.

If the possibility of crack development was observed at any moment during the shrinkage process, the plastic container was closed and the distribution of the moisture through the specimen pores was brought into equilibrium. The equilibration period was arbitrary but lasted for a few hours. The drying processes of each category in terms of loss (in negative values) of moisture and reduction (in negative values) of volume change are illustrated in Figures 5.2 to 5.6. The specimens listed in the category with "no" application of shrinkage process are not plotted. The minor loss of water and the volume change for those specimens are presented in the next section. In Figure 5.2 (a), the SH1 process of the specimens of #12 to #16 began approximately 0.71 days after the sampling phase (see section 4.4). Then, it was stopped for approximately one day. The stoppage of the drying process was meant to allow for preliminary examination of any possible cracking due to the rate of desiccation in the humidity room. The additional specimen (#17) was subjected to the drying process in the same manner as the previous specimens approximately 14 days after it was initially prepared. Although it was fairly small, the 0.25 gm loss of water per 14 days indicated that the plastic container was not permanently preventing the specimens from losing some of their moisture content. However, the majority of the reduction in volume change is demonstrated by the steep curves followed by the flattened curves toward the targeted reduction in volume (e.g., see Figure 5.2 (b)). Regardless of the inconsistency in producing identical initial conditions of the specimens, the tendency of rates of desiccation was similar, which also highlighted the reasonably homogeneous production of the specimens.

The final degree of saturation values for the specimens of #12, #13, #14, #15, #16, and #17 were 97.69%, 91.72%, 91.21%, 91.49%, 97.14%, and 95.69%, respectively.

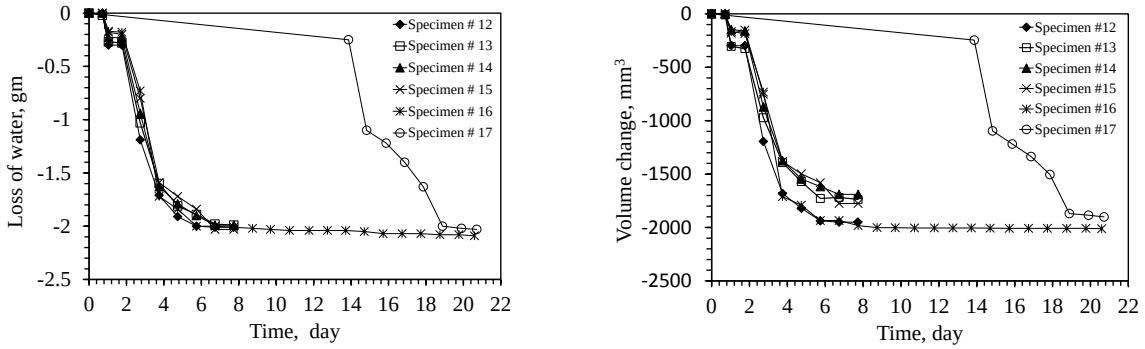

(a) (b)

Figure 5.2. Shrinkage processes of category SH1 in terms of (a) loss of water, and (b) reduction in the volume change of the specimens.

It can be observed from Figure 5.3 that the shrinkage limits for all of the specimens subjected to the SH2 process were reached before permitting the specimens to continue to dry at room temperature (at approximately 10.71 days).

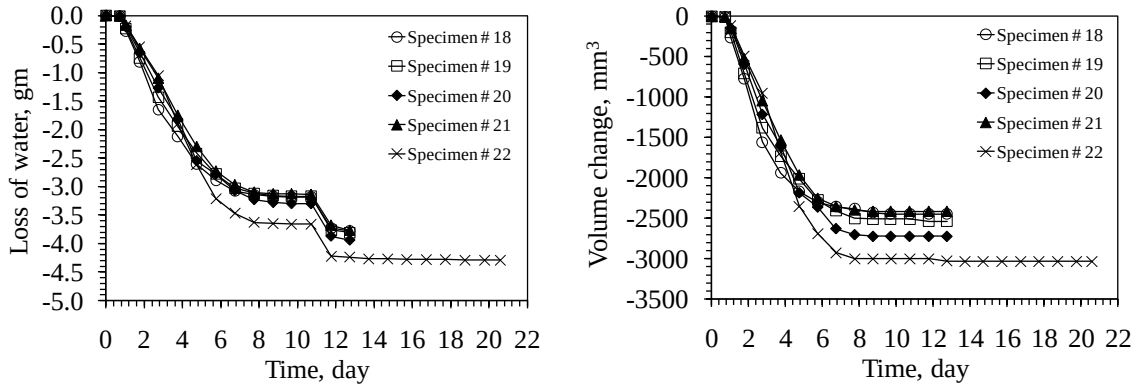

(a) (b)

Figure 5.3. Shrinkage processes of category SH2 in terms of (a) loss of water, and (b) reduction in the volume change of the specimens.

The final degree of saturation for the specimens of # 18, # 19, # 20, # 21, and # 22 are 4.82 %, 20.57 %, 19.83 %, 21.64 %, and 30.18 %, respectively. All the specimens in this group were subjected to the same period of desiccation (approximately 13 days) except for specimen #22 where its desiccation process was stopped in order to measure its soil

suction as explained later in this chapter. But depending on the initial conditions (Table 5.3) and under the same desiccation rate, specimen #18 showed the lowest degree of saturation while specimen #22 showed the highest degree of saturation. In addition, the sensitivity of the degree of saturation to the measurements of change of volumes (i.e., volume of voids and water) is critical.

It is demonstrated in Figure 5.4 that all of the specimens subjected to the SH3 process were fully saturated because of the fact that the reduction of water volume was equivalent to the reduction in the volume change of the specimen; therefore, the degree of saturation was unity (S=100%).

Given that the trend of the SH4 process was similar for all of the specimens in this category, an example of this tendency is shown in Figure 5.5. Appendix-E consists a complete illustration of the SH4 process. The final degree of saturation values of the specimens are tabulated in Table 5.4.

Specimen #	30	31	32	33	34	35	36	37	38	39	40	41
Degree of Saturation (%)	29.2	24.3	24.1	16.6	31.1	30.2	22.8	30.5	20.0	36.4	21.9	30.4

Table 5.4. The final degree of saturation values for specimens subjected to SH4 process.

In Figure 5.6, the application of the SH5 process of the designated specimens is demonstrated. The final degree of saturation values for the specimens of # 42, # 43, # 44, # 45, # 46, and # 47 were 51.38%, 65.18 %, 63.71 %, 62.09 %, 68.67 %, and 62.53 %, respectively. The final shrinkage conditions of the specimens are graphically presented in

Figure 5.7 in a form of scatter data points of moisture content and corresponding void ratio.

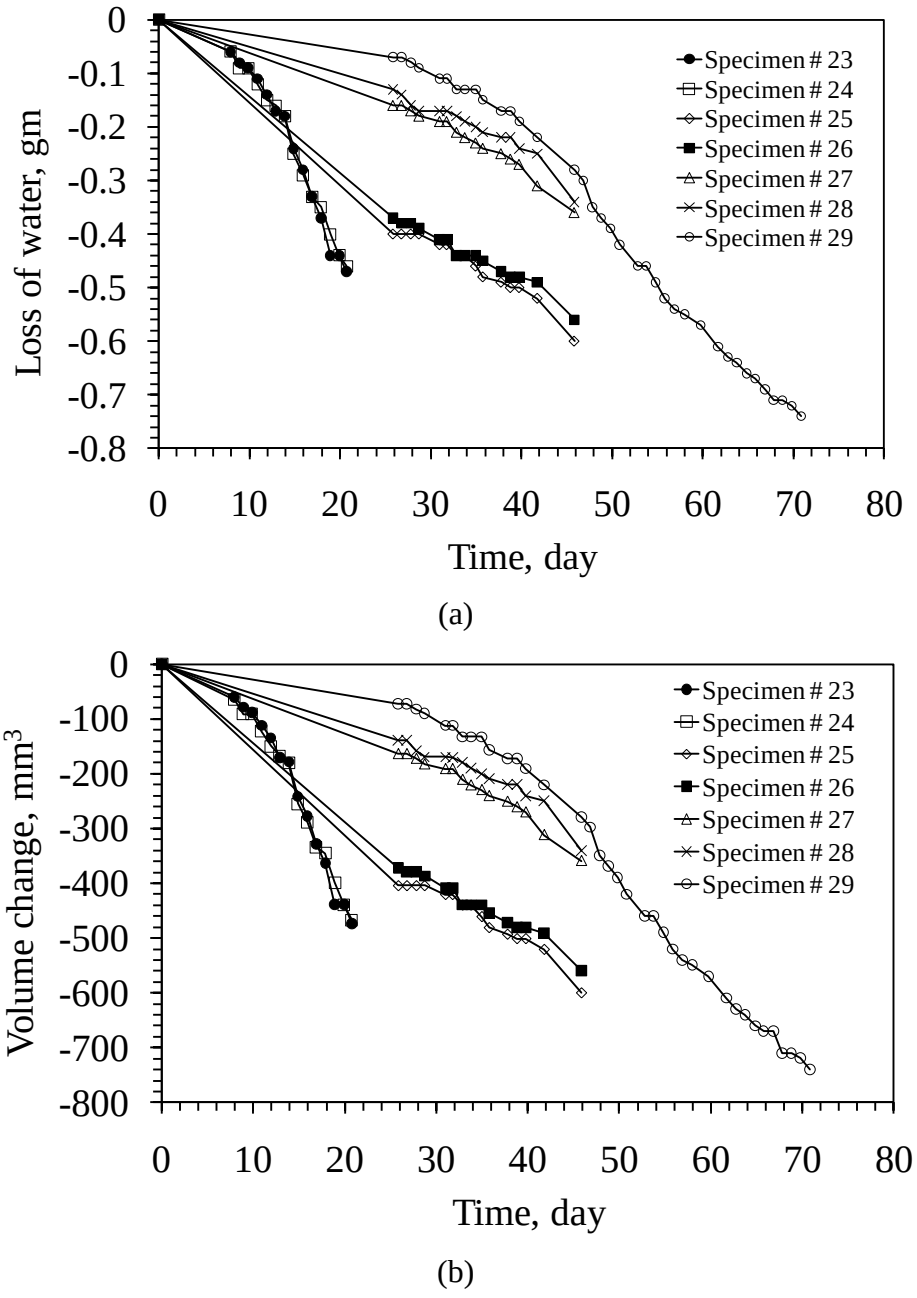

Figure 5.4. Shrinkage processes of category SH3 in terms of (a) loss of water, and (b) reduction in the volume change of the specimens.

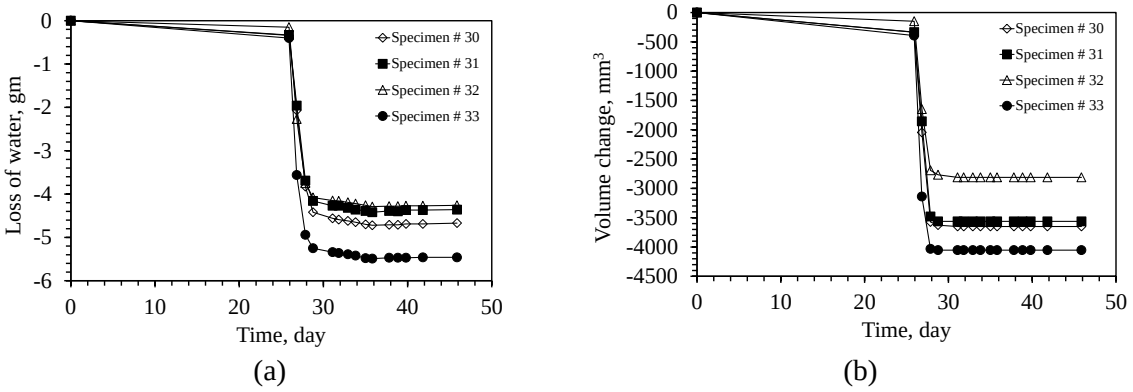

Figure 5.5. Shrinkage processes of category SH4 in terms of (a) loss of water, and (b) reduction in the volume change of the specimens.

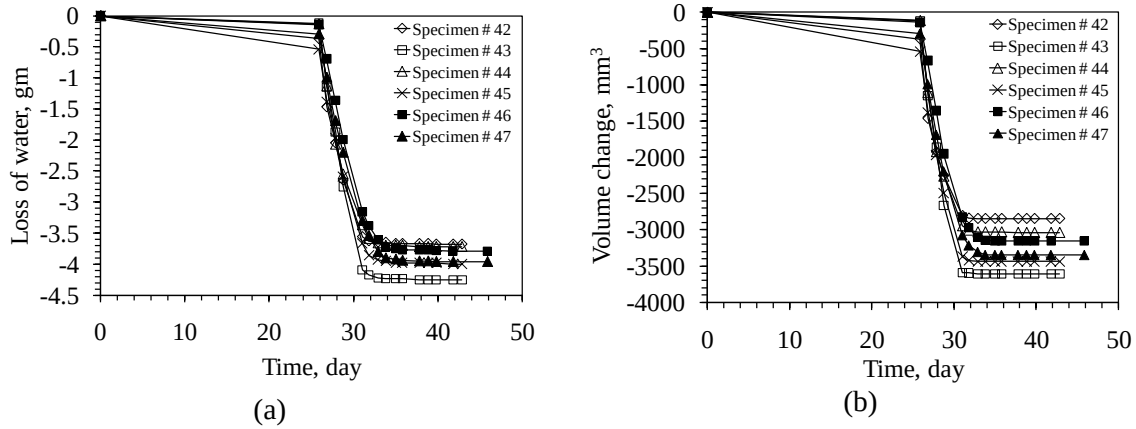

Figure 5.6. Shrinkage processes of category SH5 in terms of (a) loss of water, and (b) reduction in the volume change of the specimens.

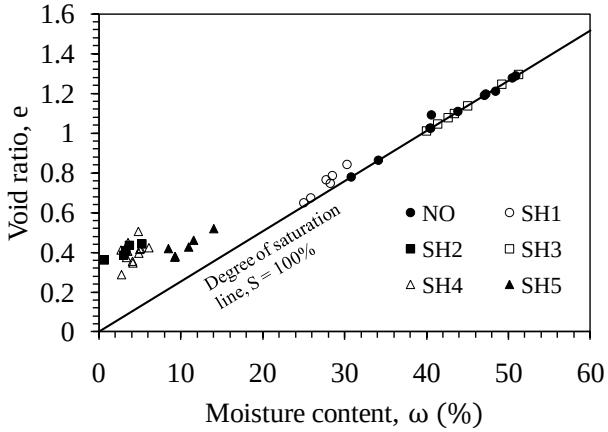

Figure 5.7. A graphical representation of the final shrinkage conditions of the specimens subjected to different shrinkage processes.

As listed in Table 5.5, the specimens were prepared for the constant volume swelling test and the one-dimensional swelling test. The shrinkage process for those specimens was not examined, but the initial void ratios and moisture contents were carefully measured and considered to be the original data points before starting the swelling tests.

Specimen #	Initial moisture content, ω_i (%)	Initial void ratio, e	Initial degree of saturation, S_i (%)	Shrinkage process
SP1	40.35	1.03	98.9	NO
SP2	33.47	0.86	98.7	SH5
SP3	28.43	0.74	97.0	SH5
SP4	24.44	0.67	92.2	SH5
SP5	22.32	0.65	86.6	SH5
SP6	20.99	0.63	83.9	SH5

Table 5.5. The initial conditions of the specimens prepared for the CVOD and the 1DST.

5.3 Free Swelling Test Results

Prior to studying the influence of the wetting rate on free swelling deformation, three wetting rates were selected to be imposed on the unconfined specimens. The wetting rates were 0.2 gm/d 0.5 gm/d and 1.0 gm/d. Moreover, some specimens were also rewetted by hygroscopically increasing their moisture content as explained in section 4.5. Therefore, the rewetting histories and the swelling processes are described in the same manner as in Section 5.2 (Tables 5.6, 5.7, and 5.8).

Letter	Description
F	Rewetting by liquid water (0.2 gm/d)
G	Rewetting by liquid water (0.5 gm/d)
H	Rewetting by liquid water (1.0 gm/d)
I	Rewetting in the humidity room (RH = 91.0 % to 93.0 %)
J	Rewetting in the desiccator container (RH = 99.0 %)
K	Fully submerged

Table 5.6. Legend key showing the description of swelling processes.

Swelling process	Rewetting history
SW1	F
SW2	G
SW3	H
SW4	I
SW5	J
SW6	K
SW7	JG
SW8	JH
SW9	IG
SW10	IH

Table 5.7. The expressions of the swelling processes according to the rewetting history.

A conceptual illustration of the histories of the swelling processes is shown in Figure 5.8.

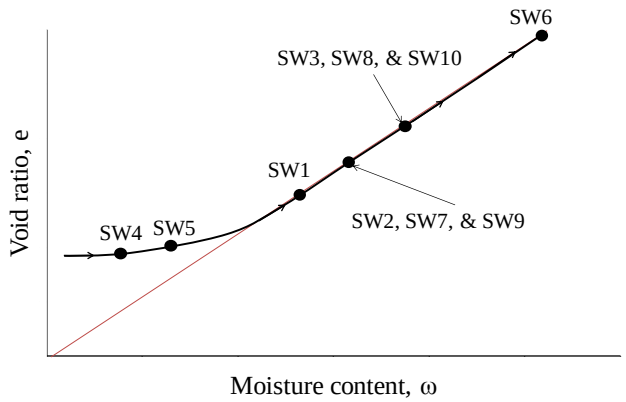

Figure 5.8. A conceptual illustration of the histories of the swelling processes during the free swelling tests.

Specimen #	Shrinkage Process	Swelling Process
1	NO	SW1
2		SW2
3		SW3
4		SW6
5		NO
6		SW2
7		SW2
8		SW3
9		SW3
10		SW6
11		NO
12	SH1	SW1
13		SW6
14		SW3
15		SW2
16		NO
17		NO
18	SH2	SW4
19		SW5
20		SW4
21		SW5
22		NO
23	SH3	NO
24		NO
25		SW2
26		SW2
27		SW3
28		SW3
29		NO
30	SH4	SW2
31		SW2
32		SW3
33		SW3
34		SW9
35		SW9
36		SW10
37		SW10
38		SW7
39		SW7
40		SW8
41		SW8
42	SH5	SW7
43		SW7
44		SW8
45		SW8
46		SW2
47		SW3

Table 5.8. The history of the swelling process for each specimen.

After adding the specified amount of water, the specimens were sealed to preserve interior humidity and allow the moisture content to equilibrate for approximately one day. The images in Figure 5.9 illustrate the volume change characteristics of several selected specimens covering both the shrinkage and the swelling deformations. It is worth noting that towards the end of the rewetting process in the presence of free water around the specimen surface, the specimen particles started to disintegrate and cause soil clumps to fall off. This in turn, caused problems in measuring the volume change as shown in Figures 5.10 (b). The theoretical lines (dash lines) in this figure explain the inaccuracy in measuring the volume change towards the end of swelling process especially for the highest wetting rate. This discrepancy between the accurate and measured data produces maximum percentage errors of 20.33%, 13.85% and 6.17% in measuring the volume changes when using 1.0 gm/d, 0.5 gm/d and 0.2 gm/d wetting rates, respectively.

Once again, the swelling process was ceased (between days 1 and 2) for all of the specimens in the early phase of the tests in order to investigate any possible cracking induced by swelling deformation. Specimen #4 was directly submerged in water; therefore, no cumulative water mass or volume change during the swelling process was measured. Figure 5.11 shows another representation of both shrinkage and swelling processes. The rest of these results are presented in Appendix-E. It can be demonstrated from both Figures 5.10 and 5.11 that regardless of the specified wetting rate for the free swelling tests, there was no drastic impact on the amount of absorbed pore water on the progression of free swelling deformation, which are indicated by more or less linearly proportional quantities. This observation strongly supported the insignificant influence of

the wetting rate on the progression of volumetric swelling as well as its independence from the initial moisture content of the specimen.

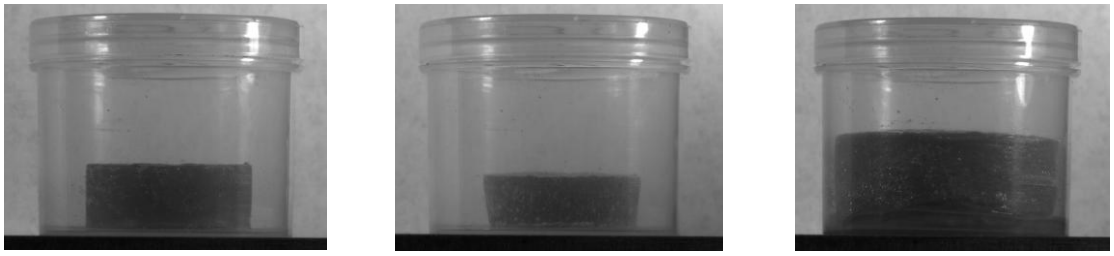

Initial condition | Final Shrinkage Process | Final Swelling Process

(a)

Initial Condition | Final Shrinkage Process | Final Swelling Process

(b)

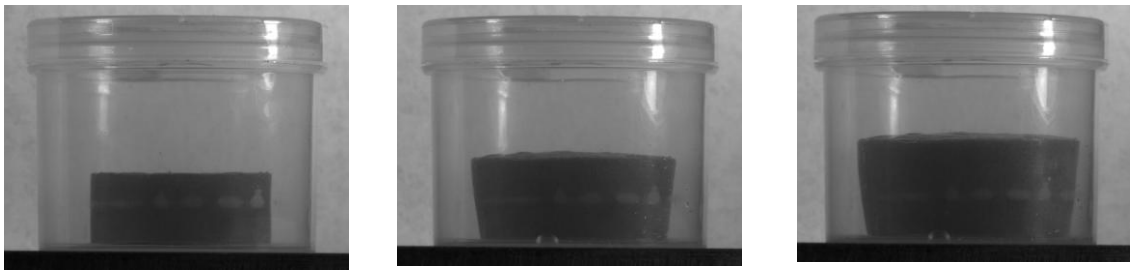

Initial Condition | After 12 Days of Swelling Process | Final Swelling Process

(c)

Figure 5.9. The selected images showing the deformation processes of (a) specimen #40, (b) specimen #47, and (c) specimen #6.

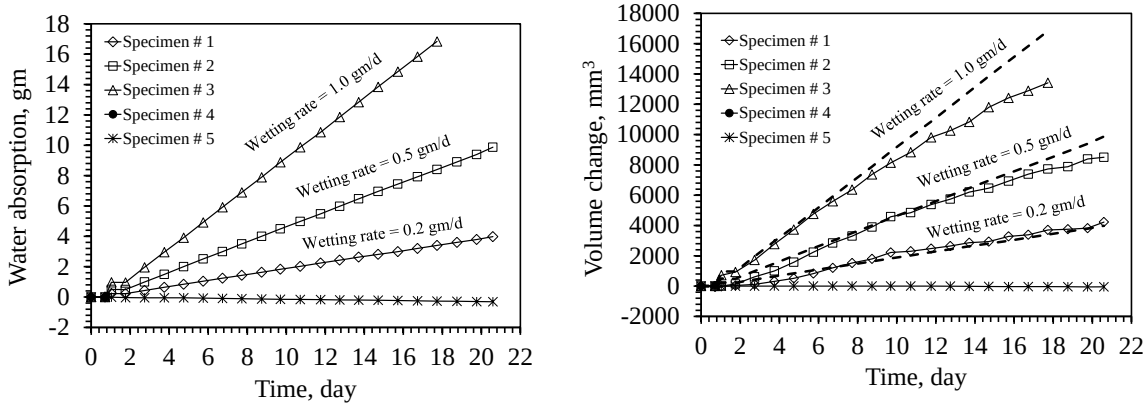

(a) (b)

Figure 5.10. Free swelling tests of the initially saturated specimens at different wetting rates showing; (a) the amount of absorbed water with time, and (b) the development of volume change with time.

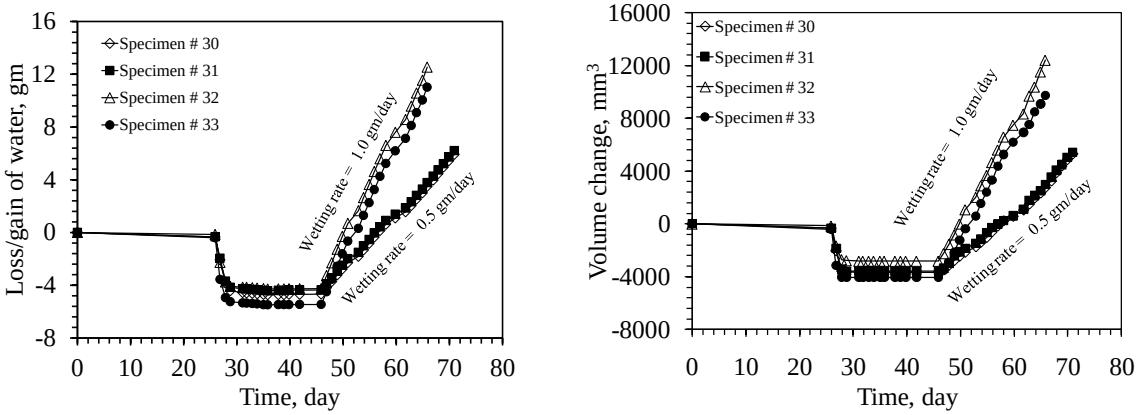

(a) (b)

Figure 5.11. Free swelling tests of the nearly dried specimens at different wetting rates showing; (a) the amount of absorbed water with time, and (b) the development of volume change with time.

The influence of wetting rate on volume changes is presented in Figure 5.12 for several specimens. While the wetting rates were substantially lower for the specimens subjected to hygroscopic moisture increase, relative to the ones wetted by liquid water, the void ratio increase was independent of the wetting rate as shown in Figure 5.12 (b).

For the hygroscopic wetting process, the average wetting rate for the duration of the test is used in this plot.

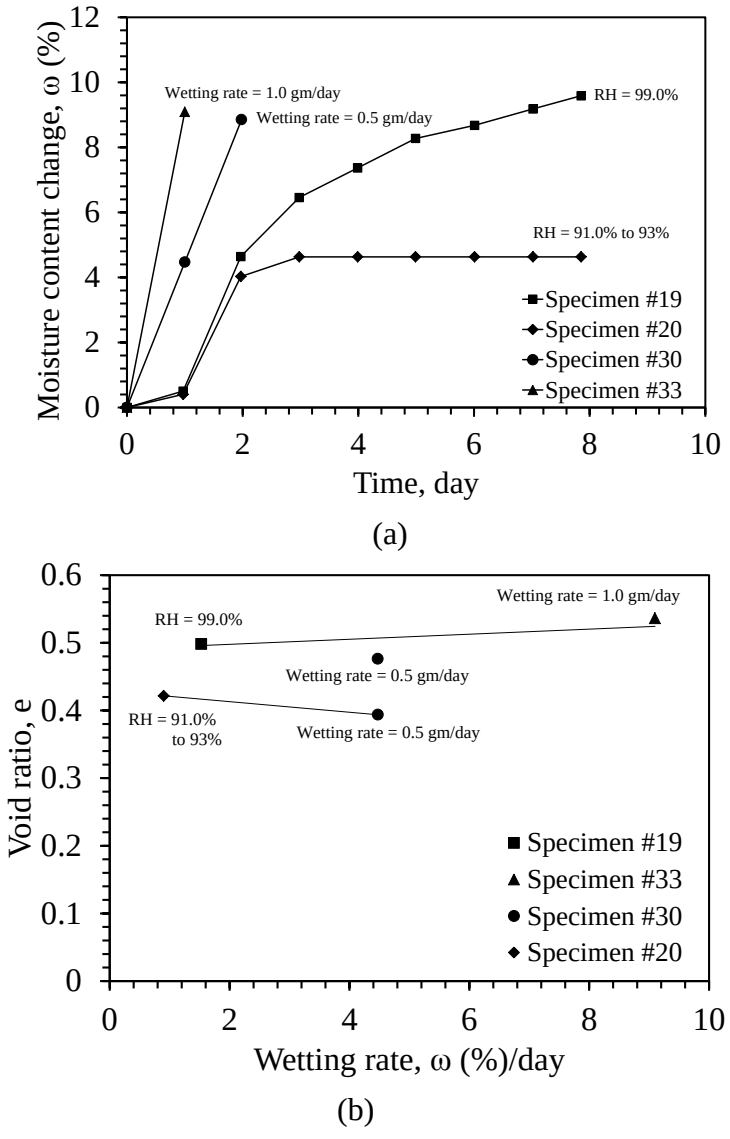

Figure 5.12. The influence of the wetting rates on the volume changes in terms of (a) moisture content change with time, and (b) void ratio with wetting rate.

The comparison between the initial and final moisture contents of the specimens is plotted in Figure 5.13. This comparison shows the achievement of the water storage capacity when the specimens were permitted to free swell.

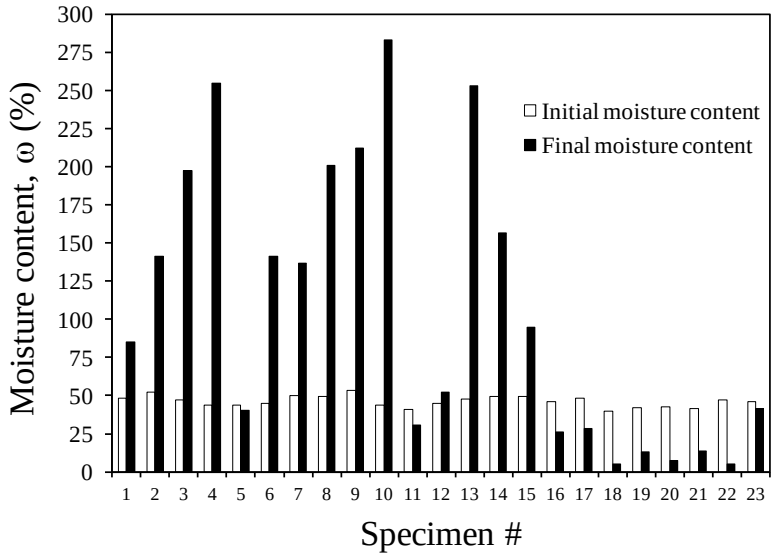

(a)

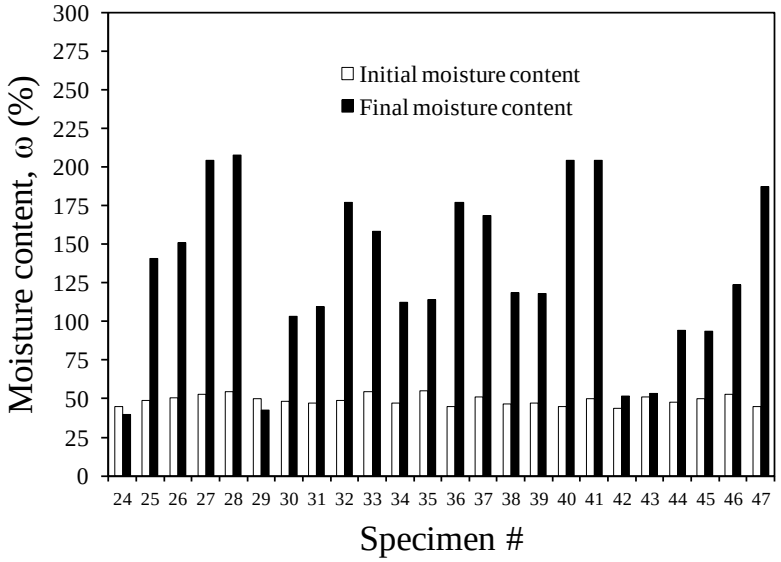

(b)

Figure 5.13. The comparison between initial and final moisture contents of (a) specimens #1 to #23, and (b) specimens #24 to #47.

5.4 Soil Suction Test Results

As described in section 4.6, the soil suction measurements, which ranged from moderate to high were conducted using the chilled mirror – dew point meter device. The low soil suction measurements were conducted using the tensiometer sensor. Those measurements were made at the final moisture contents of the specimens as illustrated in Figure 5.13. The data for both tests as a function of time were used to determine the soil suctions at equilibrium. Typically average values were collected from the measured soil suctions in the later stage of the tests. An example in Figure 5.14 shows the outputs of the chilled mirror – dew point meter device for high (142.75 MPa) and moderate (1.18 MPa) suctions. The soil suction is a direct measurement in MPa that represents the total suction of the specimen. An example in Figure 5.15 shows outputs of the tensiometer sensor for low matric suction (60.02 kPa) and very low matric suction (0.37 kPa). Appendix-E includes the other data from the soil suction measurements.

The plot of the tabulated values of soil suctions with respect to the final moisture contents (as shown in Table 5.9) is illustrated in Figure 5.16. The disadvantage of the chilled-mirror dew point device is its inability in measuring small total suctions below 100 kPa. Since most of the rewetted specimens by liquid water exhibited very high moisture contents, the total suctions obtained by the chilled-mirror dew point device were unreliable (0.1 kPa implies zero total suction in the logarithmic scale). The exception was specimens #18, #19, #20, and #21 in which the rewetting process was hygroscopically.

By including the results of the free swelling tests with those of the soil suction tests, it is generally possible to observe that the shrinkage deformation and soil suction increase as the moisture content of the specimen decreases. On the contrary, as the moisture

content of the specimen increases, swelling deformation increases whereas soil suction decreases. Moreover, the extensive deformability of the specimens is represented by the high moisture contents and low soil suction.

It is suggested, according to the preliminary information outlined from the previous tests, that the range of interest where the expansive soil in this research experiences significant deformability is under approximately 1000 kPa of soil suction. The soil suction results below 1000 kPa will be compared with the swelling pressure results as explained in Chapter 6.

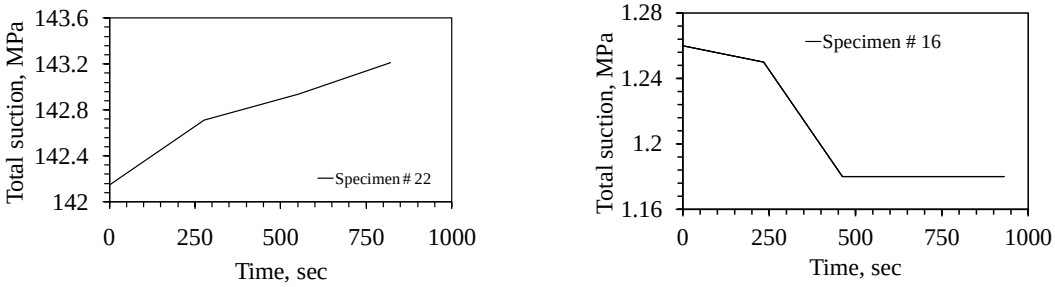

Figure 5.14. The outputs of the chilled-mirror dew point device for (a) high total suction and (b) moderate total suction.

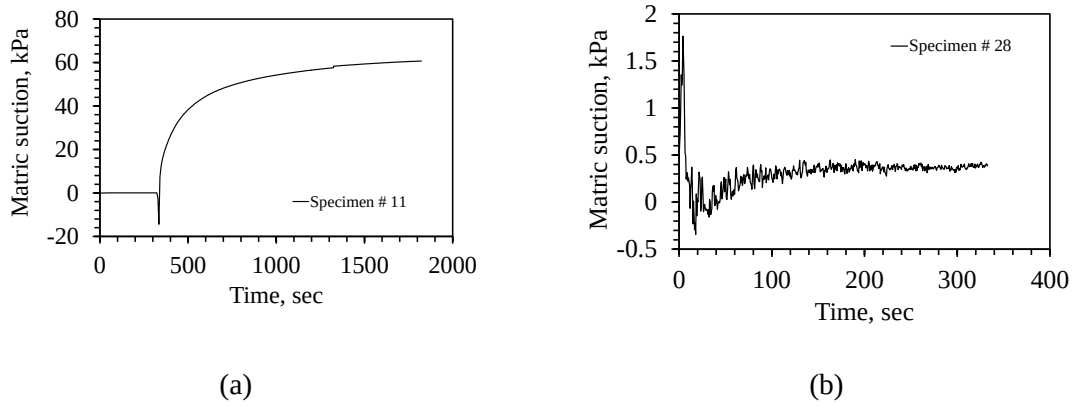

Figure 5.15. The outputs of the tensiometer sensor for (a) low matric suction and (b) very low matric suction.

Specimen #	Initial Moisture Content (%)	Final Moisture Content (%)	Soil Suction (kPa)	Remarks
1	48.47	85.15	0.0	total suction
2	52.20	141.31	0.0	total suction
3	47.06	197.42	0.0	total suction
4	43.79	254.80	130.0	Suspicious result
5	43.71	40.60	240.0	total suction
6	45.12	141.55	1.62	matric suction
7	49.77	136.65	1.22	matric suction
8	49.53	200.68	0.57	matric suction
9	53.49	212.53	0.79	matric suction
10	43.77	283.43	0.49	matric suction
11	40.78	30.77	60.02	matric suction
12	44.73	52.22	0.0	total suction
13	47.74	253.01	0.0	total suction
14	49.69	156.70	0.0	total suction
15	49.59	91.20	0.0	total suction
16	46.03	25.88	1180.0	total suction
17	48.28	28.24	493.3	total suction
18	39.50	5.31	25840.0	total suction
19	41.77	12.91	7210.0	total suction
20	42.71	7.66	28020.0	total suction
21	41.28	13.49	5700.0	total suction
22	46.92	5.27	142752.5	total suction
23	45.79	41.32	227.0	total suction
24	44.68	40.01	60.0	total suction
25	49.01	140.65	1.78	matric suction
26	50.55	151.15	1.36	matric suction
27	52.55	204.40	0.44	matric suction
28	54.39	207.86	0.37	matric suction
29	49.73	42.60	44.56	matric suction
30	48.10	103.27	4.03	matric suction
31	47.24	109.83	3.81	matric suction
32	48.91	176.97	1.01	matric suction
33	54.70	158.21	1.14	matric suction
34	47.00	112.40	2.99	matric suction
35	54.95	114.15	3.04	matric suction
36	44.95	177.14	0.53	matric suction
37	50.85	168.39	0.59	matric suction
38	46.43	118.80	2.9	matric suction
39	47.28	117.82	2.05	matric suction
40	45.06	204.09	0.59	matric suction
41	49.89	204.35	0.77	matric suction
42	43.92	51.71	29.74	matric suction
43	51.11	53.34	27.84	matric suction
44	47.53	94.39	11.48	matric suction
45	49.72	93.46	10.62	matric suction
46	52.55	123.89	3.13	matric suction
47	45.15	187.09	0.65	matric suction

Table 5.9. The soil suction results of the specimens with respect to their final moisture content.

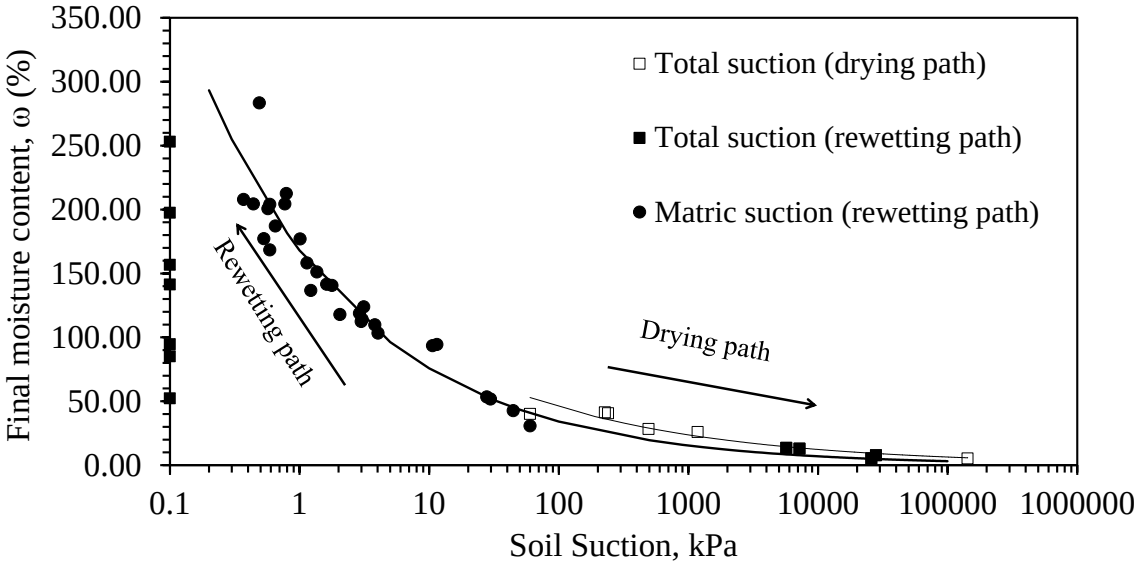

Figure 5.16. The constitutive relationship between soil suction and moisture content during the drying and rewetting processes of specimens under unconfined condition.

5.5 Constant Volume Oedometer Test (CVOT) Results

During the absorption process, the soil suction was reduced and the specimen had the tendency to swell in volume. As this volumetric swelling was prevented by the load frame, the constant setting pressure, and the rigid oedometer ring, the load cell measured pressure required to maintain the constant volume which is called the swelling pressure (p_s).

The data collected was the development of the p_s with time (Figure 5.17). When the p_s approached equilibrium state (approximately 95 kPa in Figure 5.17 (a)), the measured p_s records produced cyclic curves with fairly typical patterns. This cyclic trend was also observed in some of the other specimens tested in the same manner (see Appendix-E). As these pressure oscillation had a period of approximately 24 hours, it was concluded that they coincide with heating pattern in the lab. This prevented us from obtaining precise

determination of the p_s, but the test still produced consistent estimation of the released soil suction. Upon unloading, the specimen did not show a tendency of regenerating the p_s indicating that the soil suction was completely dissipated in the first stage.

Subsequent specimens continued to develop p_s upon unloading stages as shown in Figure 5.17 (b) for specimen #SP6. The unloading effects and the corresponding volume changes on the development of p_s will be discussed in a later section.

Figure 5.18 shows the records of the primary p_s of the specimens prepared at different initial moisture contents. It was observed that, a lower the initial moisture content was correlated with a higher primary p_s. Since the relationship between initial water content and p_s was found to be nonlinear, the power function in Figure 5.18 (b) was selected as the best fit function representing the experimental data points. The observed effect of initial moisture content on the development of the p_s is consistent with the past observations obtained by Kassiff and Ben Shalom (1971), and El-Sohby and El-Sayed (1981).

The time-rate of the swelling pressure developments can be used to determine the compressibility characteristics, such as the coefficient of volume compressibility, the hydraulic diffusivity coefficient and permeability coefficient (see Chapter 7).

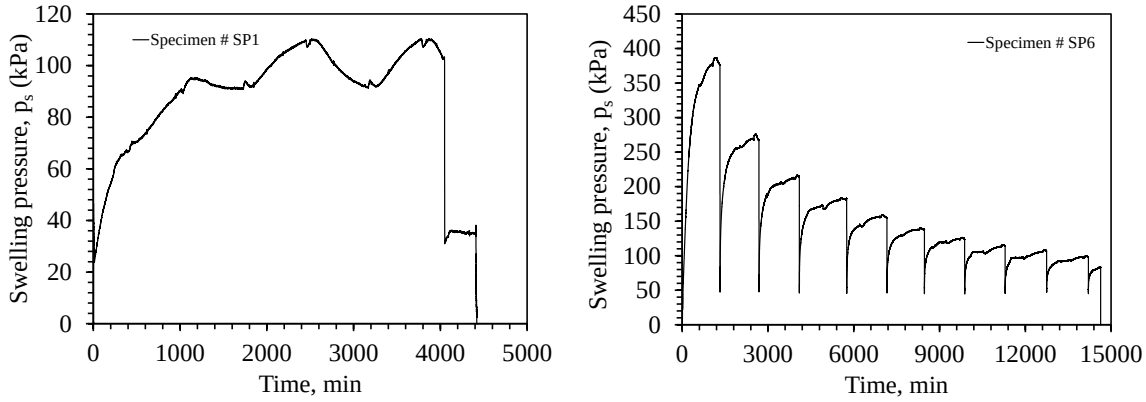

(a) (b)

Figure 5.17. The CVOT testing results of (a) the initially saturated specimen #SP1, and (b) the specimen #SP6 along with the successive unloading stages.

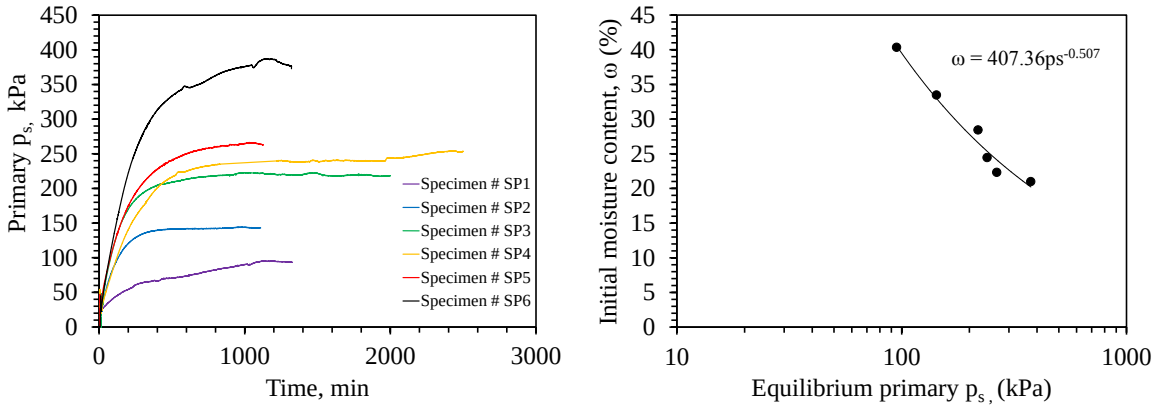

(a) (b)

Figure 5.18. The CVOT results showing (a) the primary swelling pressure developments at constant applied setting pressure, and (b) the equilibrium primary swelling pressure as a function of initial moisture content.

5.5.1 The influence of Unloading Stages on Soil Suction and Swelling Pressure

Upon the primary p_s was reached the specimen was unloaded to the original setting pressure. The required displacement during the unloading stage was measured as discussed earlier in Section 4.7.2.1. This displacement permitted the specimen to deform vertically and termed as allowable vertical deformation $d_{v(all.)}$ that was gradually

reduced the p_s in conjunction with gradual increase in soil suction (Figure 5.19). The regeneration of the p_s which corresponds to the reduction in soil suction was under constant volume (the $d_{v(all.)}$ was fixed). The overall process had led to reduced the potential of swelling because after each unloading stage all the variables ($d_{v(all.)}$, p_s, and soil suction) were monotonically reducing as they are converging to the initial surcharge pressure. This information will later on be used and combined with the other swelling test results to study the deformation and pressure characteristics of the selected expansive soil.

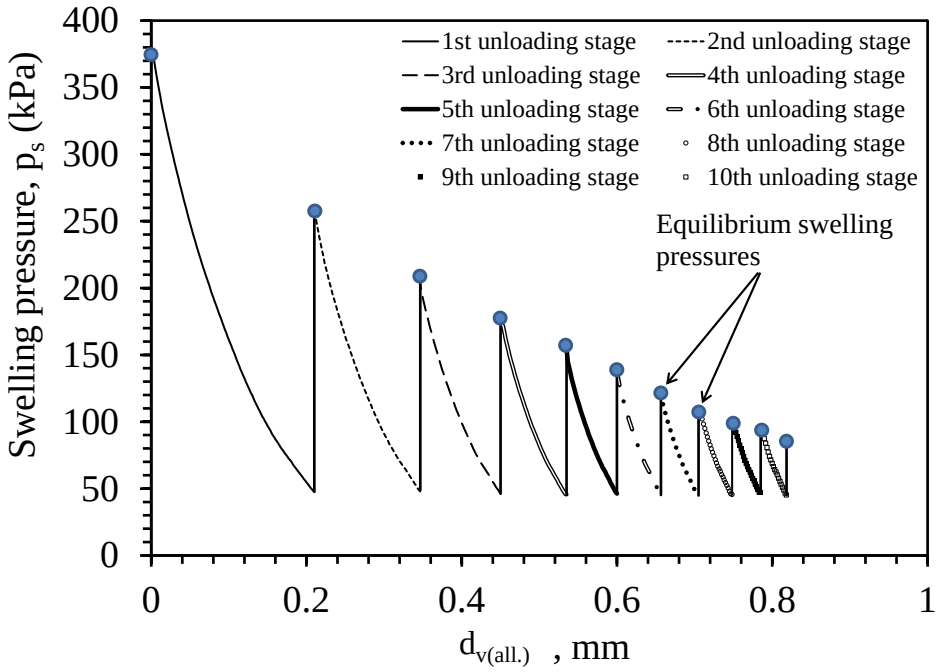

Figure 5.19. A representation of the equilibrium swelling pressure dissipation after each successive unloading stage for specimen #SP6.

5.6 One-dimensional Swelling Test (1DST) Results

As explained in section 4.7.3, the 1DST was immediately set after the CVOT. The axial swelling was monitored after applying the nominal pressure (5.0 kPa). As shown in Figure 5.20, the increase in void ratios indicate that regardless of the attempts made to

primarily reduce soil suction and minimize the rebounding effect through the end of the CVOT, the specimen still had the potential to swell. This observation may also highlight the contribution of vertical applied stress to the swelling potential, which was reduced from approximately 47.0-50.0 kPa to 5.0 kPa. The data in Figure 5.20 do not show any particular trends but a general scatter. In transferring the test cell from the CVOT setup to the 1DST setup some experimental error was induced which affected the quality of this data. As will be shown in Chapter 7, the experimental scatter had minimal effect on the overall conclusion.

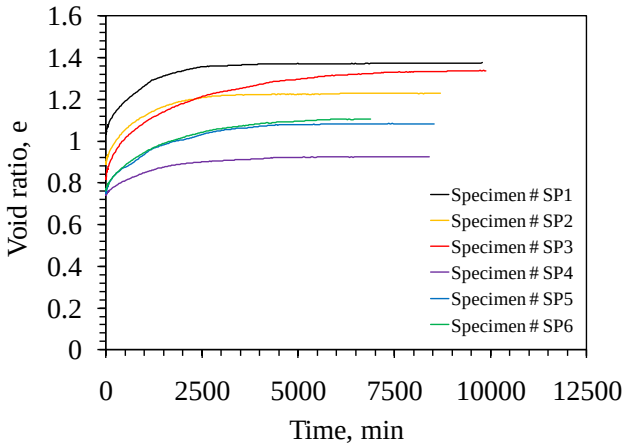

Figure 5.20. The results of void ratio developments during the 1DST.

5.7 Submergence Test Results

Finally, after performing the previous tests (section 5.6), the void ratios and moisture contents were measured before submerging the specimens. Then, the specimens were freely submerged in glass containers until the potential of swelling completely vanished. The moisture contents are plotted in Figure 5.21 (except for specimen # SP1). A sample of images during the submergence test is illustrated in Figure 5.22. The

information obtained from this test demonstrates that the significant volumetric swelling is only taking place when the surcharge pressure is completely released even if it is minimal.

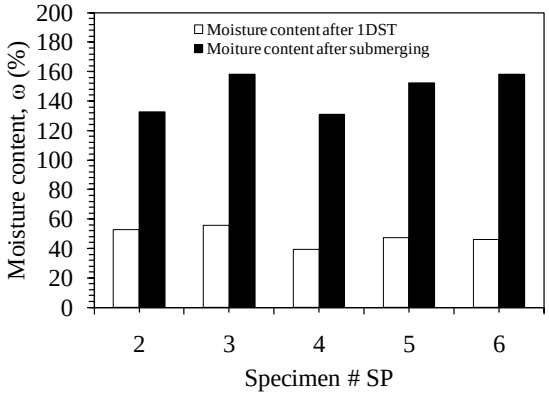

Figure 5.21. Comparison between the moisture contents obtained after the 1DST and the submergence test.

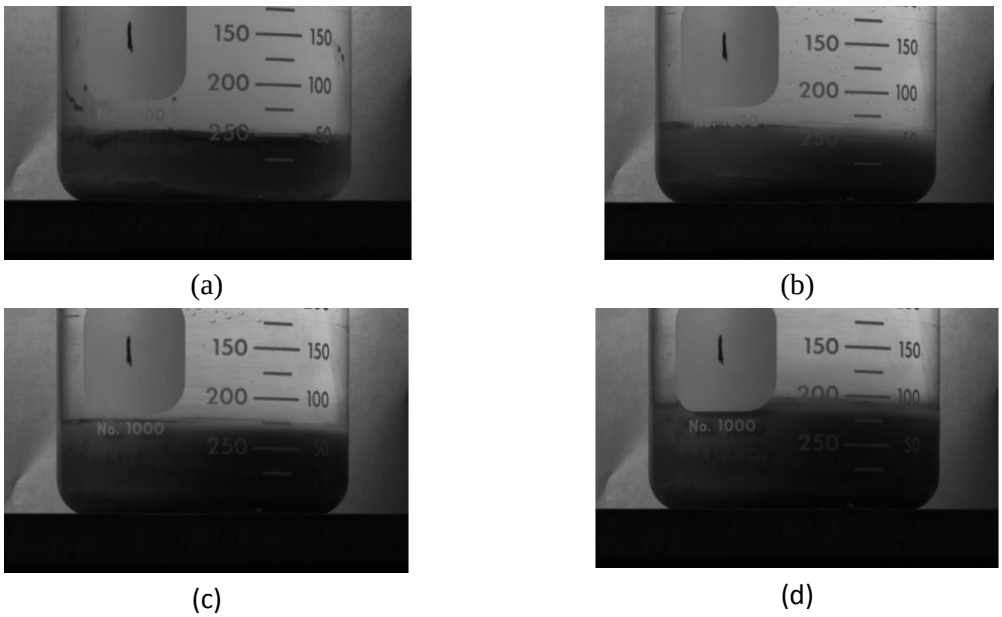

Figure 5.22. The results of the submergence test showing the free swelling potential of the specimen #SP3 after (a) 0 hr, (b) 6 hrs, (c) 40 hrs, and 143 hrs.

CHAPTER 6

ANALYSIS OF RESULTS AND DISCUSSION

6.1 Introduction

The results of the experimental investigation are quantitatively analyzed in the framework of several constitutive relationships, such as moisture content – void ratio and void ratio – swelling pressure relationships. The observations of the current results are discussed and correlated with previous research observations in order to provide a comprehensive understanding of the mechanism of the swelling process in expansive soil.

This chapter is organized into the following sections:

- Analysis and discussion of the free swelling test results, including analysis of the soil-water retention characteristic by means of the constitutive relationship of soil suction and moisture content;
- Analysis and discussion of the oedometric swelling test results, including the CVOT and the 1DST, as well as the submergence test results; and
- Comparison between the soil suction analysis and swelling pressure analysis with respect to the moisture content variation.
- A general description of the swelling behavior.

6.2. Analysis and Discussion of the Free Swelling Test Results

The constitutive relationships between the void ratio and moisture content are plotted in Figures 6.1 to 6.5. Generally, the rewetting path during the swelling process was observed to be similar in most of the specimens. Therefore, these figures show examples for each swelling process in terms of moisture content- void ratio relationship. The results of the remaining free swelling tests are plotted in Appendix-F. In some cases, the data points for the rewetting path indicate that the degree of saturation is higher than 100%. This deviation also implies the overall accuracy of measurements of the moisture content and corresponding void ratio. It should be noted that the amount of added moisture was basically measured from the imposed infiltration rate, i.e., the mass of water per day was assumed to be entirely included into the specimen's pores. This assumption is valid when some of the saturated specimens were permitted to absorb the excess water for a long enough time. The swelling process in terms of moisture content and void ratio relationship could be divided into the following two segments:

- Partially saturated zone under 80% saturation (Zone I), where the increase of moisture content is associated with the relatively slower development of the void ratio; and
- Nearly to fully saturated zone over 80% saturation (Zone II), where the water absorption is as intensive as the corresponding volumetric swelling.

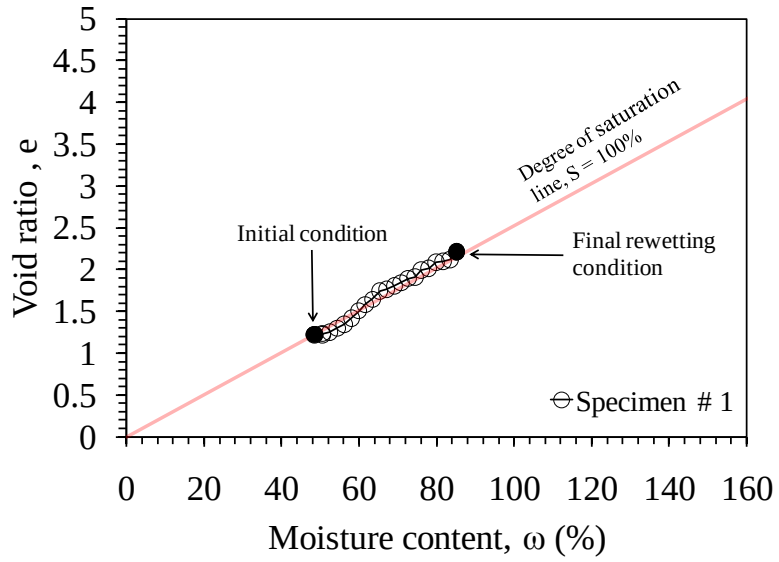

(a)

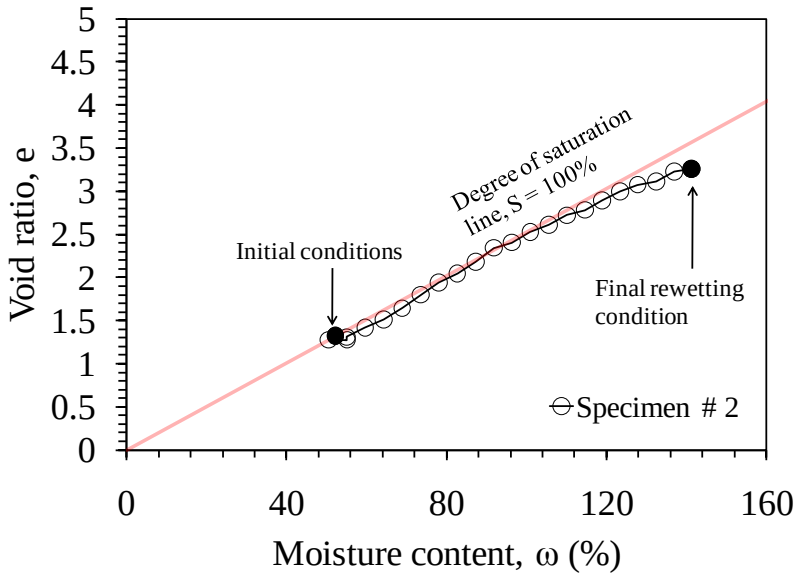

(b)

Figure 6.1: The constitutive relationship between void ratio and moisture content showing the processes of (a) SW1, and (b) SW2.

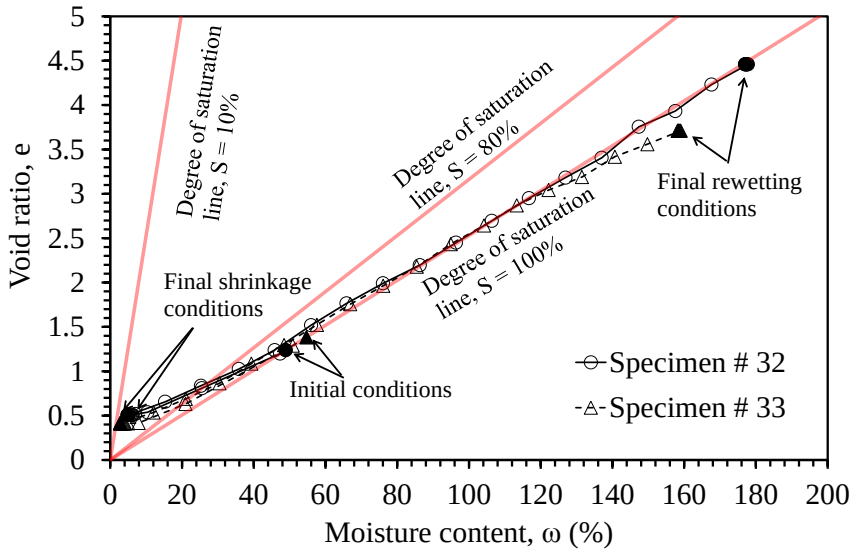

(a)

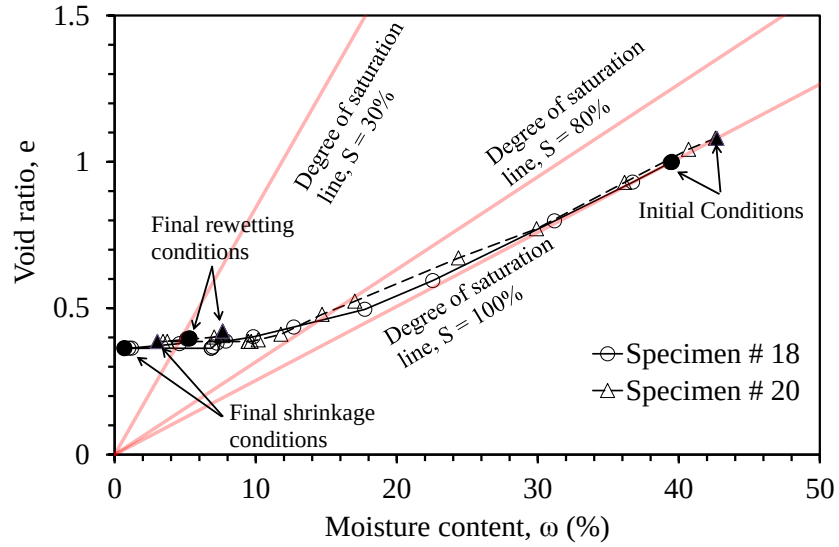

(b)

Figure 6.2: The constitutive relationship between void ratio and moisture content showing the processes of (a) SW3, and (b) SW4.

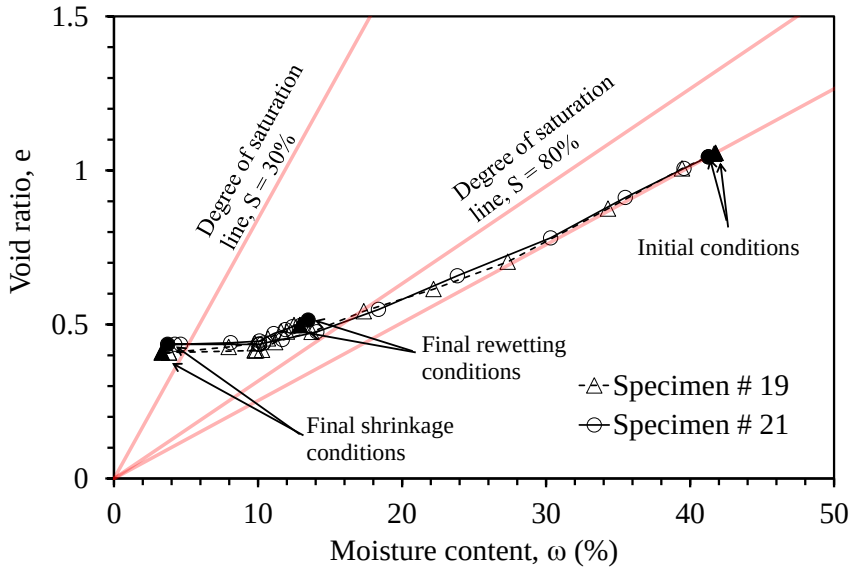

(a)

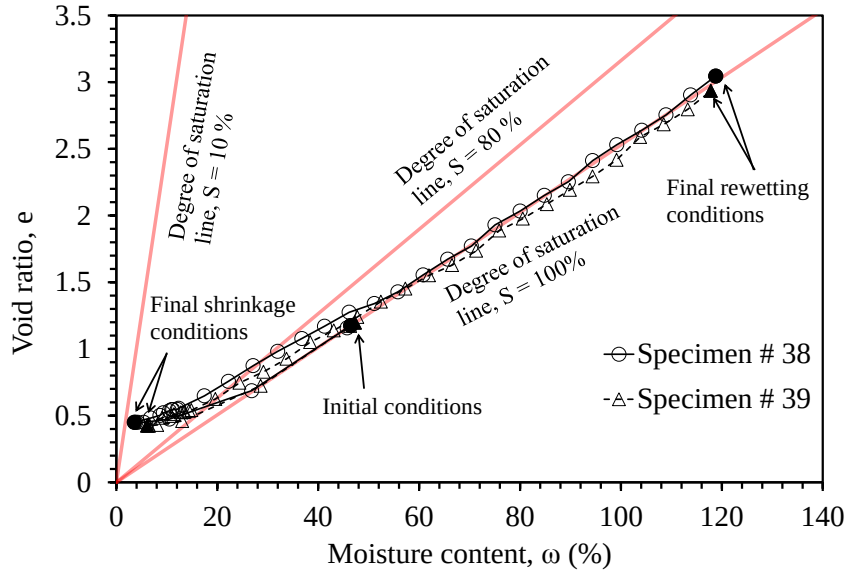

(b)

Figure 6.3: The constitutive relationship between void ratio and moisture content showing the processes of (a) SW5, and (b) SW7.

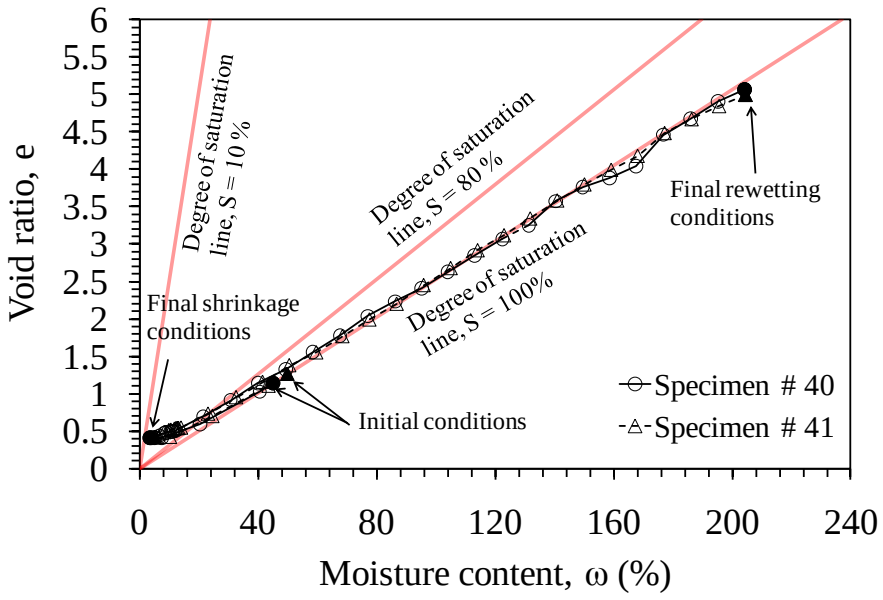

(a)

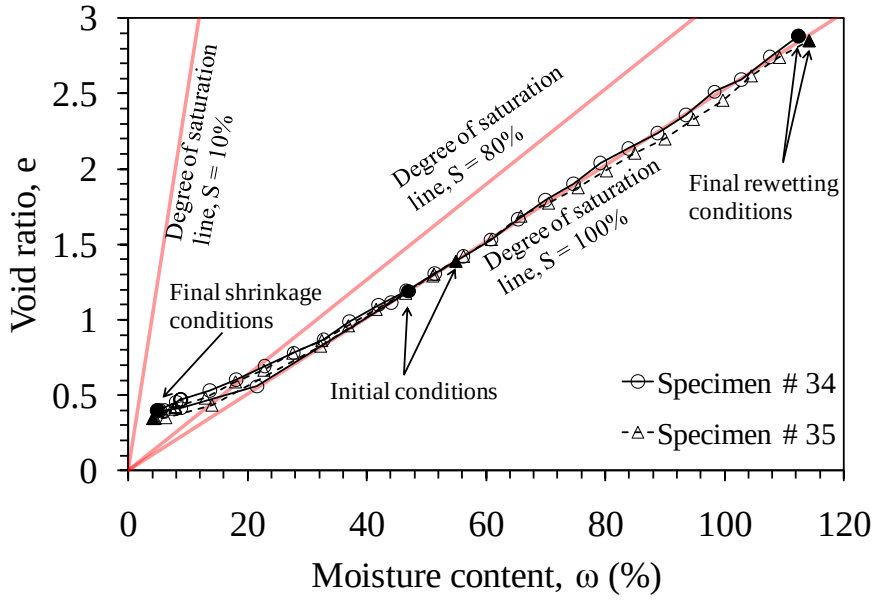

(b)

Figure 6.4: The constitutive relationship between void ratio and moisture content showing the processes of (a) SW8, and (b) SW9.

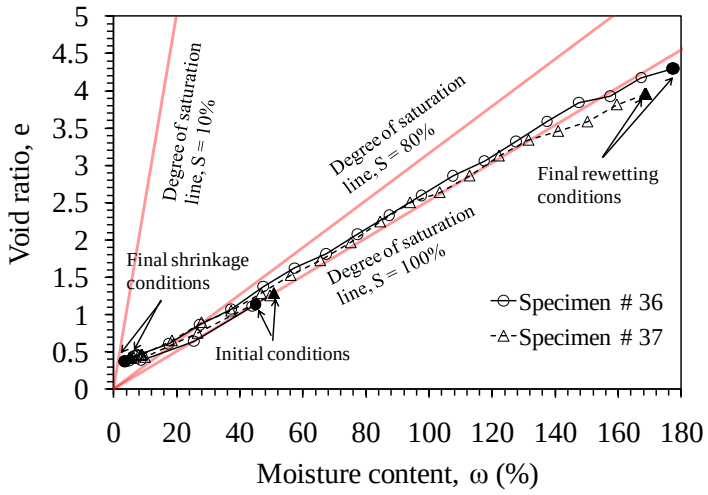

Figure 6.5: The constitutive relationship between void ratio and moisture content showing the process of SW10.

6.2.1 The Influences of Hygroscopic Absorption and Reversible/Irreversible Components on the Swelling Behavior

The degree of saturation line of 80% that separates the two zones as mentioned in the previous section is subjective. The reason of this selection is justified as shown in Figures 6.6 and 6.7 where the Zone I is magnified for the swelling processes SW4, SW5, SW7, and SW8, respectively. One can see that the hygroscopic increase in moisture content was fast during the early stage of the rewetting process followed by relatively slow increase in moisture content (each data point represents approximately 24 hours elapsed time). In all cases, the associated increase in void ratio was minimal and almost reached equilibrium before approaching 80% saturation. Keep in mind that the volumetric expansion by adding liquid water in the same zone was comparable and faster to approach the 80% saturation (Figure 6.6 (c)). It is only in the Zone II where the substantial increase in void ratio occurred towards degree of saturation of 100% and continued along 100% saturation line (Figure 6.7 (c)). By taking the two zones into

consideration, the minor development of void ratio in Zone I is called "volumetric expansion. While in Zone II, the significant development of void ratio is called "actual swelling".

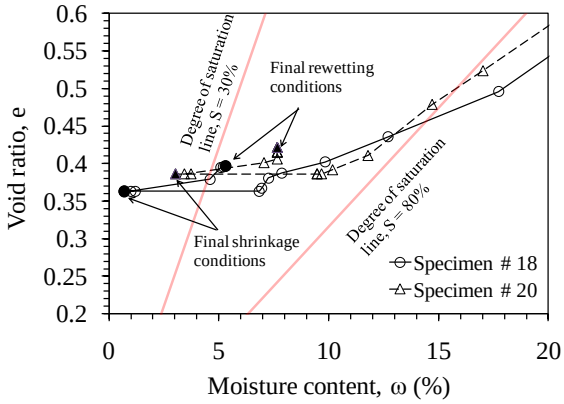

(a)

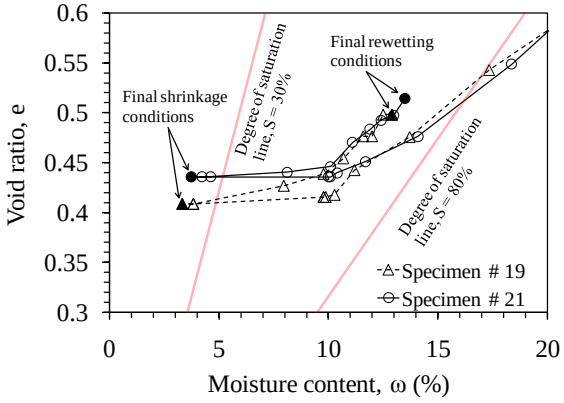

(b)

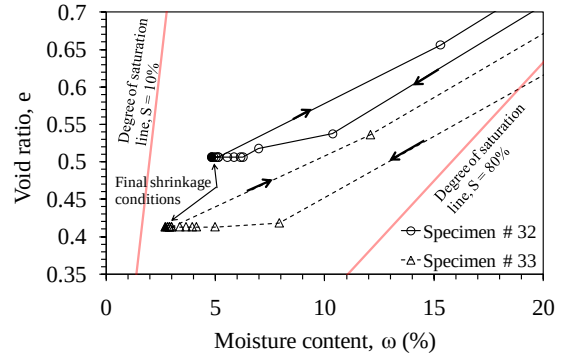

(c)

Figure 6.6: The constitutive relationship between void ratio and moisture content for Zone I showing the processes of (a) SW4, (b) SW5, and (c) SW3.

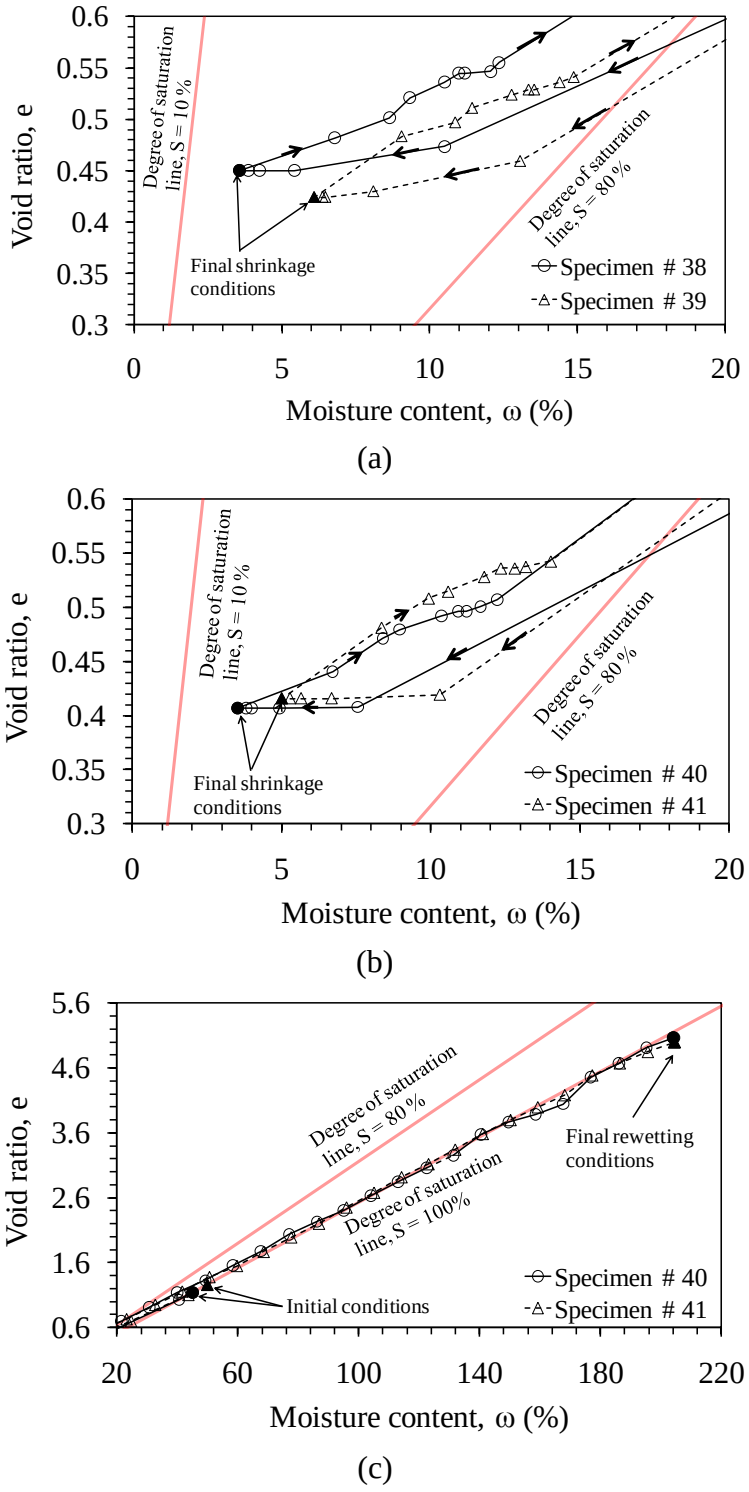

Figure 6.7: The constitutive relationship between void ratio and moisture content for Zone I showing the processes of (a) SW7, (b) SW8, and for Zone II of (c) SW8.

Various approaches have been proposed by several researchers (including Gens and Alonso, 1992; Delage et al., 1998; Alonso et al., 1999; Tripathy et al., 2002; Romero et al., 2006; Nowamooz and Masrouri, 2008) to recognize the volumetric deformation in terms of reversible and irreversible components. To better quantify these components, in most cases, the expansive soils were subjected to several cycles of wetting and drying. Although the hydraulic hysteresis effect on those components is not investigated in this study, it can be concluded by combining swelling deformation in Zone I and Zone II that the swelling path is almost reversible and thus, the early irreversible portion of the swelling path represents the minor deviation from the reversible path. Therefore, the reversible swelling is considered to be the fundamental property of the selected expansive soil in this study.

6.2.2 Contribution of Soil Suction Variation to the actual swelling of Unconfined Expansive Soil

When the degree of saturation of 80 % was approximately approached, a significant monotonic increase of void ratio as a function of water content was observed. This is, of course, due to the presence of the highly expansive clay selected in this study. The observed volume change behavior can be related to the soil suction as shown in Figure 5.15. The data in that figure indicate that at high soil suction values the change in moisture content and corresponding void ratio are relatively small demonstrating very stiff response of soil to suction changes. This stiff behavior is noticed during both drying and wetting processes that showing little to no hysteresis. As soil suction drops below approximately 1.0 MPa upon wetting, the moisture content and void ratio changes increase dramatically. For this material, the soil suction value of approximately 1.0 MPa corresponds roughly to 80% degree of saturation and to moisture content of about 16%,

which is close to the shrinkage limit for this soil. In that regard, this research was focused on the swelling behavior of expansive soil for soil suctions below 1.0 MPa.

The rewetting paths that represent the total and matric suction can be linked together, which means that the osmotic suction variation at higher level of total suction is insignificant. The distinction of the osmotic suction contribution inside or outside the range of interest requires more experimental investigations to be confirmed, as it is out of the scope of this study.

6.3 Analysis and Discussion of the Oedometric Swelling Test Results

After defining the zone where the actual swelling was distinguished (section 6.2), in that zone, it is intended to investigate the association of the swelling pressure with the actual swelling which may answer some of the inquiries such as; how does the actual swelling govern the development of swelling pressure (or soil suction reduction)? How much the confined specimen should heave in order to dissipate completely the soil suction or swelling pressure?

6.3.1 The Constant Volume Oedometer Test (CVOT)

6.3.1.1 Relationship between Primary Swelling Pressure and Soil Suction

From the CVOT, the primary p_s s at equilibrium are plotted against the initial moisture contents as shown in Figure 6.8 (a). It should be noted that the specimens were permitted to dry freely so that their soil suction and reduced moisture content could be assumed comparable to the ones obtained from the free swelling tests. In this figure, the values of the primary p_s are always lower than the corresponding soil suctions, for the same moisture content (before starting the test). Consider now two possibilities. It can be

assumed that since the shrinkage deformation of specimens was isotropic in nature, the corresponding increase in state of stress was also isotropic. During the CVOTs, the soil suction might be released under k_o-condition. Therefore, the development of swelling pressure required to maintain the constant volume would be equivalent to the reduction in soil suction. Also, the lower swelling pressure may be caused by the uneven contact surface between top platen and specimen (the specimen may not be perfectly cylindrical). The small gap in between the top platen and specimen allowed the specimen to slightly swell upon absorbing water and thus, the early development of primary p_s may not fully reflect the suction reduction.

Having the best-fit power functions that represent the drying path of the total suction and primary p_s at equilibrium, one can calculate the primary p_s corresponding to the total suction by using Equation 6.1. The relationship between the swelling pressure and soil suction obtained by Kassiff and Ben Shalom (1971) demonstrates the same phenomenon (Figure 6.8 (b)). A comparison between their experimental results, the data points obtained by using the resulted primary p_s with the power function from the total suction results, and the fitting curve obtained by using Equation 6.1, is shown in Figure 6.8(c). Keep in mind that the maximum primary p_s (at equilibrium state) of the soaked specimen was attained upon the complete absorption with water, which did not necessarily mean that the state of specimen was fully saturated. The maximum primary p_s defines the "actual swelling pressure" of an unsaturated-confined specimen.

$$p_s = 5.59\,{\psi_t}^{0.56} \tag{6.1}$$

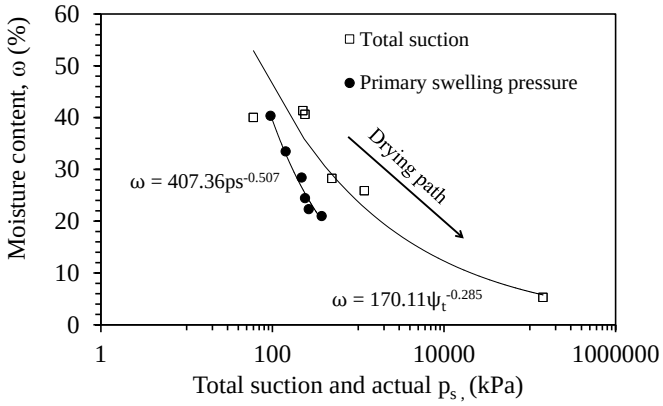

(a)

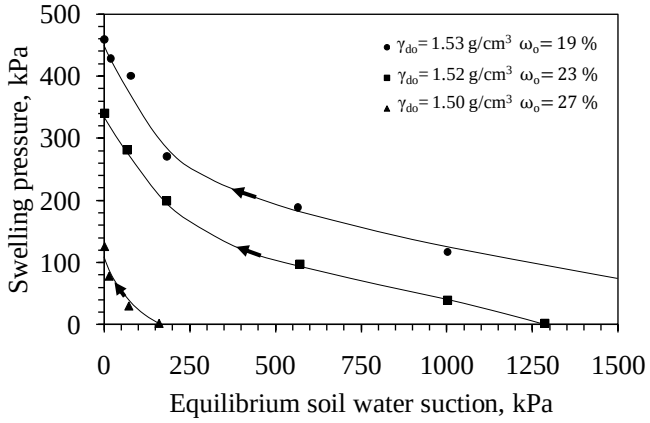

(b)

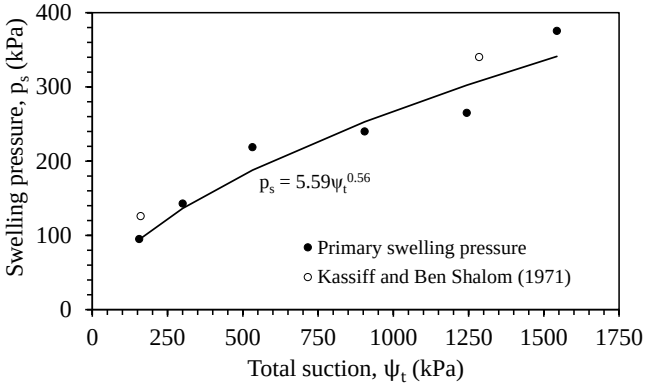

(c)

Figure 6.8. Comparison between total suction and the corresponding actual swelling pressure obtained from (a) the current research, and (b) Kassiff and Ben Shalom (1971), and (c) overall comparison between (a) and (b).

6.3.1.2 The Role of $d_{v(all.)}$ on Swelling Pressure Dissipation

As shown in Figure 5.16 (b) along with the results presented in Appendix-E, it can be deduced that the greater the actual p_s, the more the $d_{v(all.)}$ required to fully dissipate the swelling pressure. This is also shown in Figure 6.9. In this particular test, 10 unloading stages were required to reduce the actual p_s from 375.44 kPa to 83.09 kPa which is associated with the total $d_{v(all.)}$ of 0.818 mm (equivalent to 0.13 increase in void ratio). The final $d_{v(all.)}$ for all of the tests were less than 1.0 mm (see Appendix-F) causing only minor changes in the void ratio.

A comparison between analyses of all the tests is plotted in Figure 6.10. The range required to dissipate the swelling pressure toward the initial surcharge pressure is larger for specimen #SP6 than that for the specimen #SP2. This is related to the required void ratio changes of 0.130 for the specimen #SP6 and 0.034 for the specimen #SP2. However, the trends are almost identical and can be linearly approximated in the semi-logarithmic plot. It is worth mentioning that after determining the actual p_s upon a complete water absorption, the reduction in swelling pressure and soil suction during the unloading sequences signifies the rebounding effect which is the nature of any clay when they are unloaded. Therefore, the swelling index (C_s), which is the slope of linearly approximated line for each specimen (except for the specimen #SP1) is determined as shown in Table 6.1. The listed values in this table will be used to mathematically determine the coefficient of volume compressibility (m_v) as explained in Chapter 7.

Specimen #	SP2	SP3	SP4	SP5	SP6
C_s	0.099	0.173	0.139	0.173	0.201

Table 6.1. The C_s values for the unloaded specimens.

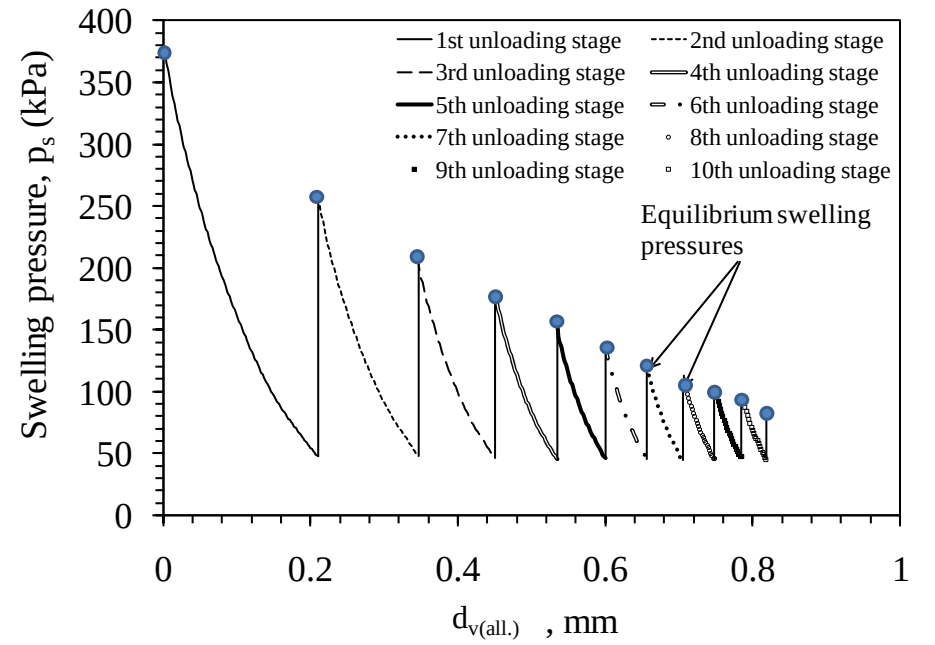

(a)

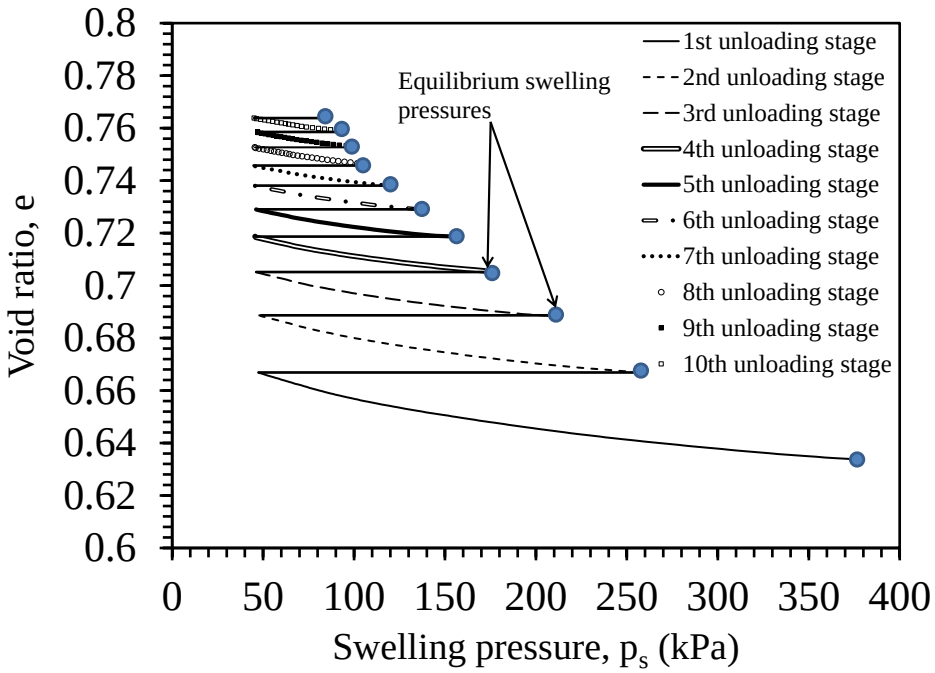

(b)

Figure 6.9. The decrement of p_s as a function of (a) $d_{v(all.)}$, and (b) void ratio for specimen # SP6.

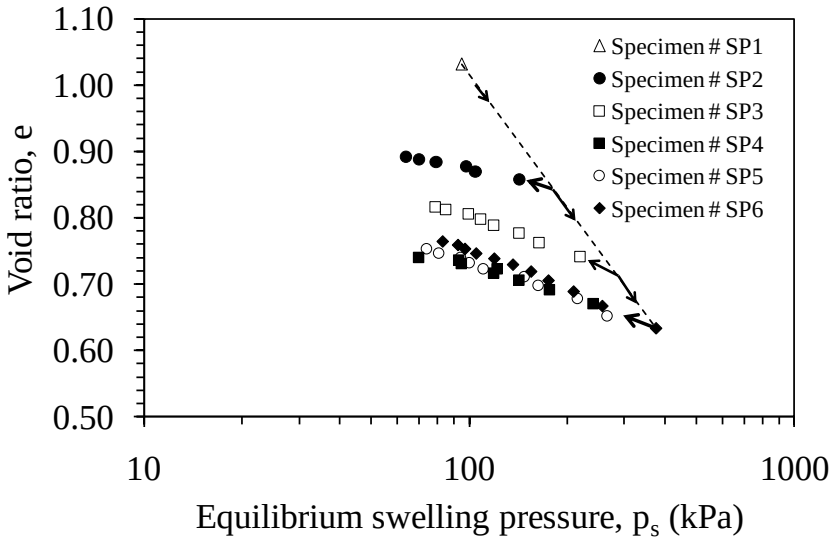

Figure 6.10. The decrement of equilibrium p_s after each unloading stage.

6.3.2 Analysis and Discussion of the Oedometric Swelling Test (1DST) and Submergence Test

The results of the 1DSTs and submergence tests were presented in Sections 5.6 and 5.7, respectively. These results are collectively analyzed and compared with those provided in the previous section, as shown in Figure 6.11. During the transition from the CVOT to the 1DST the surcharge pressure was reduced from the final surcharge pressure (after the last unloading stage) to the nominal surcharge pressure acting on the specimen. Only one data point obtained at the end of the 1DST when the equilibrium of swelling deformation was reached. It can be observed that similar trends were occurred to those from the CVOTs even though the specimens subjected to 1DST showed higher response to water absorption and void ratio changes due to the change in the magnitude of surcharge pressure.

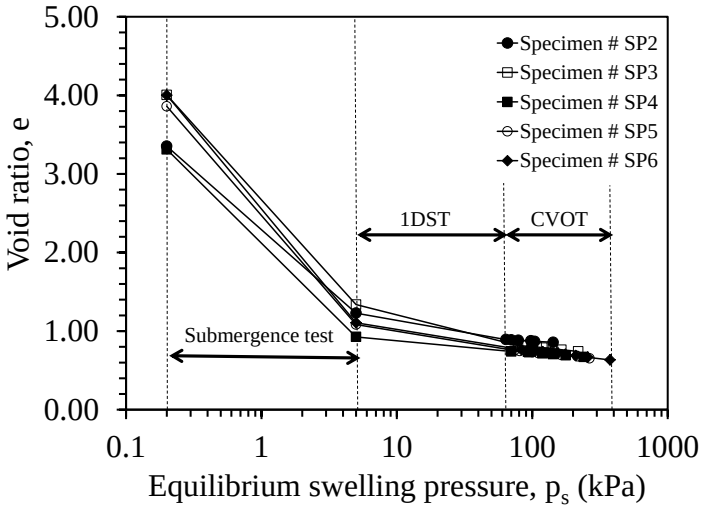

(a)

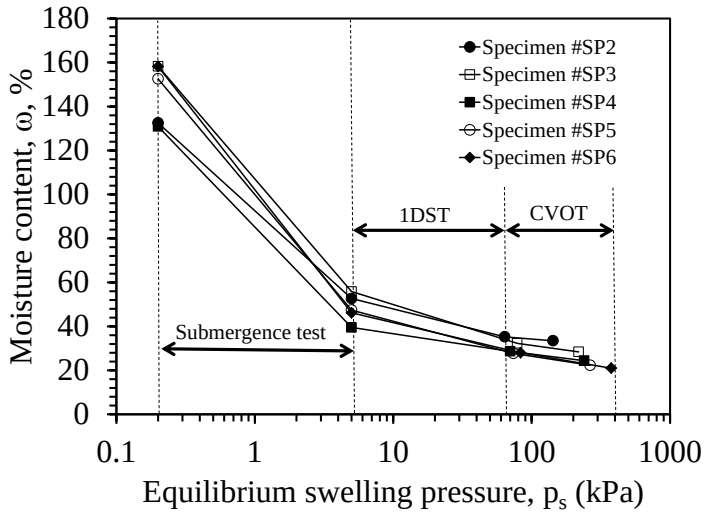

(b)

Figure 6.11. Equilibrium p_s as a function of (a) void ratio, and (b) moisture content.

Other interpretations for this analysis can be presented by plotting the moisture content-void ratio constitutive relationship as depicted in Figures 6.12 to 6.14. This alternative representation can conveniently monitor the effects of confinement conditions on the progression of actual swelling starting from the initial conditions. The three annotated data points represent the actual swelling after performing, CVOT, 1DST, and the submergence test, respectively. With the known values of void ratio after the CVOT, the values of the corresponding moisture content were calculated assuming linear

relationship between void ratio and moisture content from the initial condition to the point after the 1DST. In the case of submergence tests, the values of void ratio could be determined from the fact that the degree of saturation was 100% and from the known values of moisture content (Section 5.7).

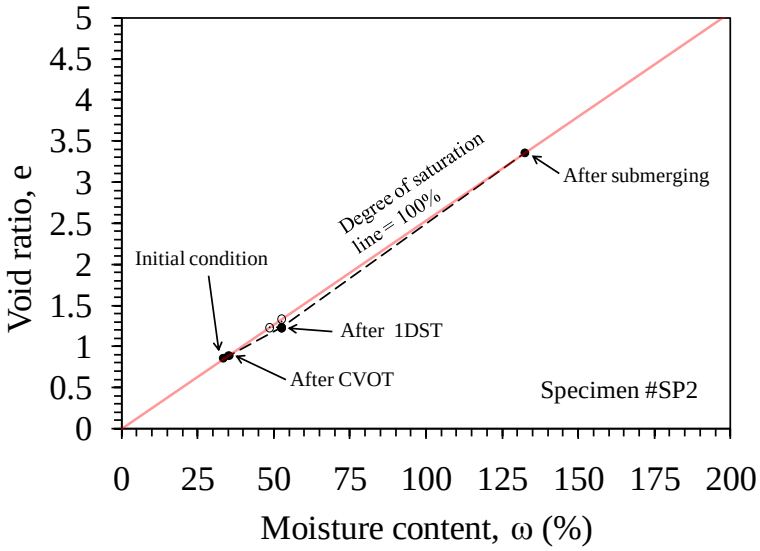

(a)

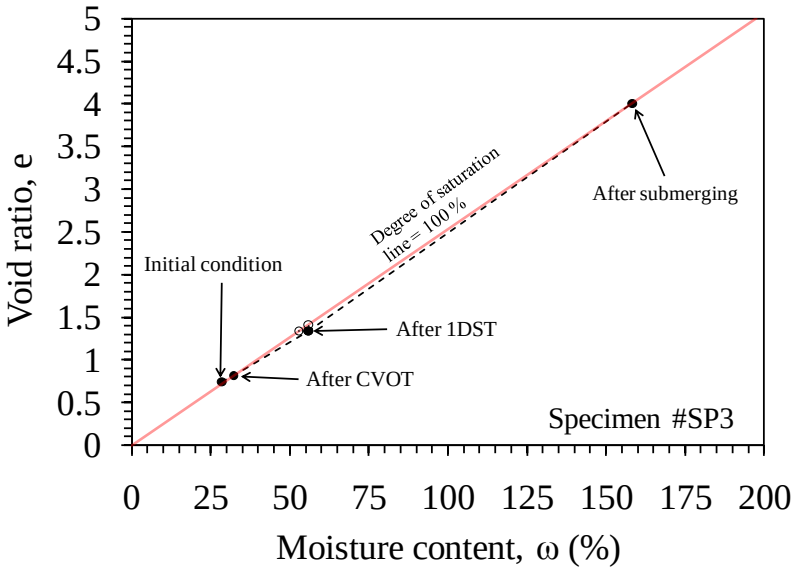

(a)

Figure 6.12. Moisture content-void ratio relationship under oedometric swelling pressure tests and submergence test for (a) the specimen #SP2 and (b) the specimen #SP3.

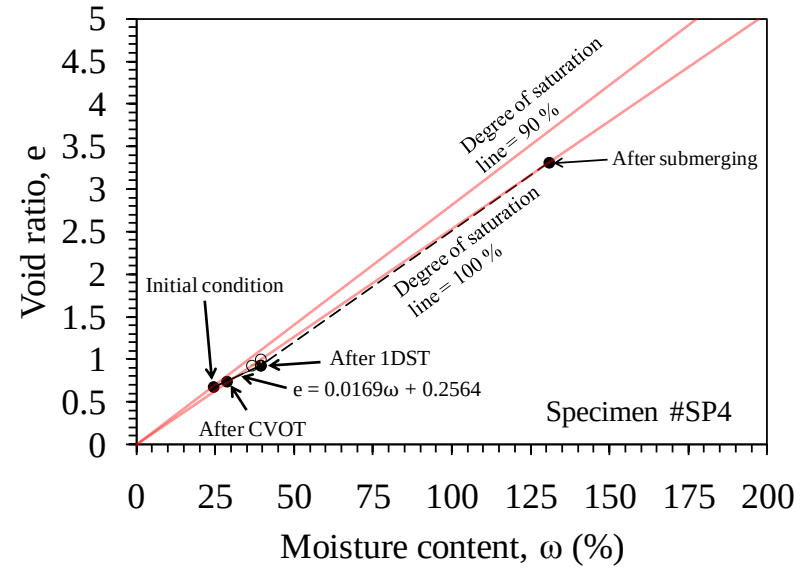

(a)

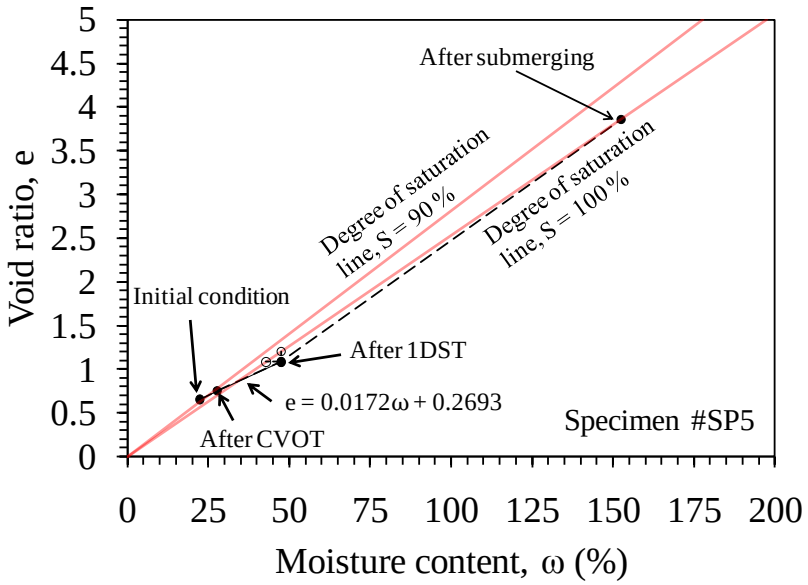

(b)

Figure 6.13. Moisture content-void ratio relationship under oedometric swelling pressure tests and submergence test for (a) the specimen #SP4 and (b) the specimen #SP5.

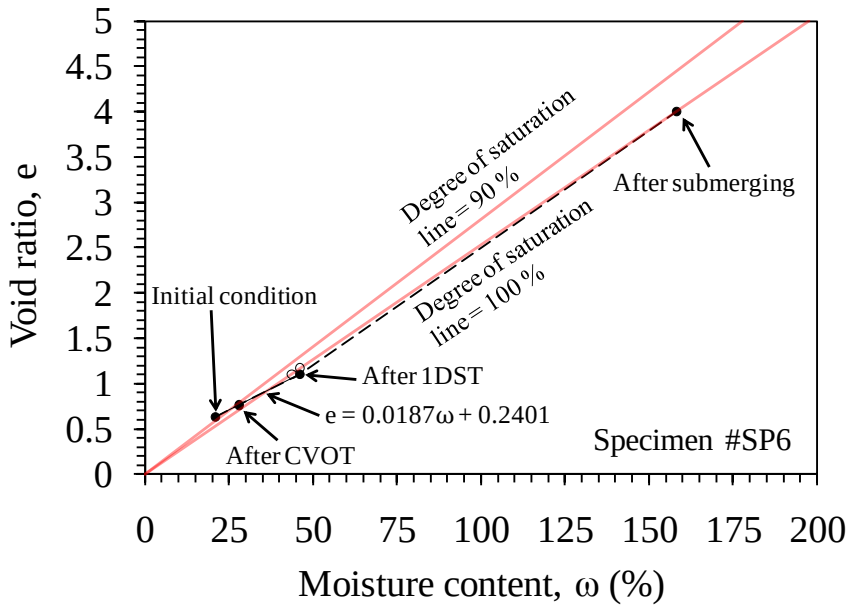

Figure 6.14. Moisture content-void ratio relationship under oedometric swelling pressure tests and submergence test for the specimen #SP6.

6.4 Comparison between Soil Suction and Swelling Pressure During Rewetting Process

The analysis of results obtained from Figure 6.11 (b) is compared with the soil suction results from the free swelling tests and plotted in Figure 6.15. The equilibrium p_s values that represent the rewetting path are, once again, lower than the soil suctions of the same path. The confinement conditions have been known to restrict the storage capacity of expansive soil during the swelling process and thus, affect the potential of water absorption (or soil suction reduction). In addition, the gradual unloading during the p_s measurements stages and soil suction dissipations appeared to exhaust the specimens' absorption abilities, to some extent, as shown by the lower final water contents than those obtained by performing the free swelling tests.

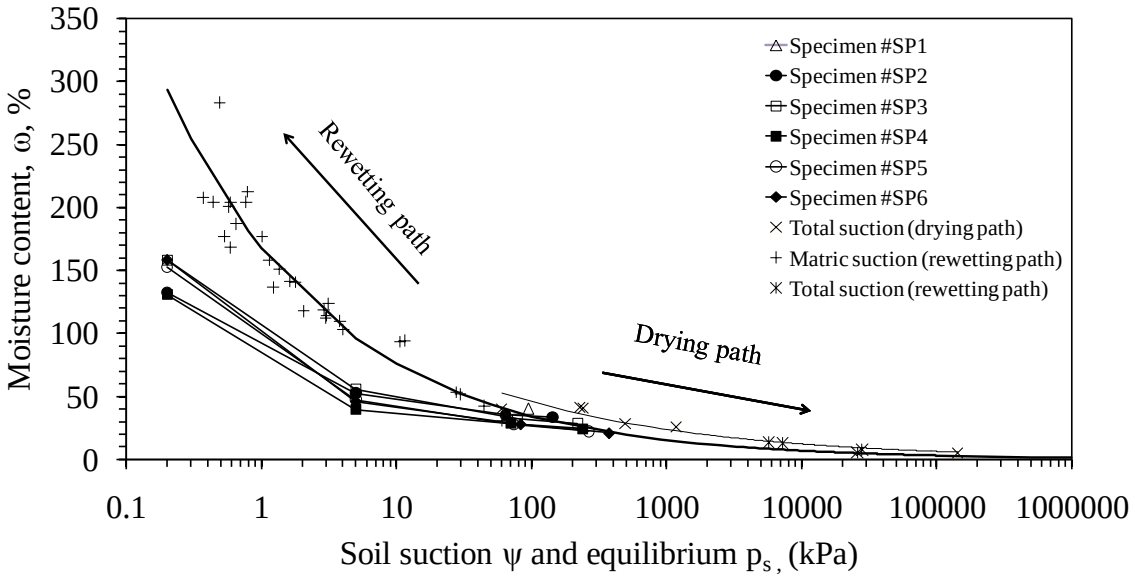

Figure 6.15. Comparison between the paths of equilibrium p_s and soil suction.

6.5 A General Description of the Swelling Behavior

The analyses of the experimental program are compared in single plot in order to provide a comprehensive understanding of the swelling behavior of the selected expansive soil in this research. Figure 6.16 consists of the rewetting path for specimen #41, the rewetting path for specimen #SP6 including its initial condition, and the matric suction curve obtained from the free swelling test. The hygroscopic increase in moisture content for the specimen #41 had a minor influence on the development of void ratio (i.e., volumetric expansion in Zone I) but significantly reduced the matric suction to approximately 1000 kPa. The subsequent increase in moisture content by liquid water had a major influence on the development of void ratio (i.e., actual swelling in Zone II) as well as the reduction in matric suction. In the Zone II where the matric suction was reduced to approximately 200 kPa, both specimens showed almost identical and minor void ratio change. After the CVOT (specimen #SP6), the change in void ratio associated with the reduction in matric suction was relatively higher. The reduction of external

pressure in the 1DST had significant effect on the development of actual swelling. This was related to a greater reduction in both the p_s and matric suction.

The overall evaluation of the swelling processes in terms of deformation for both specimens in the Zone II implies almost identical swelling behavior. This time-dependent behavior is affected by the confinement and surcharge pressure conditions in which it delays the swelling deformation during water absorption but not the swelling deformation path.

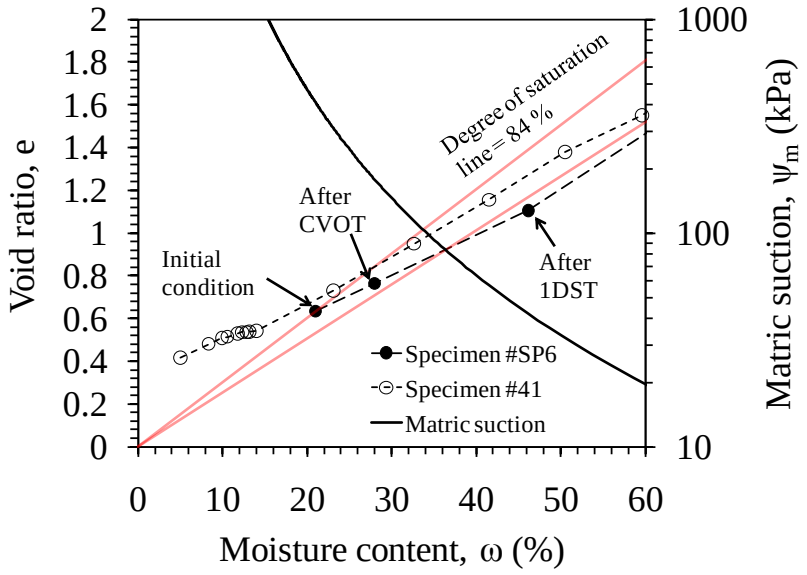

Figure 6.16. A general comparison between the swelling tests results.

CHAPTER 7

TIME-DEPENDENT ONE-DIMENSIONAL SWELLING

7.1 Introduction

The progression of water absorption and actual swelling under oedometric condition tests (CVOT and 1DST) is having only one-dimensional perspective (vertical direction). In addition to that, if the compressibility of water and soil particles is assumed to be negligible, then the concept of time rate of consolidation theory (Terzaghi, 1925) may apply to investigate the time-dependent one-dimensional swelling in this study (Appendix-B). As discussed in Chapter 6, the actual swelling during every unloading stage produces small increase in void ratio that can be averaged and used as a constant value for the whole swelling process. But the coefficients of volume compressibility and permeability are not constants as investigated theoretically and experimentally herein.

In order to distinguish between the compressibility characteristics due to consolidation and the ones due to swelling, the coefficient of consolidation (c_v) is considered as the hydraulic diffusivity (D). While the coefficient of volume compressibility (m_v) and the coefficient of permeability (k) will not be rephrased since they describe the same physical meanings whether during consolidation of swelling processes.

In this chapter, the original equation of D (Appendix-A) is simply modified and proposed. Then, the aforementioned coefficients are determined by using both experimental and theoretical approaches.

7.2 Theoretical Estimation for the Hydraulic Diffusivity *D*

The analyses related to the matric suction of the rewetting path and the CVOTs (see Chapter 6) are used to modify the mathematical expression of D as derived in the Appendix-A. The modified D equation is expressed as follows:

$$D = \frac{k(1+e_i)}{S\,{\partial e}/{\partial \psi_m}} \tag{7.1}$$

where, k is the constant coefficient of permeability (m/sec) during each unloading stage. The constant value of k is changing with the small change in the initial void ratio e_i during every unloading stage. S is the dimensionless degree of saturation. ${\partial e}/{\partial \psi_m}$ is the derivative of void ratio with respect to matric suction that has similar physical meaning as the coefficient of compressibility.

The change in S during the unloading stages was very small thus, it can be considered as a constant value ranged from 0.84 to 1. The $S = 0.84$ is based on the lowest initial S value obtained from specimen #SP6. With G_s to be constant during the swelling process, the ${\partial e}/{\partial \psi_m}$ term in Equation 7.1 can be substituted by the following equation:

$${\partial e}/{\partial \psi_m} = \left({\gamma_w G_s}/{S}\right) {\partial \omega}/{\partial h_m} \tag{7.2}$$

where, $G_s = 2.53$ and ω is the dimensionless moisture content which is a function of suction head h_m (m). γ_w is the unit weight of water = 9.81 $^{kN}/_{m^3}$. Therefore, the change of void ratio with matric suction change is related to the response of moisture content to suction head.

As shown in Figure 7.1, the power function obtained from the suction head-moisture content relationship for the rewetting path of free swelling tests is derived and substituted in Equation 7.2:

$$^{\partial e}/_{\partial \psi_m} = \frac{6.552\ h_m^{-1.346}}{S} \tag{7.3}$$

By substituting Equation 7.3 into Equation 7.1, the D (m^2/sec) is equal to:

$$D = 0.153k(1 + e_i)\ h_m^{1.346} \tag{7.4}$$

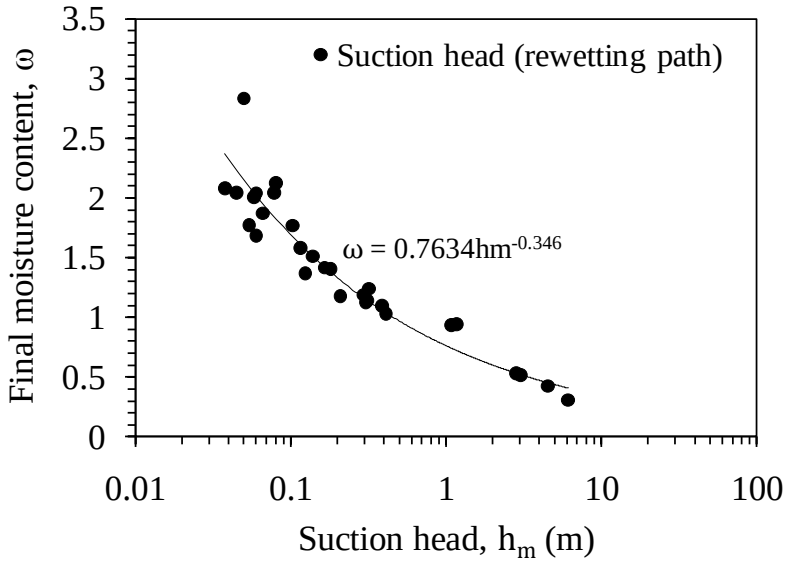

Figure 7.1. The rewetting path of the SWRC obtained from the free swelling tests.

The proposed Equation 7.4 can be used as a simple mathematical model to justify the determination of either the D or the k where the e_i change is small after each

unloading stage during the CVOTs. This implies that the e_i can be averaged indicating the great impact of the magnitude of D or k to the variation of $\partial e/\partial \psi_m$ (see Equation 7.1).

7.3 Experimental and Theoretical Determination of the m_v, D, and k for the CVOTs and 1DSTs

It is convenient to use the oedometer for evaluating the compressibility characteristics while it is under displacement control mode. It is basically the reverse process of one-dimensional consolidation in which one can expect the gradual increase in volumetric swelling is actually a consequence of the increase of excess pore water pressure (u_e). Moreover, the p_s at equilibrium after every unloading stage can be the representative of the effective stress (σ') at any time during the swelling process. In this manner, the decrease in p_s (or σ') is directly related to the increase in u_e.

7.3.1 Determination of m_v

For the CVOTs**,** the expression of m_v below is derived from the relationship between the m_v and the C_s as follows:

$$m_v = \frac{0.435\ C_s}{(1 + e_{avg})\sigma'_{v(avg)}} \tag{7.5}$$

where, C_s is the constant swelling index (determined in Chapter 6). e_{avg} and $\sigma'_{v(avg)}$ are the average of the initial and final values of void ratios and vertical effective stresses (or $p_{s_{(avg)}}$), respectively.

Because the testing condition of the 1DST was slightly different from the CVOT, the swelling mechanism response may produce slightly different C_s. Therefore, it is decided to use the following equation to determine the actual m_v values for the 1DSTs :

$$m_v = \frac{\Delta e}{\left(1 + e_i\left(or\ e_{avg}\right)\right)\Delta p_s} \tag{7.6}$$

An example the evolution of m_v as a function of p_s is depicted in Figure 7.2. Since the equilibrium p_s was not minimized to the averaged swelling pressure value in the 1DST when performing the unloading stages during the CVOT, the increments of m_v were extrapolated (dashed curve) by using Equation 7.5. The m_v values obtained from the 1DST by using Equation 7.6 were higher than the ones extrapolated from the CVOT at the same equilibrium p_s level. Also, this discrepancy is evident for the other tests as shown in the Appendix-F.

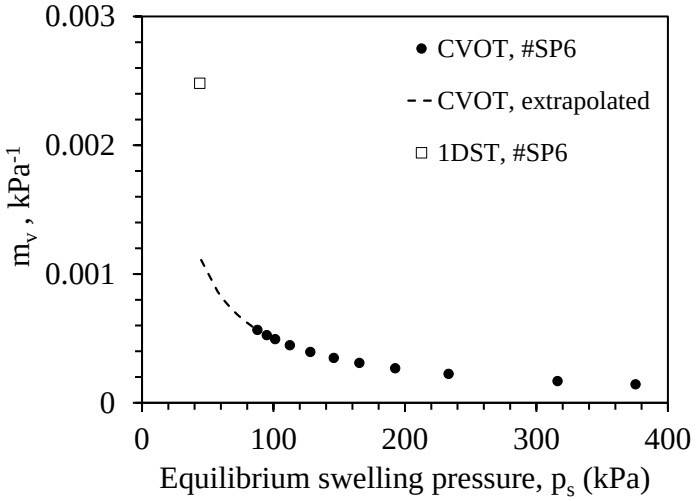

Figure 7.2. The evolution of m_v as a function of p_s for specimen #SP6.

The comparison between the m_v values for all of the CVOTs and the 1DSTs is shown in Figure 7.3.

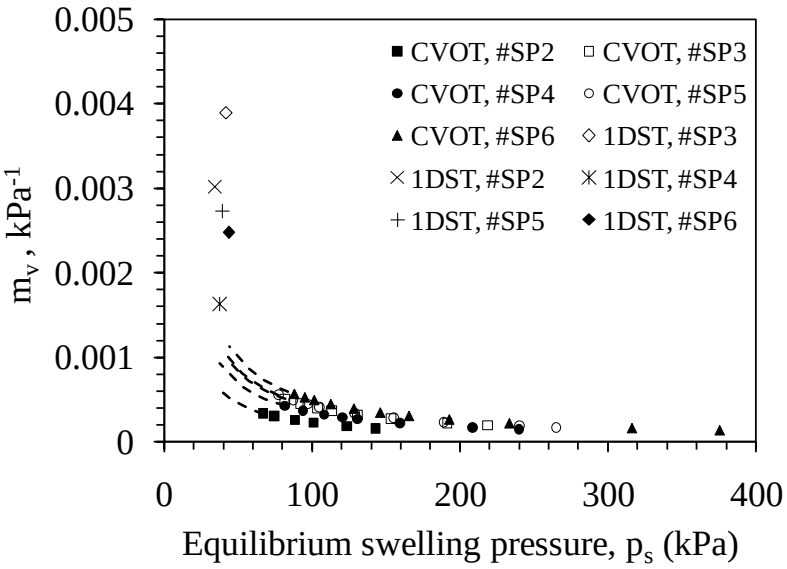

Figure 7.3. The evolution m_v as a function of equilibrium p_s for all of the swelling pressure tests.

The values of equilibrium void ratio resulted from the 1DSTs caused the values of m_v to be inconsistent at almost the same swelling pressure level (40 kPa). But one can observe at this swelling pressure level that the m_v can be as high as approximately 0.004 kPa^{-1}.

7.3.2 Determination of D and k

7.3.2.1 Degree of Consolidation

It is advisable to recall the basic concept of degree of consolidation as mathematically formulated below (Craig, 2004):

$$U_z = \frac{e_o - e}{e_o - e_1} \tag{7.7}$$

where e_o and e_1 are initial and final void ratios, respectively. e is void ratio at any time during consolidation process. U_z is the degree of consolidation at any time, at depth z.

If the relationship of $e - \sigma'$ is linearly related as schematically shown in Figure 7.4, then Equation 7.7 can be reformulated as follows:

$$U_z = \frac{\sigma' - \sigma_o'}{\sigma_1' - \sigma_o'} \tag{7.8}$$

where σ_o' and σ_1' are effective stresses before and after consolidation process, respectively. σ' is effective stress any time during consolidation process. If the effective stresses of the above expression are substituted with p_s, one can change U_z into so called degree of swelling ($\mathcal{S}_v$) as follows:

$$\mathcal{S}_v = \frac{p_s - p_{s_o}}{p_{s_1} - p_{s_0}} \tag{7.9}$$

where p_s, p_{s_0}, and p_{s_1} follow the same physical meaning as for the effective stresses in Equation 6.3.

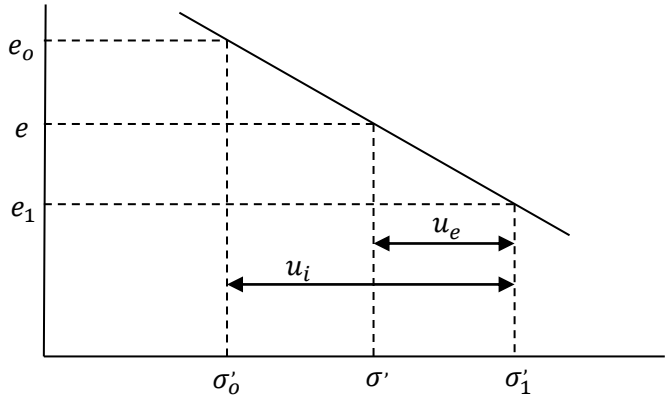

Figure 7.4. Assumed linear $e - \sigma'$ relationship (after Craig, 2004).

The physical and mathematical understanding from this discussion is that the $\mathcal{S}_v$ can be equivalently expressed by either terms of void ratio or p_s variations. This knowledge justifies the use of time-rate of $p_s$instead of time-rate of displacement for determining the square root of time of 90% averaged degree of swelling.

7.3.2.2. Average Degree of Consolidation

It is well-known that the average degree of consolidation $\mathcal{U}$ of the whole soil layer is more important than U_z, as expressed below (Craig, 2004):

$$\mathcal{U} = 1 - \frac{(1/2h)\int_0^{2h} u_e dz}{u_i} \tag{7.10}$$

where u_i and u_e are constant initial excess pore water pressure and excess pore water pressure at any time during consolidation process, respectively. h is the height of the longest drainage path.

The solution of u_e can be obtained by solving the partial differential equation of one dimensional consolidation. In that solution, the embedded time factor T_v (dimensionless) is conveniently used to substitute the c_v ,time t , and h as follows:

$$T_v = \frac{c_v t}{h^2} \tag{7.11}$$

If the theoretical relationship between $\mathcal{U}$ and T_v is plotted in terms of $\mathcal{U}$ vs $\log(T_v)$ or $\mathcal{U}$ vs$\sqrt{T_v}$, the tendency of their curves are comparable with those determined experimentally. Therefore, the above relationships can be used to determine c_v graphically as commonly known as log-time method (by Casagrande and Fadum,1940) or square root of time method (by Taylor, 1942). The square root of time method is selected once the secondary consolidation curve used in log-time method requires very long time to be noticeable. Normally, the gradual pressure is controlled to determine the

consolidation rate. In this study, the gradual $d_{v_{(all.)}}$ is controlled to determine the swelling pressure rate as shown in Figure 7.5.

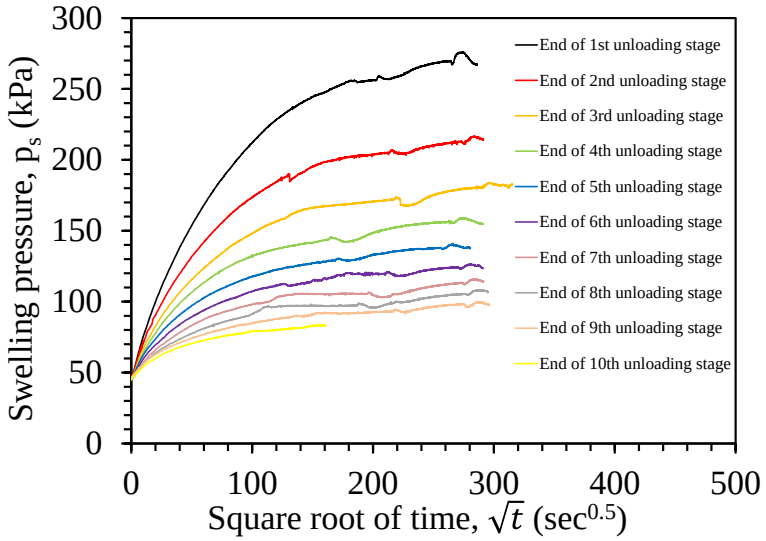

Figure 7.5. The rate of p_s obtained by controlling $d_{v_{(all.)}}$ for the specimen #SP6.

Rearranging Equation 7.13 has led to D given by:

$$D = \frac{0.848\, h^2}{t_{90}} \tag{7.12}$$

where the factor 0.848 is the same factor of T_v corresponding to 90% of $\mathcal{U}$. The t_{90} is the time corresponds to 90% of $\mathcal{U}$.The h in this case is half a thickness of the specimen due to two-way drainage path length. Once again, h can be assumed constant as the imposed $d_{v_{(all.)}}$ is relatively very small with respect to the specimen thickness.

A typical example of the square root of time method used for determining t_{90} is graphically presented in Figure 7.6 (a). Appendix-F consists of the remaining of this presentation including the ones for all of the other tests. The evolution of D for each

CVOT (including the only data point obtained from specimen #SP1) is analyzed in Figure 7.6(b).

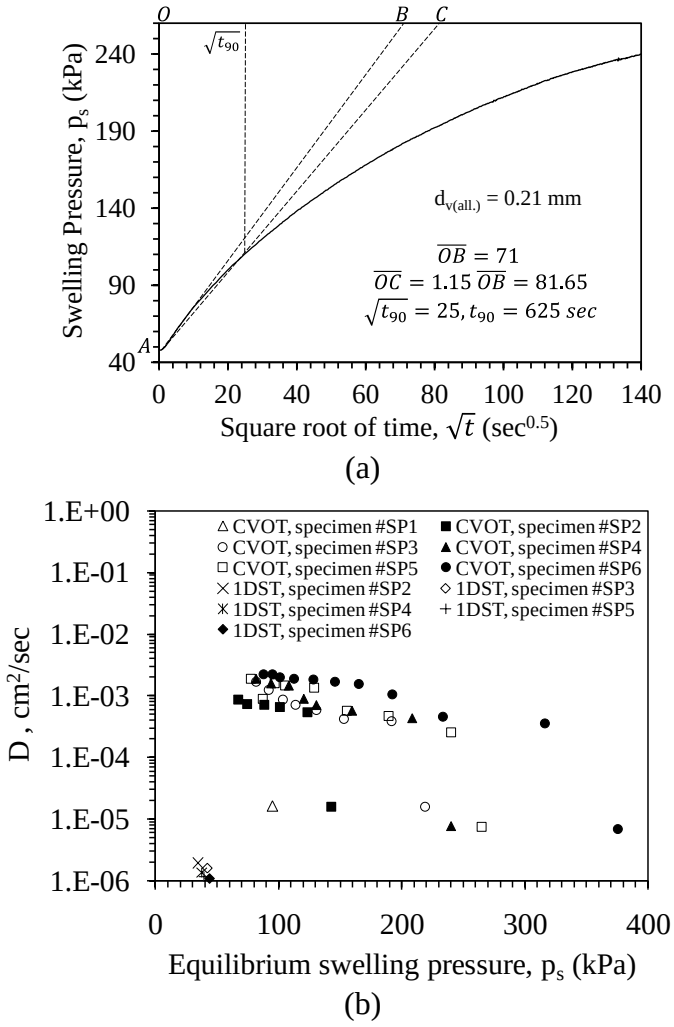

Figure 7.6. Graphical illustrations of (a) the typical example for determining $\sqrt{t_{90}}$ by using square root of time method for specimen #SP6 (1st unloading stage), and (b) the evolution of D during the CVOTs and the 1DSTs.

Generally, the high increase in D values from -6.0 order of magnitude to approximately -3.0 order of magnitude occurring at the end of the first unloading stage. The subsequent evolution of D was relatively lower. The highest final D value was resulted by the specimen #SP6 in which it had the lowest initial moisture content and the highest primary p_s.

The intersection of some of the D paths was occurred as the p_s converged with the initial surcharge pressure. This is because of several issues such as; a consequence of experimental error, the specimen may behave differently in response to each unloading stage, or the fact that the determination of D values was somewhat subjective. The values of D obtained from the 1DSTs were significantly smaller than those obtained from the last unloading stage in the CVOTs. This was due to the higher t_{90}values required in the 1DSTs to reach the 90% of averaged degree of swelling than those required for unloading stages in the CVOTs (Appendix-F). These issues will certainly affect the determination of k values as shown in the next section.

7.3.2.3 Determination of k

Normally, the k is assumed to be constant even during the consolidation process of saturated clay. This is the most convenient way for the determination of c_v as a constant coefficient of the partial differential equation derived in Appendix-B. In this study, it is preferable to consider the k to be variable and consistent with the changes in D and m_v by using the expression below:

$$k = D\, m_v\, \gamma_w \tag{7.13}$$

The evolution of k during the CVOTs was proportional to the D and m_v as demonstrated in Figure 7.7. In case of the 1DSTs, the drop of k values resulted by the inconsistent evaluation of the corresponding D values. An alternative demonstration regarding the evolution of k as a function of void ratio during the CVOTs is shown in Figure 7.8. The very small change in void ratio associated with high increase in k value at the end of first unloading stage indicates that the change in degree of saturation may

have independent impact on the volume change of porous medium when the specimens were unsaturated.

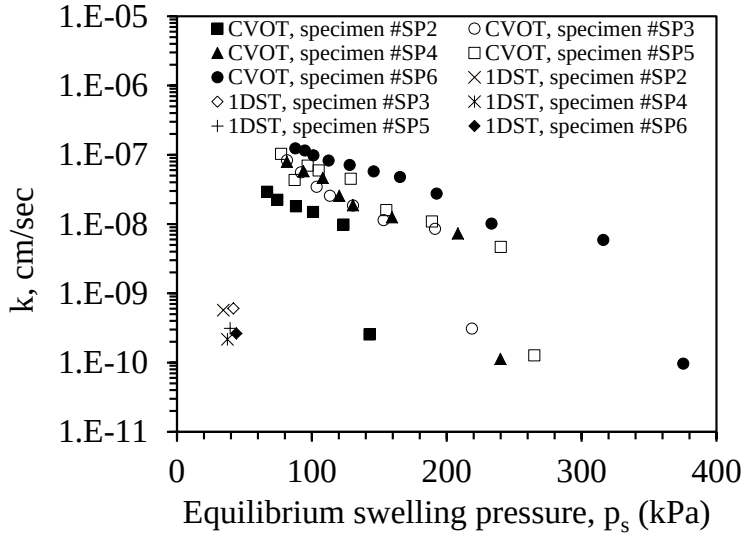

Figure 7.7. The evolution of *k* during the CVOTs and the 1DSTs.

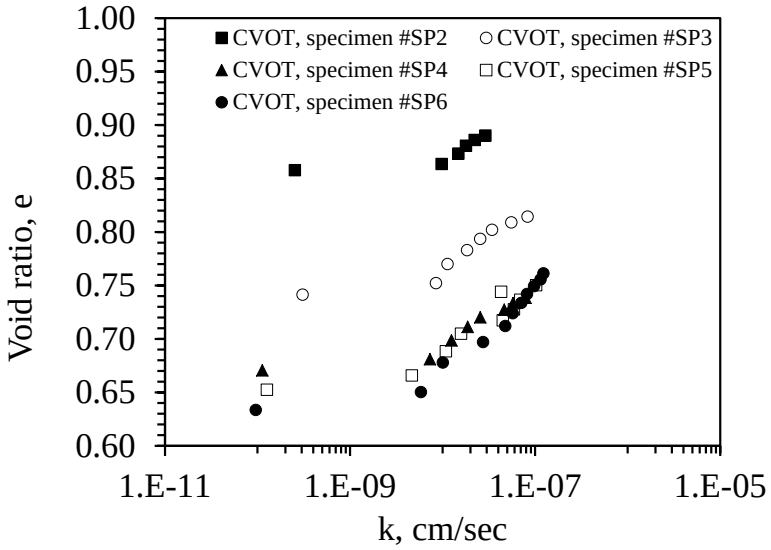

Figure 7.8. The evolution of *k* during the CVOTs as a function of void ratio.

CHAPTER 8

CONCLUSIONS AND RECOMMENDATIONS

8.1 Summary of Research Contribution

Focus of this research was to quantitatively understand the swelling mechanism of expansive soil. In particular, the swelling potential was studied by means of two measures, namely; swelling deformation and swelling pressure. Two factors had been controlled to study the swelling deformation behavior: relative humidity and moisture content. The swelling pressure behavior was investigated by restricting the specimens' axial deformation in the oedometer.

The experimental program in this study had two main parts with one part to measure the deformation of specimen under free swelling condition and identify the actual swelling zone, and another part consisting of a series of constant volume oedometer test (CVOT) and one-dimensional swelling test (1DST) to define correlations between the significant swelling deformation and both, the soil suction and the swelling pressure.

The experimental results were analyzed based on several constitutive relationships, such as void ratio- moisture content, moisture content- soil suction (SWRC), void ratio- swelling pressure, and cross relationships between these components.

Moreover, the experimental system facilitated the characterization of the coefficient of compressibility, coefficient of permeability and hydraulic diffusivity.

8.2 Conclusions

- Results from the free swelling tests on the soil in this study indicated the actual swelling for a degree of saturation higher than 80%. While for a degree of saturation lower than 80%, the deformation during swelling identified only the volumetric expansion associated with suction decrease, by which the specimens were mostly recovering their loss of total volume caused by the shrinkage processes.
- In this study, hygroscopic increase of moisture content and associated soil suction reduction for a range higher than 1.0 MPa were observed to have minimal effect on the volume change of the specimens, as the specimen are very stiff in that suction range. In the range of low soil suction (less than 1.0 MPa), the volume of the specimens was significantly increasing in the presence of liquid water until the soil was completely disintegrated.
- The CVOTs results indicated that the swelling pressure increased as the initial moisture content decreased. The sequence of the swelling pressure regeneration after each unloading stage signified only the swelling pressure due to soil suction dissipation.
- The 1DSTs results showed further increase of swelling deformation consistent with further dissipation of the associated residual suction and swelling pressure from the CVOTs.

- The measured values of m_v extrapolated from the CVOTs gave smaller values compared to those obtained from the 1DSTs. Irrespective of the dramatic increase of these values at the same swelling pressure level, the corresponding k values were always lower because the process required to equilibrate the change in volume lasted much longer during the 1DSTs.
- This apparent inconsistency, that the k values at higher void ratio were significantly reduced indicates that the rate of swelling may not be controlled by the hydraulic conductivity but rather by the ability of expansive clay material to absorb water. This means that the rate of swelling may not be controlled by Darcy's law at very low soil suction range (or very high moisture content).

8.3 Recommendations

Some of subjects and suggestions that could be pursued in the future research:

- Based on the experience gained from this research, improvements over the testing methodologies are recommended to obtain better quality data. Better controlled experiments with reliable moisture and suction control for saturation above 80% need to be developed in order to characterize the soil swelling in that range. This is particularly important as the most volume change takes place in that saturation range.
- The relationship between the swelling pressure and soil suction requires more experimental investigations in order to examine the influence of the confinement and surcharge pressure conditions on these inversely proportional stresses. This will help understand this relationship more deeply and will be useful in constructing analytical or numerical models.

- The experimental data obtained in this research can be used to obtain parameters for future analytical or numerical modeling.
- The conflict between the k values obtained from the CVOTs and 1DSTs at the same swelling pressure level indicates the need of more research to investigate the validation of using Darcy's law to describe the transient flow of water through the high expansive soils at low suction range since it has strong impact on the volume change behavior.

REFERENCES

Abdulla, W. S., and A-Abadi, A. M. (2010). "Cationic-electrokinetic improvement of an expansive soil," Applied Clay Science, 47, 343-350.

Abedi-Koupai, J., and Mehdizadeh, H. (2008). "Estimation of Osmotic Suction from Electrical Conductivity and Water Content Measurements in Unsaturated Soils," Geotechnical Testing Journal © ASTM, Vol. 31, No. 2, pp. 1-7.

Agus, S. S., Schanz, T., and Fredlund, D. G. (2010), "Measurements of suction versus water content for bentonite-sand mixtures," Can. Geotech. J., 47, 583-594.

Al-Homoud, A. S., Basma, A. A., Malkawi, A. I. H., and Al Bashabsheh, M. A. (1995). "Cyclic Swelling Behavior of Clay," Journal of Geotechnical Engineering, 562-565.

Alonso, E. E., Romero, E., Hoffmann, C., and Garcia-Escudero, E. (2005). "Expansive bentonite-sand mixture in cyclic controlled-suction drying and wetting," Engineering Geology, 81, 213-226.

Alonso, E. E., Vaunat, J., and Gens, A. (1999). "Modelling the mechanical behavior of expansive clays," Engineering Geology, 54, 173-183.

American Society for Testing and Materials (ASTM), (2007). "Standard Test Methods for Liquid Limit, Plastic Limit, and Plasticity Index of Soils," Designation ASTM D4318-05, Annual Book of ASTM Standards, Section 4, Volume 04.08, pp. 542-557.

American Society for Testing and Materials (ASTM), (2007). "Standard Test Methods for Specific Gravity of Soil Solids by Water Pycnometer," Designation ASTM D854-06 e1, Annual Book of ASTM Standards, Section 4, Volume 04.08, pp. 96-102.

American Society for Testing and Materials (ASTM), (2007). "Standard Test Method for Measurement of Soil Potential (Suction) using Filter Paper," Designation ASTM D5298-03, Annual Book of ASTM Standards, Section 4, Volume 04.08, pp. 1125-1130.

American Society for Testing and Materials (ASTM), (2007). "Standard Test Method for Pore Water Extraction and Determination of Soluble Salt Content of Soils by Refractometer,"

Designation ASTM D4542-07, Annual Book of ASTM Standards, Section 4, Volume 04.08, pp. 686-690.

American Society for Testing and Materials (ASTM), (2007). "Standard Test Methods for One-Dimensional Swell or Settlement Potential of Cohesive Soil," Designation ASTM D4546-08, Annual Book of ASTM Standards, Section 4, Volume 04.08, pp. 698-704.

Ashayeri, I., and Yasrebi, S. (2008). "Free-Swell and Swelling Pressure of Unsaturated Compacted Clays; Experiments and Neural Networks Modeling," Geotech. Geol. Eng., 137-153.

Baille, W., Tripathy, S., and Schanz, T. (2010). "Swelling pressure and one-dimensional compressibility behaviour of bentonite at large pressures," Applied Clay Science, 48, 324-333.

Basma, A. A., Al-Homoud, A. S., and Malkawi, A. H. (1995). "Laboratory assessment of swelling pressure of expansive soils," Applied Clay Science, 9, 355-368.

Basma, A. A., Al-Homoud, A. S., Malkawi, A. I. H., and Albashabsheh, M. A. (1996). "Swelling-shrinkage behavior of natural expansive clays," Applied Clay Science, 11, 211-227.

Bicalho, K. V. (1999). "MODELING WATER FLOW IN AN UNSATURATED COMPACTED SOIL," Doctoral Thesis, University of Colorado at Boulder.

Casagrande, and Fadum (1940). "Notes on Soil Testing for Engineering Purposes," Harvard University Graduate School Engineering Publication No.8.

Castellanos, E., Gens, A., Lloret, A., and Romero, E. (2006). "Influence of Water Chemistry on the Swelling Capacity of a High-Density Bentonite," ASCE, 692-972.

Chao, K. C., Nelson, J. D., Overton, D. D., and Cumbers, J. M. (2008). "Soil water retention curves for remolded expansive soils," Proceedings of the 1st European Conference on Unsaturated Soils, Durham, UK, pp. 243-248.

Chen, F. H. (1975). “FOUNDATIONS ON EXPANSIVE SOILS,” Elsevier Scientific Publishing Company, Amsterdam.

Cornelis, W.M., Corluy, J., Medina, H., Diaz, J., Hartmann, R., Van Meirvenne, M., and Ruiz, M. E. (2006). “Measuring and modeling the soil shrinkage characteristic curve,” Geoderma, 137, 179-191.

Craig, R. F. (2004). “Craig’s Soil Mechanics,” 7th edition, New York, Spon Press.

Cui, Y. J., Tang, A. M., Loiseau, C., and Delage, P. (2008). “ Determining the unsaturated hydraulic conductivity of a compacted sand-bentonite mixture under constant-volume and free-swell conditions,” Physics and Chemistry of the Earth, 33, S462-S471.

Cui, Y. J., Yahia-Aissa, M., and Delage, P. (2002). “A model for the volume change behavior of heavily compacted swelling clays,” Engineering Geology, 64, 223-250.

Cuisinier, O., and Masrouri, F. (2005). “Hydromechanical behaviour of a compacted swelling soil over a wide suction range,” Engineering Geology, 81, 204-212.

Das, B. M. (1998). “Pronciples of Geotechnical Engineering,” International Thomson Publishing.

Davidson, S. E., and Page, J. B. (1956). “Factors Influencing Swelling and Shrinking in Soils,” SSSA Proceedings, vol 20, 320-324.

Dawson, R. F. (1953). “Movement of small houses erected on an expansive clay soil,” Proc. 3rd Int. Conf. Soil Mech. Found. Eng., 1:346-350.

De Veaux, R., and Steele, J. M. (1989). “ACE Guided-Teansformation Method for Estimation of the Coefficient of Soil-Water Diffusivity,” Technometrics, Vol. 31, No. 1, pp. 91-97.

Delage, P., Howat, M. D., and, Cui, Y.J. (1998). “ The relationship between suction and swelling properties in a heavily compacted unsaturated clay,” Engineering Geology, 50, 31-48.

El-Sohby, M. A., and El-Sayed, A. R. (1981). “SOME FACTORS AFFECTING SWELLING OF CLAYEY SOILS,” Geotechnical Engineering, Vol. 12, 19-39.

Fattom, M., and Barakat, S. (2000). "Investigation of Three methods for Evaluating Swelling pressure of Soils," Environmental & Engineering Geoscience, Vol. VI, No. 3, pp. 293-299.

Ferber, V., Auriol, J., Cui, Y., and Magnan, J. (2009). "On the swelling potential of compacted high plasticity clays," Engineering Geology, 104, 200-210.

Fityus, S., and Buzzi, O. (2009). " The place of expansive clays in the framework of unsaturated soil mechanics," Applied Clay Science, 43, 150-155.

Fredlund, D. G. (1967). "Comparison of soil suction and one-dimensional consolidation characteristics of a highly plastic clay," The Emergence of Unsaturated Soil Mechanics, pp. 193-201.

Fredlund, D. G., and Rahardjo, H. (1993). "SOIL MECHANICS FOR UNSATURATED SOILS," John Wiley & Sons, Inc.

Freeze, R. A., and Cherry, J. A. (1979). "GROUNDWATER," A Simon & Schuster Company.

Gardner, W. H., and Gardner, W. (1951). "Flow of Soil Moisture in the Unsaturated State," Soil Science Society of America Journal, Vol. 15, Issue 15, pp. 42-50.

Gardner, W. H., and Hsieh, J. C. (1956). "Water Velocity in Unsaturated Porous Materials," Soil Science Society of America Journal, Vol. 20, No. 2, pp. 157-161.

Gens, A., and Alonso, E. E. (1992), " A framework for the behaviour of unsaturated expansive clays," Can. Geotech. J., 29, 1013-1032.

Guney, Y., Sari, D., Cetin, M., and Tuncan, M. (2007). " Impact of cyclic wetting-drying on swelling behavior of lime-stabilized soil," Building and Environment, 42, 681-688.

Holtz, W. G., and Gibbs, H. J. (1954). "ENGINEERING PROPERTIES OF EXPANSIVE CLAYS," American Society of Civil Engineers, Vol. 80, No. 516, pp. 1-15.

Hwang, C. (2002). "DETERMINATION OF MATERIAL FUNCTIONS FOR UNSATURATED FLOW," Doctoral Thesis, University of Colorado at Boulder.

Jennings, J. E. B., and Knight, K. (1957). “THE PREDICTION OF TOTAL HEAVE FROM THE DOUBLE OEDOMOTER TEST,” Proc. Symp. Expansive Clays (South Africa Inst. Of Civil Engineers, Johannesburg), Vol. 7, No. 9, pp. 13-19.

Jones, D. E., and Holtz, W. G. (1973). “ Expansive soils – the hidden disaster,” Civil Eng., ASCE, 43(8), 49-51.

Kariuki, P. C., and van der Meer, F. (2004). “A unified swelling potential index for expansive soils,” Engineering Geology, 72, 1-8.

Kassiff, G., and Ben Shalom, A. (1971). “Experimental Relationship Between Swell Pressure And Suction,” Geotechnique, vol. 21, Issue 3, 245-255.

Kehres, A. (1983). “ Isothermes de deshydration des argilles, energies d’hydration – Diagrammes de pores surface internes et externs,” Doctoral Thesis, Universite Paul Sabatier de Toulouse.

Kim, D. J., Jaramillo, R. A., Vauclin, M., and Feyen, J. (1999). “Modeling of soil deformation and water flow in a swelling soil,” Geoderma, 92, 217-238.

Komine, H. (2004). “Simplified evaluation for swelling characteristics of bentonites,” Engineering Geology, 71, 265-279.

Komine, H. (2008). “Theoritical equations on hydraulic conductivities of bentonite based buffer and backfill for underground disposal of radioactive wastes,” Geotechnical and Geoenvironmental Engineering, American Society of Civil Engineers (ASCE), 134 (4), 497-508.

Komine, H. (2010). “Predicting hydraulic conductivity of sand-bentonite mixture backfill before and after swelling deformation for underground disposal of radioactive wastes,” Engineering Geology, 114, 123-134.

Komine, H., and Ogata, N. (1994). “Experimental study on swelling characteristics of compacted bentonite,” Can. Geotech. J, 31, 478-490.

Komornik, A., and David, D. (1969). “PREDICTION OF SWELLING PRESSURE OF CLAYS,” Journal of the SOIL MECHANICS AND FOUNDATIONS DIVISION, Proceedings of the American Society of Civil Engineers, Vol. 95 No.SM1, 209-225.

Laird, D. A., Shang, C., and Thompston, M. L. (1995). ‘ Hysteresis in Crystalline Swelling of Smectites,” Journal of Colloid and Interface Science, 171, 240-245.

Laird, D. A. (2006). “ Influence of layer charge on swelling of smectites,” Applied Clay Science, 34, 74-87.

Leong, E. C., He, L., and Rahardjo, H. (2002). “ Factors Affecting the Filter Paper Method for Total and Matric Suction Measurements,” J Geotechnical Testing © ASTM, Vol. 25, No. 3, pp. 1-12.

Leong, E. C., Tripathy, S., and Rahardjo, R. (2003). “Total suction measurement of unsaturated soils with a device using the chilled-mirror dew-point technique,” Geotechnique, vol. 53, issue 2, pp. 173-182.

Likos, W. J., and Lu, N. (2003). “ Automated Humidity System for Measuring Total Suction Characteristics of Clay,” Geotechnical Testing Journal © ASTM, Vol. 26, No.2, pp. 1-12.

Likos, W. J. (2004). “Measurement of Crystalline Swelling in Expansive Clay,” Geotechnical Testing Journal © ASTM, Vol. 27, No. 6, pp. 1-7.

Lu, N., and Likos, W. (2004). “UNSATURATED SOIL MECHANICS,” John Wiley & Sons, Inc.

Madsen, F. T., and Müller-Vonmoos, M. (1989). “The swelling behavior of clays,” Appl. Clay Sci., 4, 143-156.

Masrouri, F., Bicalho, K. V., and Kawai, K. (2008). “Laboratory Hydraulic Testing in Unsaturated Soils,” Geotech. Geol. Eng., 26, 691-704.

Miao, L., Jing, F., and Huoston, S. L. (2006). “ Soil-water Characteristic Curve of Remolded Expansive Soils,” ASCE, Unsaturated Soils, 997-1004.

Miao, L., Liu, S., and Lai, Y. (2002). " Research of soil-water characteristics and shear strength features of Nanyang exoansive soil," Engineering Geology, 65, 261-267.

Miller, D. J., and Nelson, J. D. (2006). " Osmotic Suction in Unsaturated Soil Mechanics," ASCE, Unsaturated Soils, 1382-1393.

Mitchell, J. K., and Soga, K. (2005). "FUNDAMENTALS OF SOIL BEHAVIOR," JOHN WILEY & SONS, INC.

Murray, H. H. (2007). "APPLIED CLAY MINERALOGY: OCCURRENCES, PROCESSING AND APPLICATION OF KAOLINS, BENTONITES, PALYGORSKITE-SEPIOLITE, AND COMMON CLAYS," Elsevier.

Nakano, M., Amemya, Y., and Fujii, K. (1986). "SATURATED AND UNSATURATED HYDRAULIC CONDUCTIVITY OF SWELLING CLAYS," Soil Science, Vol. 141, No. 1, pp. 1-8.

Nelson, J. D., and Miller, D. J. (1992). "EXPANSIVE SOILS: PROBLEMS AND PRACTICE IN FOUNDATION AND PAVEMENT ENGINEERING," John Wiley & Sons, Inc.

Nowamooz, H., and Masrouri, F. (2008). " Hydromechanical behaviour of an expansive bentonite/silt mixture in cyclic suction-controlled drying and wetting tests," Engineering Geology, 101, 154-164.

Nowamooz, H., and Masrouri, F. (2009). "Density-dependent hydromechanical behaviour of a compacted expansive soil," Engineering Geology, 106, 105-115.

Nowamooz, H., and Masrouri, F. (2010). "Relationships between soil fabric and suction cycles in compacted swelling soils," Engineering Geology, 114, 444-455.

Olsen, H. W., Repola, K, and Wienecke, C. J. (2008), "Chilled Mirror Measurement of Soil Water Retention Curves," ASCE, GEO-VELOPMENT, geotechnical practice publication No. 5, 127-141.

Patrick, P. K., Olsen, H. W., and Higgins, J. D. (2007). "Comparison of Chilled-mirror Measurements and Filter Paper Estimates of Total Soil Suction," Geotechnical Testing Journal, Vol. 30, No. 5, 1-8.

Peck, A. J., and Rabbidge , R. M. (1966). "Soil water potential: direct measurement by a new technique," Sience, N.Y., 151, 1385-6.

Philip, J. R. (1968). "KINETICS OF SORPTION AND VOLUME CHANGE IN CLAY-COLLOID PASTES," Aus. J. Soil Res., 6, 249-267.

Philip, J. R. (1969). "Hydrostatics and Hydrodynamics in Swelling Soils," Water Resources Research, Vol. 5, No. 5, 1070-1077.

Puppala, A. J., Punthutaecha, K., and Vanapalli, S. K. (2006). " Soil-Water Characteristics Curves of Stabilized Expansive Soils," Journal of Geotechnical and Geoenvironmental Engineering © ASCE, 736-750.

Pusch, R., and Carlsson, T. (1985). "THE PHYSICAL STATE OF PORE WATER OF Na SMECTITE USED AS BARRIER COMPONENT," Engineering geology, 21, 257-265.

Pusch, R., and Yong, R. N. (2006). "Microstructure of Smectite Clays and Engineering Performance," Taylor & Francis.

Rao, S. M., and Shivananda, P. (2005). "Role of osmotic suction in swelling of salt-amended clays," Can. Geotech. J., 42, 307-315.

Romero, E., Alonso, E. E., and Hoffmann, C. (2006). "Behavior of bentonite-sand mixtures subjected to cyclic drying and wetting paths," ASCE, Unsaturated Soils, 1005-1016.

Scott, R. (1963). "PRINCIPLES OF SOIL MECHANICS," ADDISON-WESLEY PUBLISHING COMPANY, INC.

Shanker, N. B., Rao, A. S., and Swamy, A. S. R. (1982). "Swelling Behaviour of Undisturbed and Remoulded Samples of Black Cotton Clay," Indian Geotechnical Journal, vol. 12, 152-159.

Shanker, N. B., Ratnam, M. V., and Rao, A. S. (1987). "Multi-dimensional Swell Behaviour of Expansive Clays," Proceedings, 6th International Conference of Expansive Soils, New Delhi, India, 143-147.

Sharma, R. S. (1998). "Mechanical Behavior of Unsaturated Highly Expansive Clays," Doctoral Thesis, University of Oxford.

Shuai, F. (1996). "SIMULATION OF SWELLING PRESSURE MEASUREMENTS ON EXPANSIVE SOILS," Doctoral Thesis, University of Saskatchewan.

Smiles, D. E., and Rosenthal, M. J. (1968). "THE MOVEMENT OF WATER IN SWELLING MATERIALS," Aust. J. Soil Res., 6, 237-248.

Sreedeep, S., and Singh, D. N. (2006). "Methodology for determination of osmotic suction of soils," Geotechnical and Geological Engineering ©Springer, 24, 1469-1479.

Taylor, D. W. (1942). "Research on Consolidation of Clays," Serial No. 82, Department of Civil and Sanitary Engineering, Massachusettes Institute of Technology, Cambridgem Mass.

Terzaghi, K. (1925). "Erdbaumechanik auf Bodenphysikalischer Grundlager," Deuticke, Vienna.

Thompson, R. W., Perko, H. A., and Rethamel, W. D. (2006). "Comparison of Constant Volume Swell Pressure and Oedometer Load-Back Pressure," Unsaturated Soil (GSP), vol. 2, No. 147, pp. 1787-1798.

Tripathy S., Subba Rao, K. S., and Fredlund, D. G. (2002)."Water content – void ratio swell-shrink paths of compacted expansive soils," Can. Geotech. J., 39, 938-959.

Villar, M. V., and Lloret, A. (2008). "Influence of dry density and water content on the swelling of a compacted bentonite," Applied Clay Science, 39, 38-49.

Wayllace, A., and Likos, W. (2007). "Microstructural Fabric Model for Upscaling Interlayer Volume Changes in Expansive Clay," ASCE, Geo-Denver, 1-9.

Windal, T., and Shahrour, I. (2002). "Study of the swelling behavior of a compacted soil using flexible odometer," Mechanics Research Communications, 29, 375-382.

Yevnin, A., and Zaslavsky, D. (1970). “Some factors affecting compacted clay swelling,” Canadian Geotechnical Journal, Vol. 7, Issue 1, 79-89.

Yitagesu, F. A., van der Meer, F., van der Werff, H., and Zigterman, W. (2009). “Quantifying engineering parameters of expansive soils from their reflectance spectra,” Engineering Geology, 105, 151-160.

Yong, R. N. (1999). “Soil suction and soil-water potential in swelling clays in engineering clay barriers,” Engineering Geology, 54, 3-13.

Zhou, J., and Yu, J. (2005). “Influences affecting the soil-water characteristic curve,” J Zhejiang Univ SCI, 6A (8), 797-804.

Zur, B. (1966). “Osmotic control of the matric soil-water potential; I. Soil-water system,” Soil Sci. U.S.A., 102, No. 6, 394-398.

APPENDIX - A

A.1 Principle of Mass Conservation (After Lu and Likos, 2004)

Figure A.1.1 shows elemental volume of soil where the principle of mass conservation applied. The mass of liquid (e.g., water) is conserved by assuming that the net flux of inflow and outflow is equal to the amount of water being lost or gained in the elemental volume of soil. By setting three-dimensional Cartesian coordinate system together with assigning the positive directions, inflow Equation (A.1) and outflow Equation (A.2) are derived as follows:

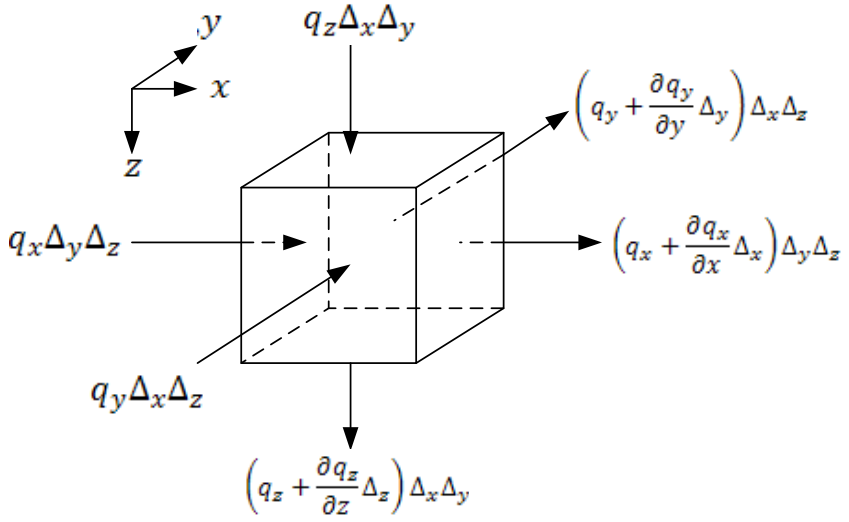

Figure A.1.1. Elemental volume of soil and continuity requirements for fluid flow (after Lu and Likos , 2004)

$$q_{in} = \rho_f\left(q_x\Delta_y\Delta_z + q_y\Delta_x\Delta_z + q_z\Delta_x\Delta_y\right) \tag{a.1}$$

$$q_{out} = \rho_f\left[\left(q_x+\frac{\partial q_x}{\partial x}\Delta_x\right)\Delta_y\Delta_z + \left(q_y+\frac{\partial q_y}{\partial y}\Delta_y\right)\Delta_x\Delta_z + \left(q_z+\frac{\partial q_z}{\partial z}\Delta_z\right)\Delta_x\Delta_y\right] \tag{a.2}$$

where, ρ_f is the density of fluid (mass/length^3); q_x, q_y and q_z (length/time) are the flow rate of fluid in directions of x,y and z respectively; and Δ_x, Δ_y and Δ_z are the dimensions of elemental volume of soil in directions of x,y and z respectively.

The loss or gain of water is also expressed as storage of fluid, which is the net mass change of fluid (e.g., water) in the elemental volume of soil per rate change of time as follows:

$$\frac{\partial m_f}{\partial t} \tag{a.3}$$

$$m_f = \rho_f V_f \tag{a.4}$$

Where, m_f if the mass of fluid, ρ_f is the density of fluid, V_f is the volume of fluid, and t is the period of time of fluid flow through soil voids.

By substituting $n = {V_v}/{V_t}$ and $S = {V_f}/{V_v}$ into Equation A.4, where, n is the soil porosity, S is the degree of saturation, and V_v, and V_t are volume of void and total volume, respectively; the storage term (A.3) is equal to:

$$\frac{\partial m_f}{\partial t} = \frac{\partial}{\partial t}\left(\rho_f\, S\, n\right) \Delta_x \Delta_y \Delta_z \tag{a.5}$$

$$\frac{\partial m_f}{\partial t} = \frac{\partial\left(\rho_f \theta\right)}{\partial t} \Delta_x \Delta_y \Delta_z \tag{a.6}$$

where, θ is the volumetric water content that describes how much volume of water in the unit volume of soil.

The governing equation of transient flow through soil is therefore, can be derived by equalizing the principle of mass conservation with the storage term as follows:

$$-\rho_f\left(\frac{\partial q_x}{\partial x}\Delta_x\Delta_y\Delta_z+\frac{\partial q_y}{\partial y}\Delta_y\Delta_x\Delta_z+\frac{\partial q_z}{\partial z}\Delta_z\Delta_x\Delta_y\right)=\frac{\partial\left(\rho_f\theta\right)}{\partial t}\Delta_x\Delta_y\Delta_z \qquad \text{(a.7)}$$

By simplifying the above equation:

$$-\rho_f\left(\frac{\partial q_x}{\partial x}+\frac{\partial q_y}{\partial y}+\frac{\partial q_z}{\partial z}\right)=\frac{\partial\left(\rho_f\theta\right)}{\partial t} \qquad \text{(a.8)}$$

The governing Equation (A.8) is also called continuity equation of transient flow. The general continuity equation can be designated according to soil conditions as follows:

1. $\left(\frac{\partial q_x}{\partial x}+\frac{\partial q_y}{\partial y}+\frac{\partial q_z}{\partial z}\right)=0$ is a condition where a soil is saturated and incompressible and seepage through the soil is at steady state condition (water flow through saturated soil problem). The density of fluid is constant.
2. $-\left(\frac{\partial q_x}{\partial x}+\frac{\partial q_y}{\partial y}+\frac{\partial q_z}{\partial z}\right)=\frac{\partial n}{\partial t}$ is a condition where a soil is saturated and compressible (consolidation of saturated soil problem). The density of fluid is constant.
3. $-\left(\frac{\partial q_x}{\partial x}+\frac{\partial q_y}{\partial y}+\frac{\partial q_z}{\partial z}\right)=n\frac{\partial S}{\partial t}$ is a condition where soil is unsaturated and incompressible (flow of water through unsaturated incompressible soil problem). The density of fluid is constant.
4. $-\left(\frac{\partial q_x}{\partial x}+\frac{\partial q_y}{\partial y}+\frac{\partial q_z}{\partial z}\right)=n\frac{\partial S}{\partial t}+S\frac{\partial n}{\partial t}$ is a condition where a soil is unsaturated and compressible (flow of water through unsaturated compressible soil problem). The density of fluid is constant.

A.2 Transient flow in saturated soil

If the soil is saturated, isotropic and homogeneous, two additional conditions may apply to the governing equation as follows:

1. $q_x = q_y = q_z = q = -k\,i = -k\frac{dh}{dl}$, where k is hydraulic conductivity of saturated soil, i is hydraulic gradient, h is total head loss per a given distance .
2. $\frac{\partial(\rho_f\, n)}{\partial t} = \rho_f S_s \frac{\partial h}{\partial t}$, where S_s is a specific storage term.

Thus, the general governing equation can be rewritten in the form of diffusion partial differential equation by assuming a constant fluid density:

$$\frac{\partial^2 h}{\partial x^2} + \frac{\partial^2 h}{\partial y^2} + \frac{\partial^2 h}{\partial z^2} = \frac{S_s}{k}\frac{\partial h}{\partial t} \tag{a.9}$$

or,

$$D\left(\frac{\partial^2 h}{\partial x^2} + \frac{\partial^2 h}{\partial y^2} + \frac{\partial^2 h}{\partial z^2}\right) = \frac{\partial h}{\partial t} \tag{a.10}$$

Where, $D\left(L^2/T\right) = \frac{k}{S_s}$ is hydraulic diffusivity of transient flow in saturated soil.

A.3 Transient flow in unsaturated soil

The hydraulic conductivity of unsaturated soil is a function of soil suction. The soil suction is generalized as matric suction ψ_m or negative pore water pressure head. If the osmotic suction ψ_o is negligible, the total head loss h is algebraic sum of matric suction head and elevation head ψ_g. Therefore, the governing equation can be rewritten as follows:

$$\frac{\partial}{\partial x}\left[k_x(\psi_m)\frac{\partial \psi_m}{\partial x}\right]+\frac{\partial}{\partial y}\left[k_y(\psi_m)\frac{\partial \psi_m}{\partial y}\right]+\frac{\partial}{\partial z}\left[k_z(\psi_m)\frac{\partial \psi_m}{\partial z}+1\right]=\frac{\partial \theta}{\partial \psi_m}\frac{\partial \psi_m}{\partial t} \qquad \text{(a.12)}$$

where, $\frac{\partial \theta}{\partial \psi_m}=C(\psi_m)$ is the specific moisture capacity that requires SWCC to be achieved.

The k function of unsaturated soil can also be a function of θ if the Darcy's law is rewritten as follows:

$$q=-k(\theta)\frac{\partial h}{\partial \theta}\frac{\partial \theta}{\partial l}=-D(\theta)\frac{\partial \theta}{\partial l} \qquad \text{(a.13)}$$

where, l is the a position (length) at specified flow directions $\left(x, y, or\ z\ (gravity\ direction)\right)$, and $D(\theta)={}^{k(\theta)}\!/_{C(\theta)}$ is the hydraulic diffusivity.

By incorporating Equation (a.13) into Equation (a.8), the following Equation (a.14) can be expressed as follows:

$$\frac{\partial}{\partial x}\left[D_x(\theta)\frac{\partial \theta}{\partial x}\right]+\frac{\partial}{\partial y}\left[D_y(\theta)\frac{\partial \theta}{\partial y}\right]+\frac{\partial}{\partial z}\left[D_z(\theta)\frac{\partial \theta}{\partial z}\right]+\frac{\partial k_z(\theta)}{\partial z}=\frac{\partial \theta}{\partial t} \qquad \text{(a.14)}$$

A typical relationship between SWCC and specific moisture capacity function for a silty soil is shown in Figure A.3.1.

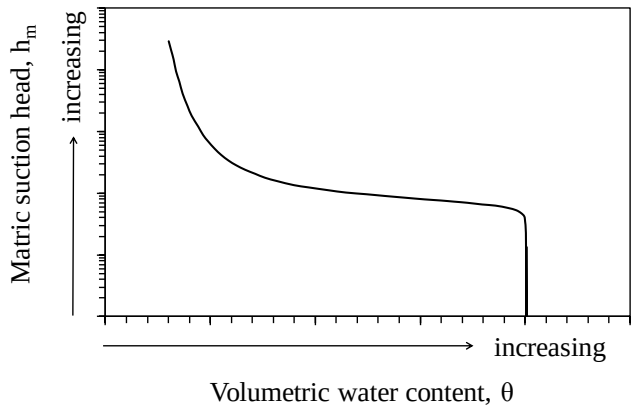

(a)

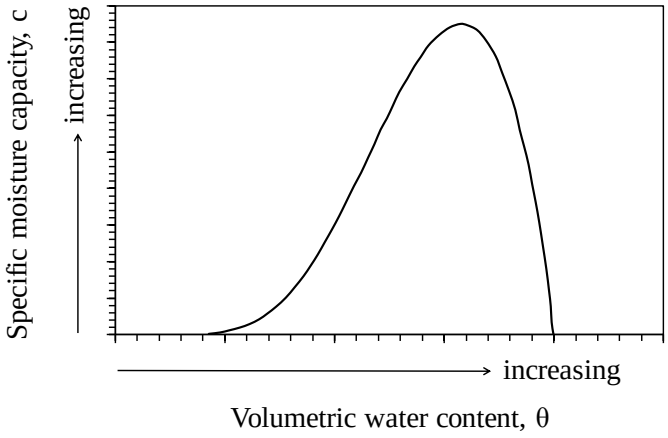

(b)

Figure A.3.1. (a) Soil-water characteristic curve and (b) specific moisture capacity function for typical silty soil (after Lu and Likos, 2004).

APPENDIX – B

B.1 Time Rate of Consolidation (After Das, 1998)

The flow of water in one direction frame is one of the assumptions used to mathematically derive the time rate consolidation theory developed by Terzaghi (1925), as shown in Figure B.1.1. This theory considers the rate of volume change to be equal to the net flux of inflow and outflow of water through an elemental soil volume.

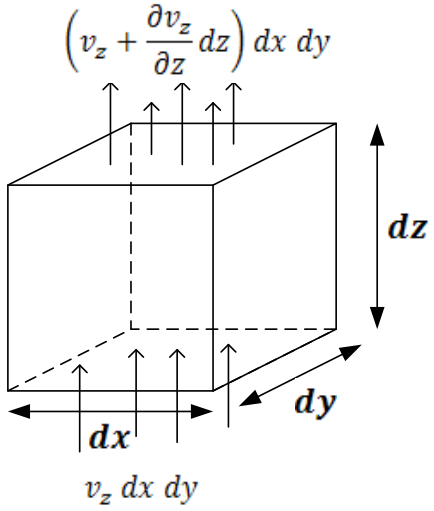

Figure B.1.1: One directional flow of water during consolidation (after Das, 1998).

Thus,

$$\left(v_z + \frac{\partial v_z}{\partial z} dz\right) dx\ dy - v_z\ dx\ dy = \frac{\partial V}{dt} \qquad \text{(b.1)}$$

where, V is volume of the soil element, and v_z is the velocity of flow in z direction.

By simplifying Equation (b.1) and applying Darcy's law, the following equation can be derived:

$$-\frac{k}{\gamma_w}\frac{\partial^2 u}{\partial z^2} = \frac{1}{dx\ dy\ dz}\frac{\partial V}{\partial t} \qquad \text{(b.2)}$$

where, V_s is volume of soil solids, and V_v is volume of voids.

Since the soil solids are incompressible, there is no change in volume of solids with time. Thus:

$$\frac{\partial V_s}{\partial t} = 0 \qquad \text{(b.4)}$$

and,

$$V_s = \frac{V}{1+e_o} = \frac{dx\ dy\ dz}{1+e_o} \qquad \text{(b.5)}$$

Substitution for Equations (b.4) and (b.5) in Equation (b.3) yields to

$$\frac{\partial V}{\partial t} = \frac{dx\ dy\ dz}{1+e_o}\frac{\partial e}{\partial t} \qquad \text{(b.6)}$$

where, e_o is the initial void ratio.

Substitution for Equation (b.6) in Equation (b.2) yields to

$$-\frac{k}{\gamma_w}\frac{\partial^2 u}{\partial z^2} = \frac{1}{1+e_o}\frac{\partial e}{\partial t} \qquad \text{(b.7)}$$

The change in void ration is assumed to be linearly related to the increase of effective stress (that is, decrease of excess pore water pressure). The ratio of the change in void ration to the change in pre water pressure is called coefficient of compressibility a_v and can be assumed constant for a narrow range of pressure increase:

$$\partial e = a_v \partial(\Delta p') = -a_v \partial u \tag{b.8}$$

where, $\partial(\Delta p')$ is the change in effective pressure, a_v is coefficient of compressibility.

By combining Equations (b.8) and (b.7) leads to:

$$-\frac{k}{\gamma_w}\frac{\partial^2 u}{\partial z^2} = -\frac{a_v}{1+e_o}\frac{\partial u}{\partial t} = -m_v \frac{\partial u}{\partial t} \tag{b.9}$$

where, m_v is the coefficient of volume compressibility.
or,

$$c_v \frac{\partial^2 u}{\partial z^2} = \frac{\partial u}{\partial t} \tag{b.10}$$

where, c_v is the coefficient of coefficient of consolidation.

Thus,

$$c_v = \frac{k}{\gamma_w \, m_v} \tag{b.11}$$

APPENDIX-C

C.1 Weight-Volume Relationship of Soil (After Das, 1998)

Naturally, the soil element has three phases namely; solids, water, and air. Figure C.1.1(a) shows the natural state of the soil element and Figure C.1.1(b) shows the three phases of it.

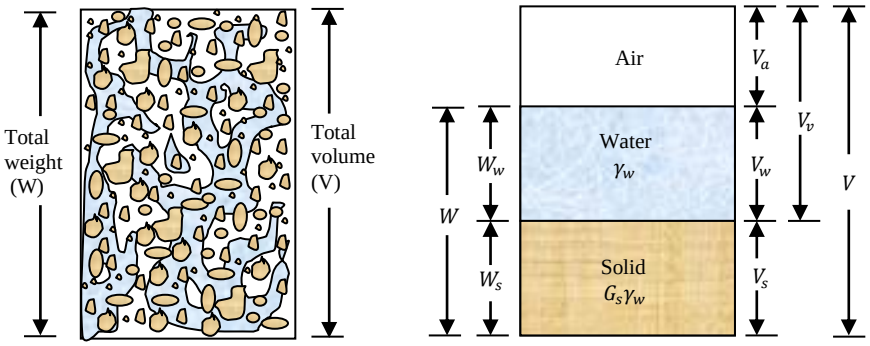

Figure C.1.1. (a) Soil element in natural state; (b) three phases of the soil element (after Das, 1998).

The total volume can be expressed as:

$$V = V_s + V_v = V_s + V_w + V_a \qquad \text{(c.1.1)}$$

where, V is total volume; V_s is volume of solids; V_v is volume of voids, V_w is volume of water in the voids; and V_a is volume of air in the voids.

Similarly, the total weight of the soil element can be expressed as:

$$W = W_s + W_w \qquad \text{(c.1.2)}$$

where, W_s is weight of soil solids, and W_w is weight of water.

Three volume relationships can be obtained from the above figure which are:

$$e = \frac{V_v}{V_s} \quad \text{(c.1.3)}$$

where, e is volume of voids,

$$n = \frac{V_v}{V} \quad \text{(c.1.4)}$$

where, n is porosity, and

$$S = \frac{V_w}{V_v} \quad \text{(c.1.5)}$$

where, S is degree of saturation.

Three general weight relationships can be obtained from the previous figure which are:

$$\omega = \frac{W_w}{W_s} \quad \text{(c.1.6)}$$

where , ω is moisture content,

$$\gamma = \frac{W}{V} \quad \text{(c.1.7)}$$

where, γ is unit weight of soil, and

$$\gamma_d = \frac{W_s}{V} \quad \text{(c.1.8)}$$

where, γ_d is dry unit weight.

By considering the unity of V_s, the volume-weight relationship can be obtained as follows:

$$W_s = G_s \gamma_w \quad \text{(c.1.9)}$$

where, G_s is specific gravity of soil solids, and γ_w is unit weight of water.

By substituting Equation c.1.9 into Equation c.1.6:

$$W_w = \omega W_s = \omega G_s \gamma_w \quad \text{(c.1.10)}$$

Substitution of Equation c.1.9 into c.1.7 yields to:

$$\gamma = \frac{W}{V} = \frac{W_s + W_w}{V} = \frac{G_s\gamma_w + \omega G_s\gamma_w}{1+e} = \frac{(1+\omega)G_s\gamma_w}{1+e} \quad \text{(c.1.11)}$$

By combining Equation c.1.9 with Equation c.1.8 leads to:

$$\gamma_d = \frac{W_s}{V} = \frac{G_s\gamma_w}{1+e} \quad \text{(c.1.12)}$$

Rearranging the above Equation leads to:

$$e = \frac{G_s\gamma_w}{\gamma_d} - 1 \quad \text{(c.1.13)}$$

Considering the fact that:

$$V_w = \frac{W_w}{\gamma_w} = \frac{\omega G_s\gamma_w}{\gamma_w} = \omega G_s \quad \text{(c.1.14)}$$

thus,

$$S = \frac{V_w}{V_v} = \frac{\omega G_s}{e} \quad \text{(c.1.15)}$$

or,

$$Se = \omega G_s \quad \text{(c.1.16)}$$

APPENDIX-D

D.1 A Summary of ATT Instruction Manual for Chilled-Mirror Dew Point Meter

1. The first step was to warm up the device (about thirty minutes) and ensure that the suction and temperature readings were set to zero on the main menu screen. Then, the equilibration solution (Potassium Chloride (KCl)) was poured in the device cup and the test specimen was placed in another device cup (with the lid on) on black circle spots on top of the device to let the device, the KCl, and the specimen equilibrate. The specimen, the cup, and the lid were then, weighed.
2. The device was set to "continuous" mode so that the elapsed time, temperature and suction measurements were continuously recorded after about every four minutes.
3. The device was set to a set-point temperature equal to or slightly higher than the estimated highest room temperature (preferably less than 0.5^0 C).
4. The personal computer was then, turn on to check the communication between it and the device.
5. After the device and personal computer setups were accomplished, the KCl cup was inserted in the device drawer and carefully slid into chamber. The device would read the the difference between the base temperature (Tb) and the solution (or specimen) temperature (Ts). It was ensured that the solution temperature is less than the base temperature and thus, the reading of Ts-Tb must be between 0^0 C to -1^0 C. If Ts was greater than Tb, the device would chill the KCl or the specimen temperature down to a targeted temperature.

6. Once the drawer knob was turn to “read” position, the device started to take the measurements and ported (after four minutes of measurement cycle) to the personal computer. The test was run until the equilibration state of temperature and suction had been reached with time.
7. After equilibrating the device, the knob was turned to “open” and the solution cup was carefully removed from the chamber drawer and discarded.
8. The device was then ready for the test and the steps 5 to 7 were used for testing the specimen.
9. The specimen and its cup with the lid on were weighed. After that, the lid was removed and the cup with the specimen was oven dried, cooled in desiccators and weighed.

APPENDIX-E

E.1 The Shrinkage Test and the Free Swelling Test Results

This section consists of the experimental data obtained from the shrinkage tests and the free swelling tests as shown in Figures E.1.1. to E.1.3.

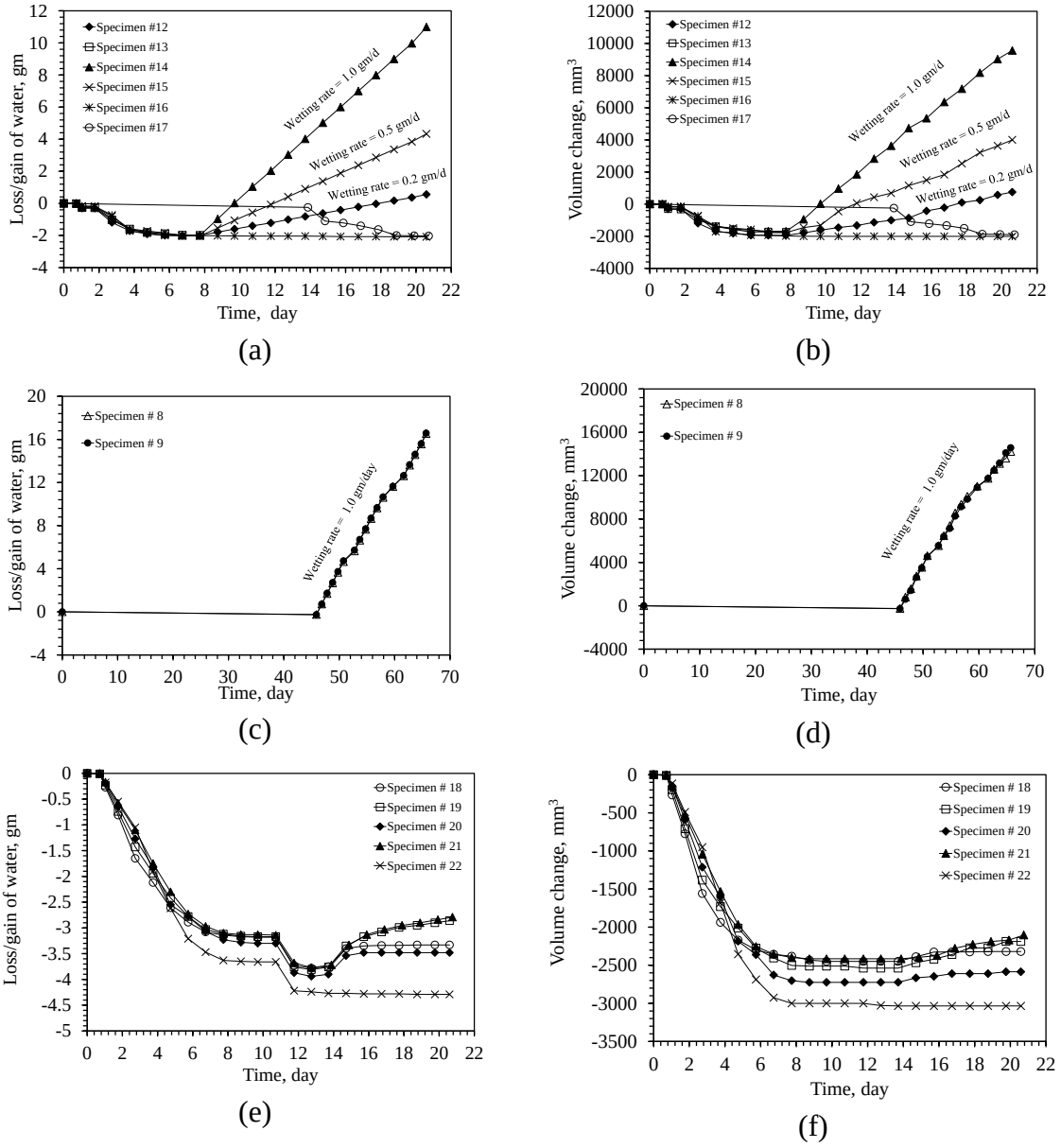

Figure E.1.1. The shrinkage and free swelling tests in terms of loss/ gain of water (a, c, and e) and the corresponding volume change (b, d, and f).

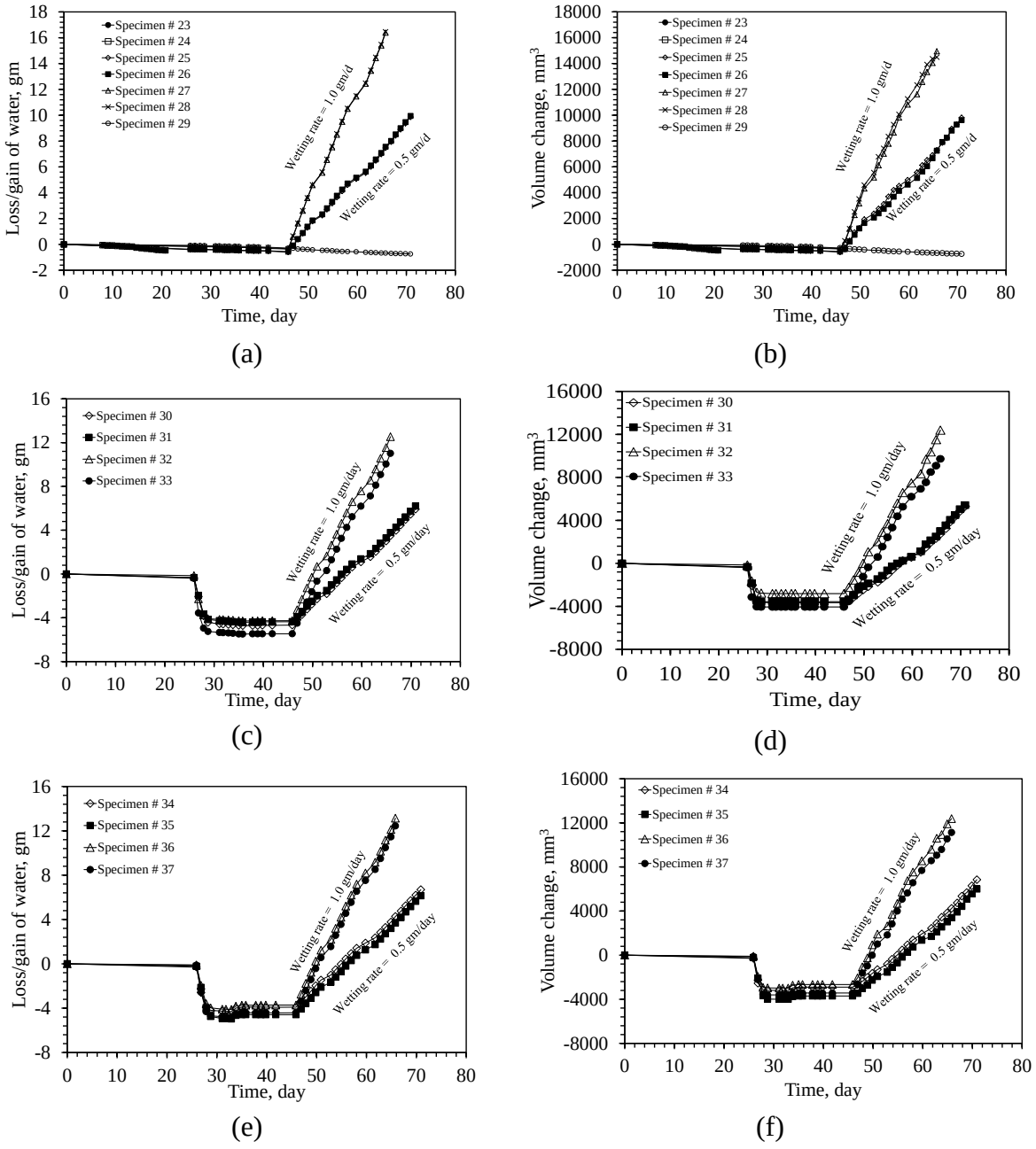

Figure E.1.2. The shrinkage and free swelling tests in terms of loss/ gain of water (a, c, and e) and the corresponding volume change (b, d, and f).

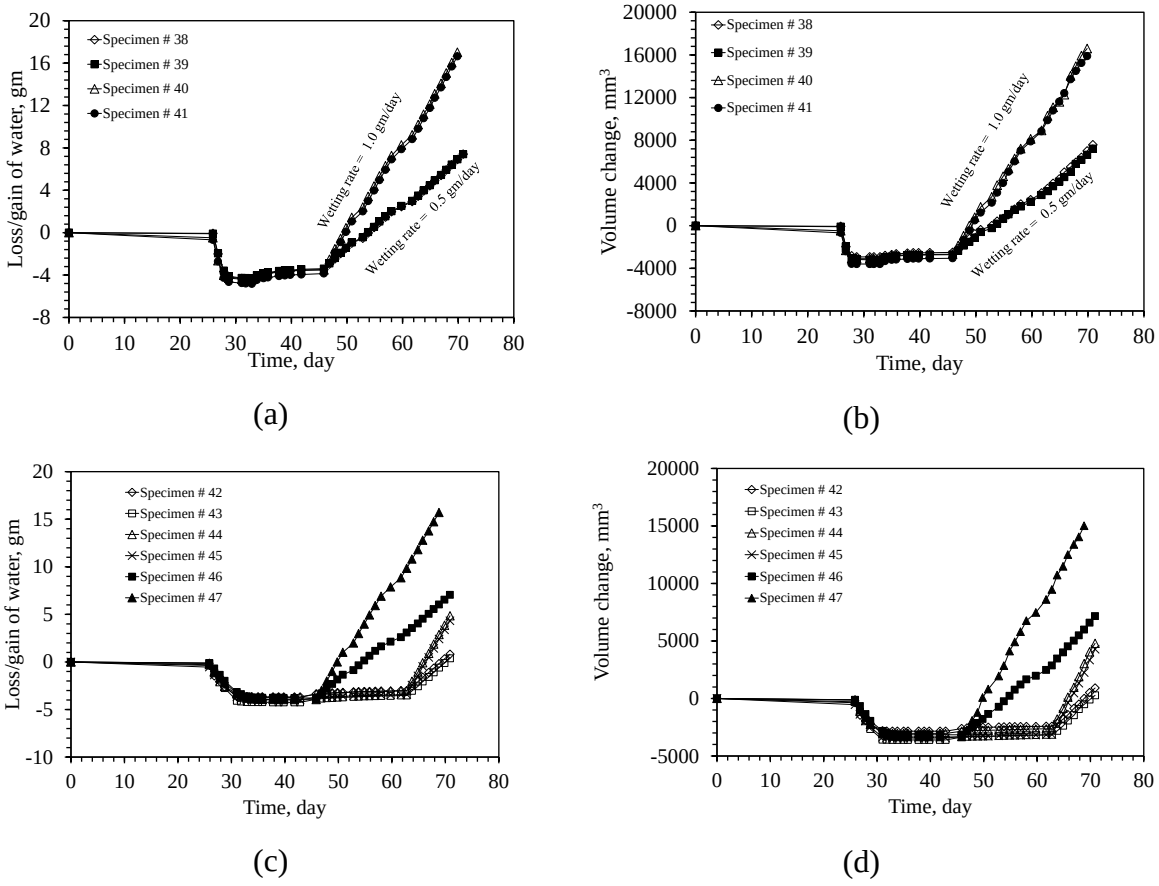

Figure E.1.3. The shrinkage and free swelling tests in terms of loss/ gain of water (a and c) and the corresponding volume change (b and d).

E.2 Soil Suction Test Results

E.2.1 Results Obtained by the Chilled-Mirror Dew Point Device (WP4-T)

This section consists of the experimental data obtained by using chilled-mirror dew point device (WP4-T) as shown in Figure E.1.1.

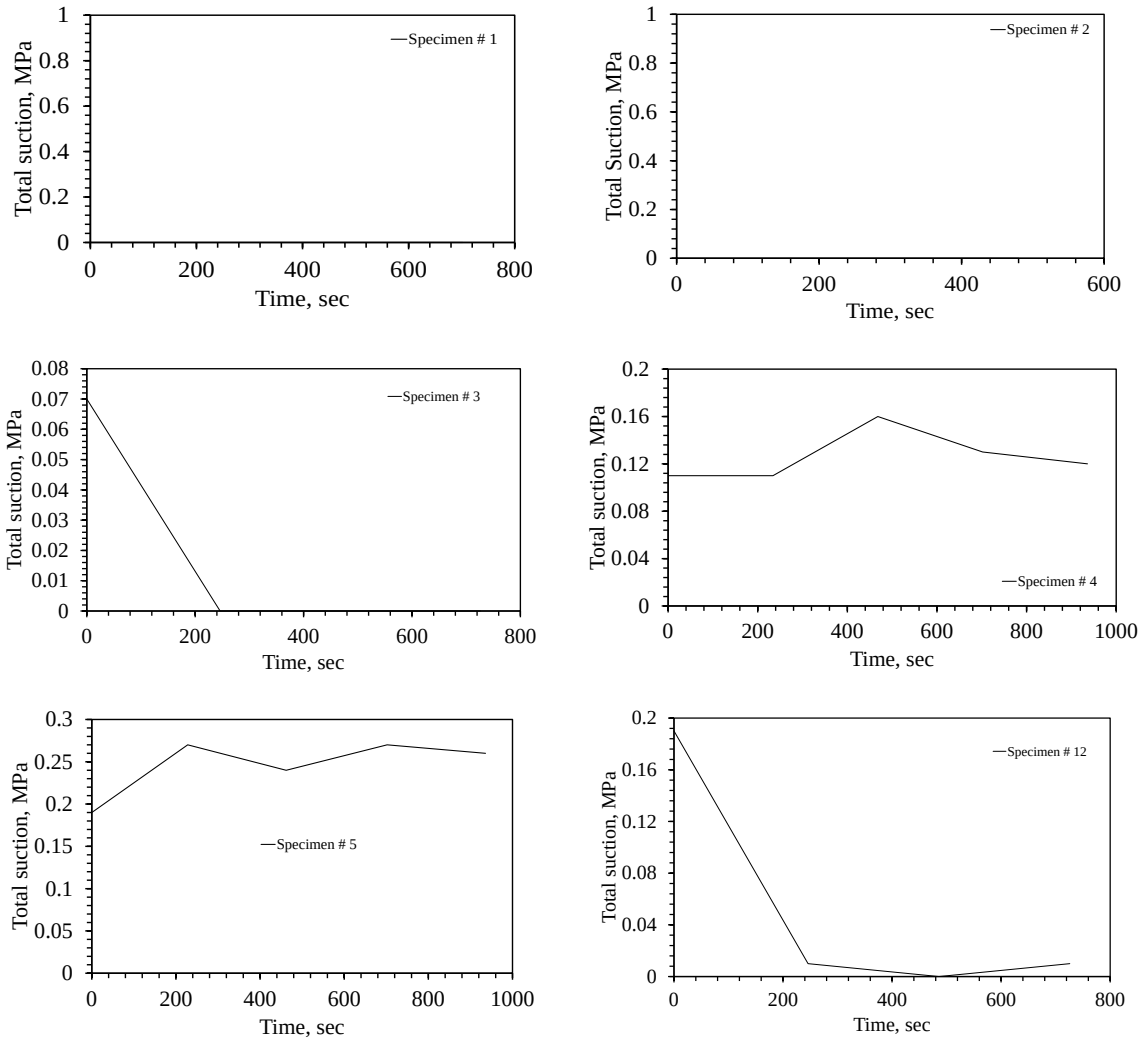

Figure E.2.1. The data of total suction with time obtained by WP4-T device.

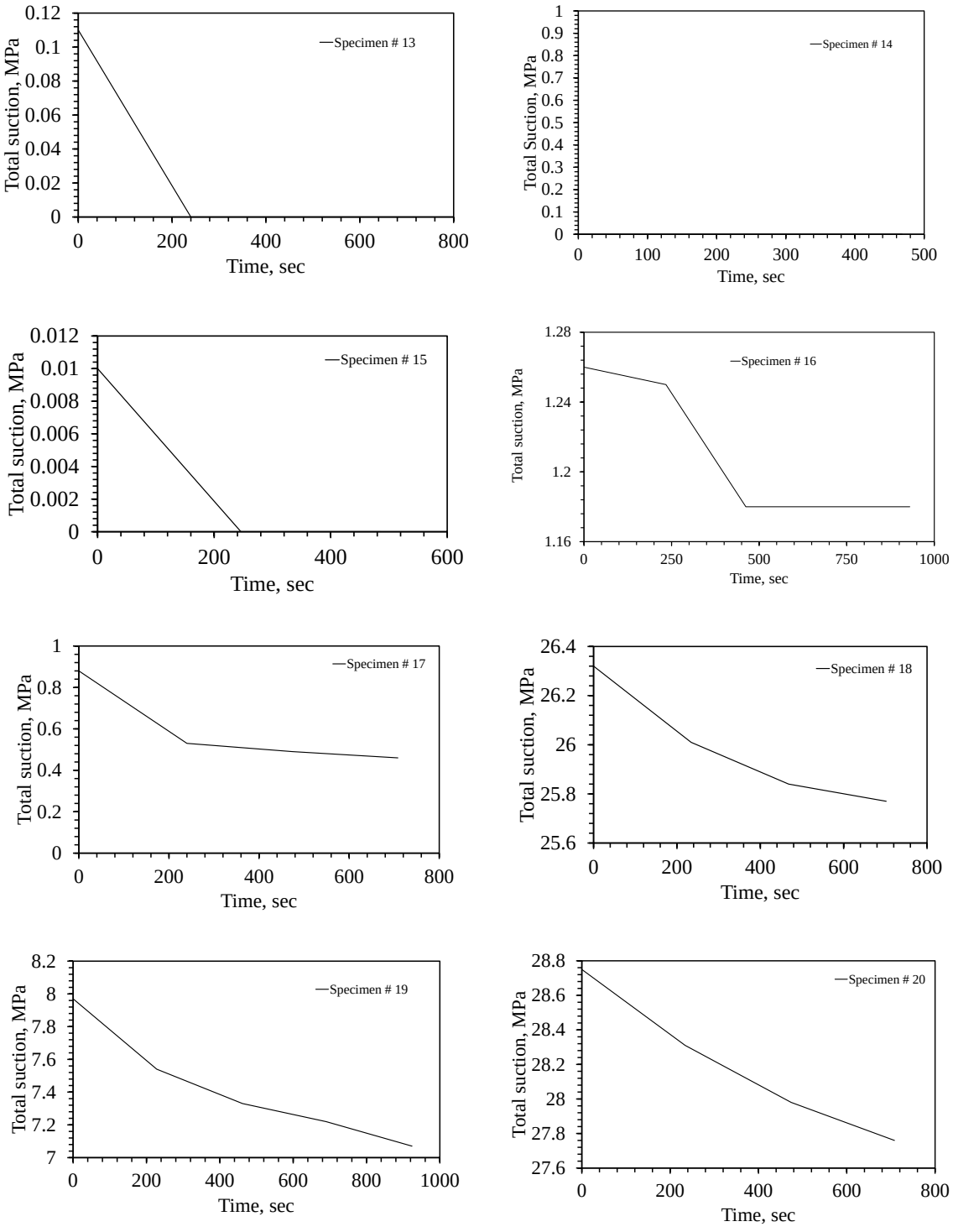

Figure E.2.1. (continued).

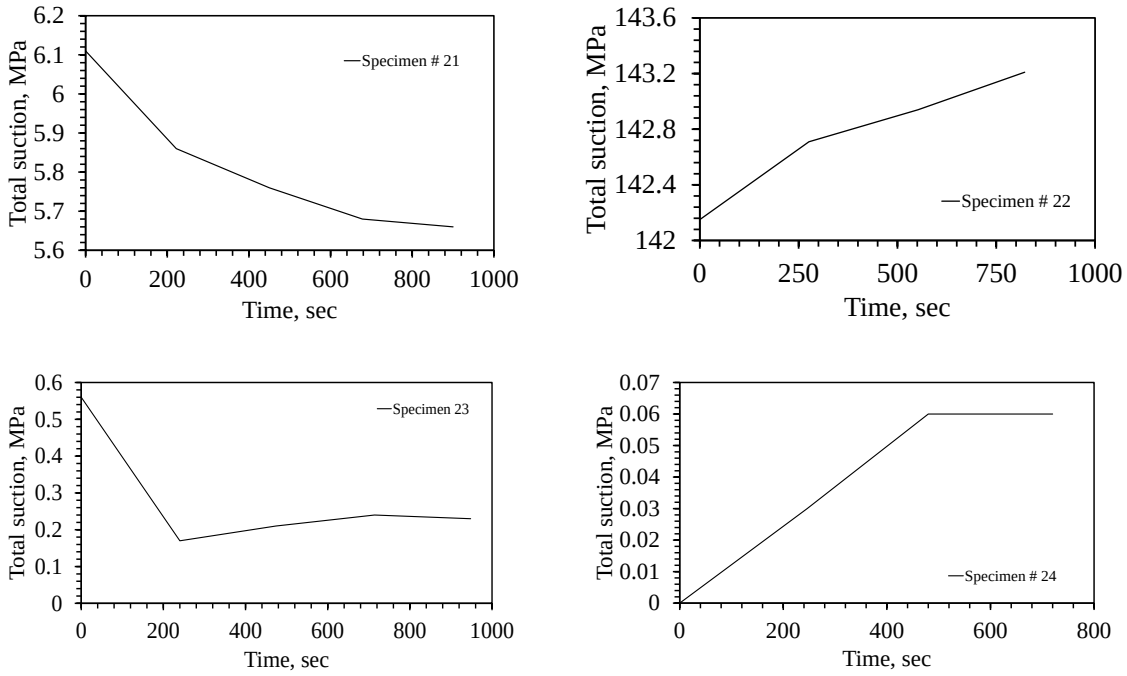

Figure E.2.1. (continued).

E.2.2 Calibration Curve and the Results Obtained by the Tensiometer Sensor

This section consists of the calibration curve (Figure E2.2.1.) used to determine the conversion factor as well as the experimental data obtained by using the tensiometer sensor (Figure E.2.2.2.).

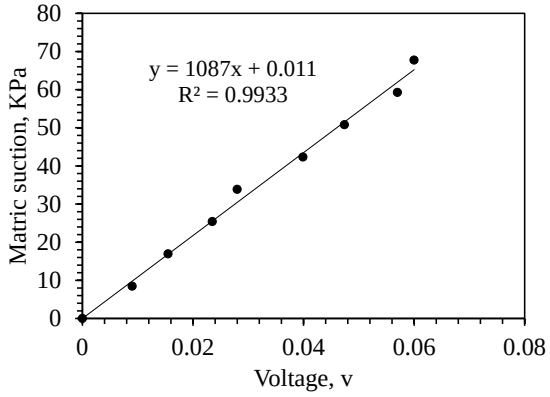

Figure E.2.2.1. Calibration curve used to determine the conversion factor.

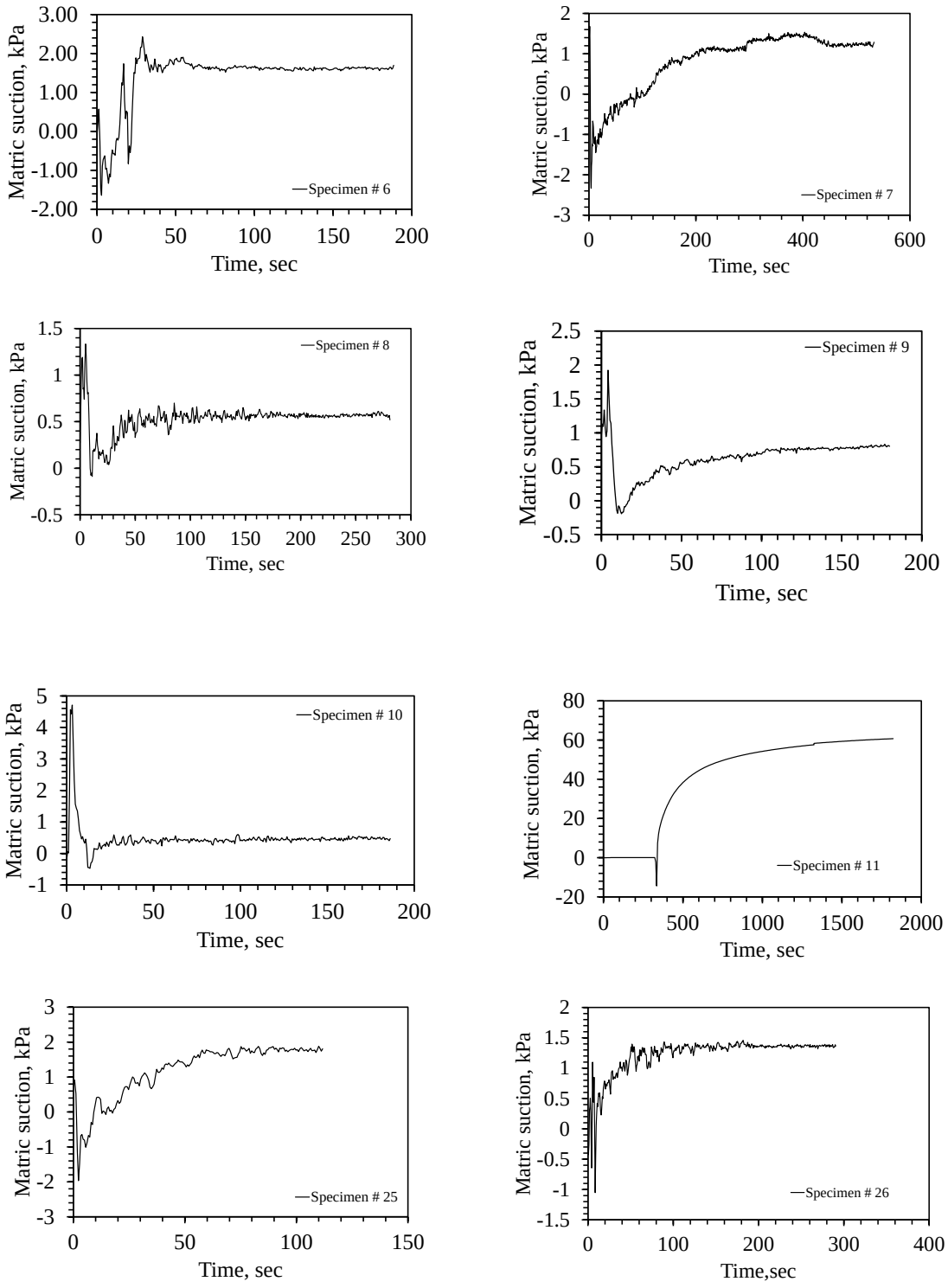

Figure E.2.2.2. The experimental data of matric suction obtained by the tensiometer sensor.

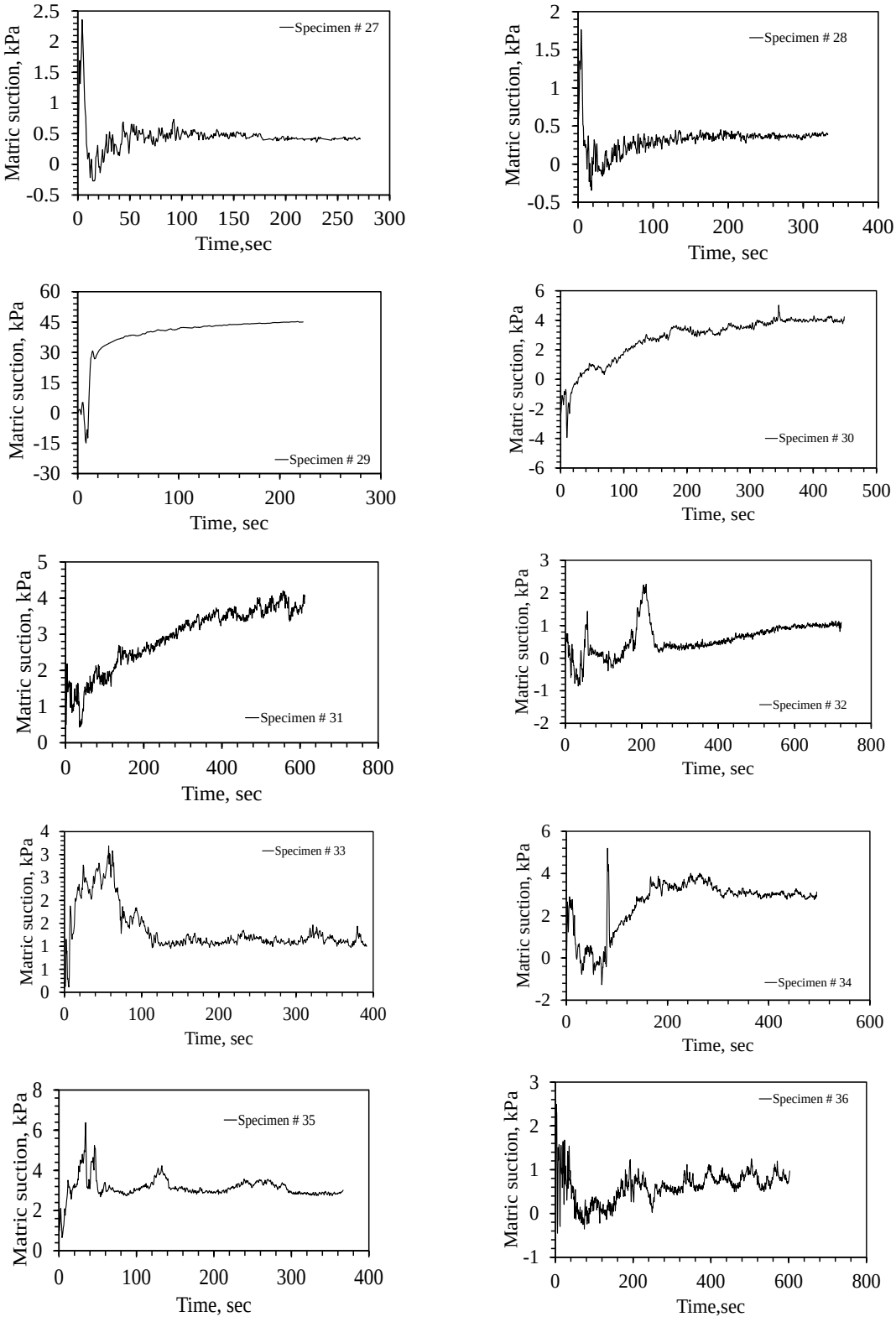

Figure E.2.2.2. (continued)

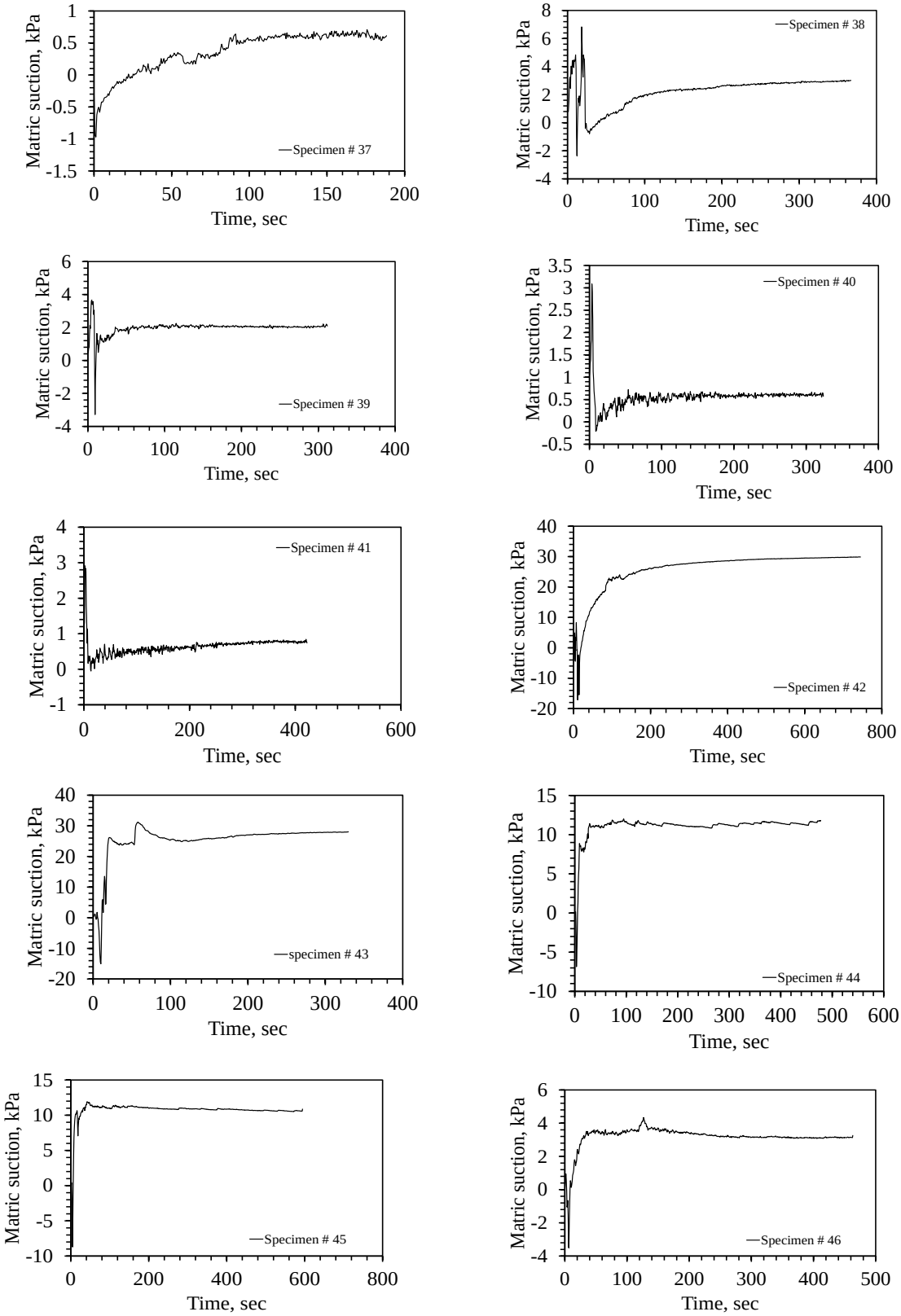

Figure E.2.2.2. (continued)

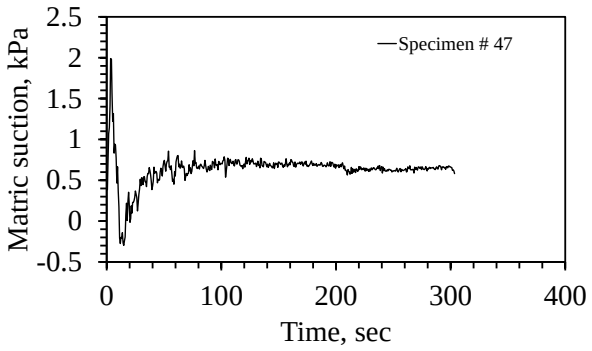

Figure E.2.2.2. (continued)

E.3 The CVOTs Results

This section consists of the rest of data obtained by performing the CVOT as shown in Figure E.3.1.

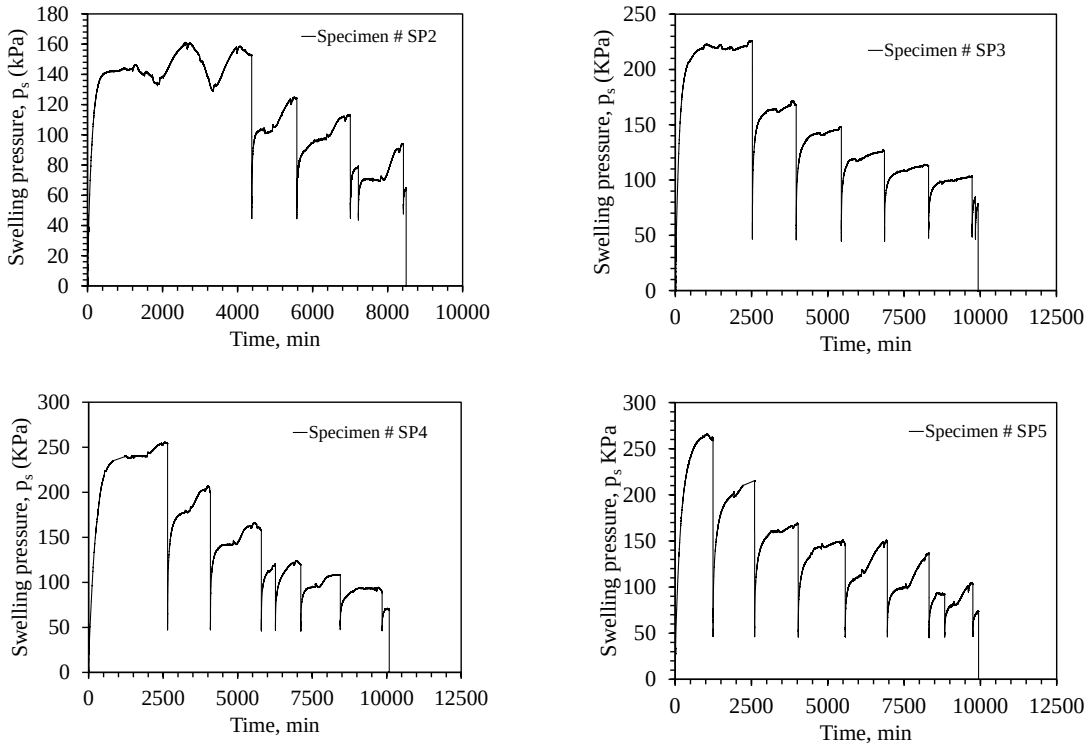

Figure E.3.1. Measurements of p_s with time by performing the CVOT.

APPENDIX-F

F.1 Analysis of the Free Swell Test Results

In this section, the rest of the analysis of free swelling test results is presented herein as shown in Figure F.1.1.

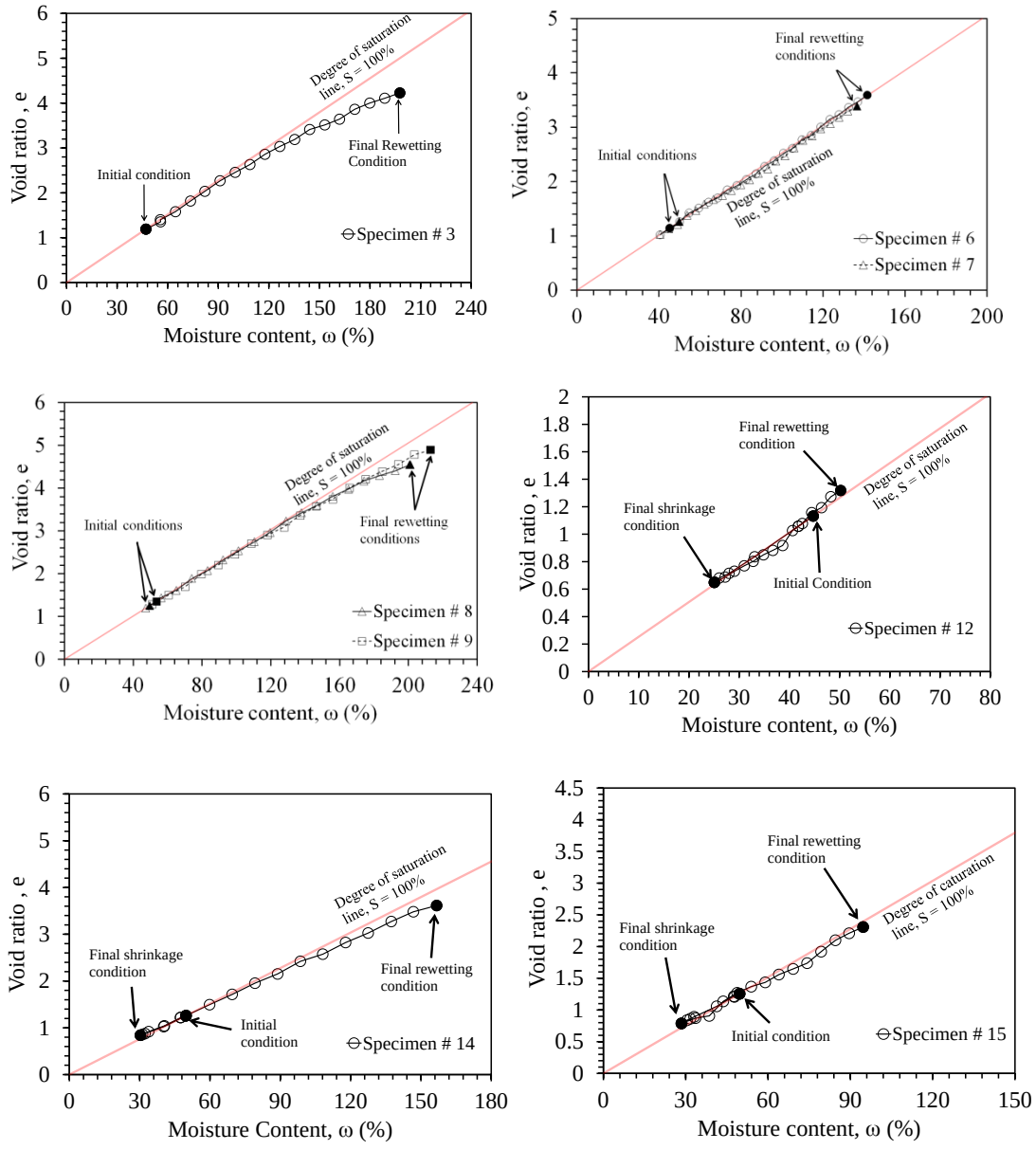

Figure F.1.1. Void ratio-moisture content relationships resulted from the free swelling tests.

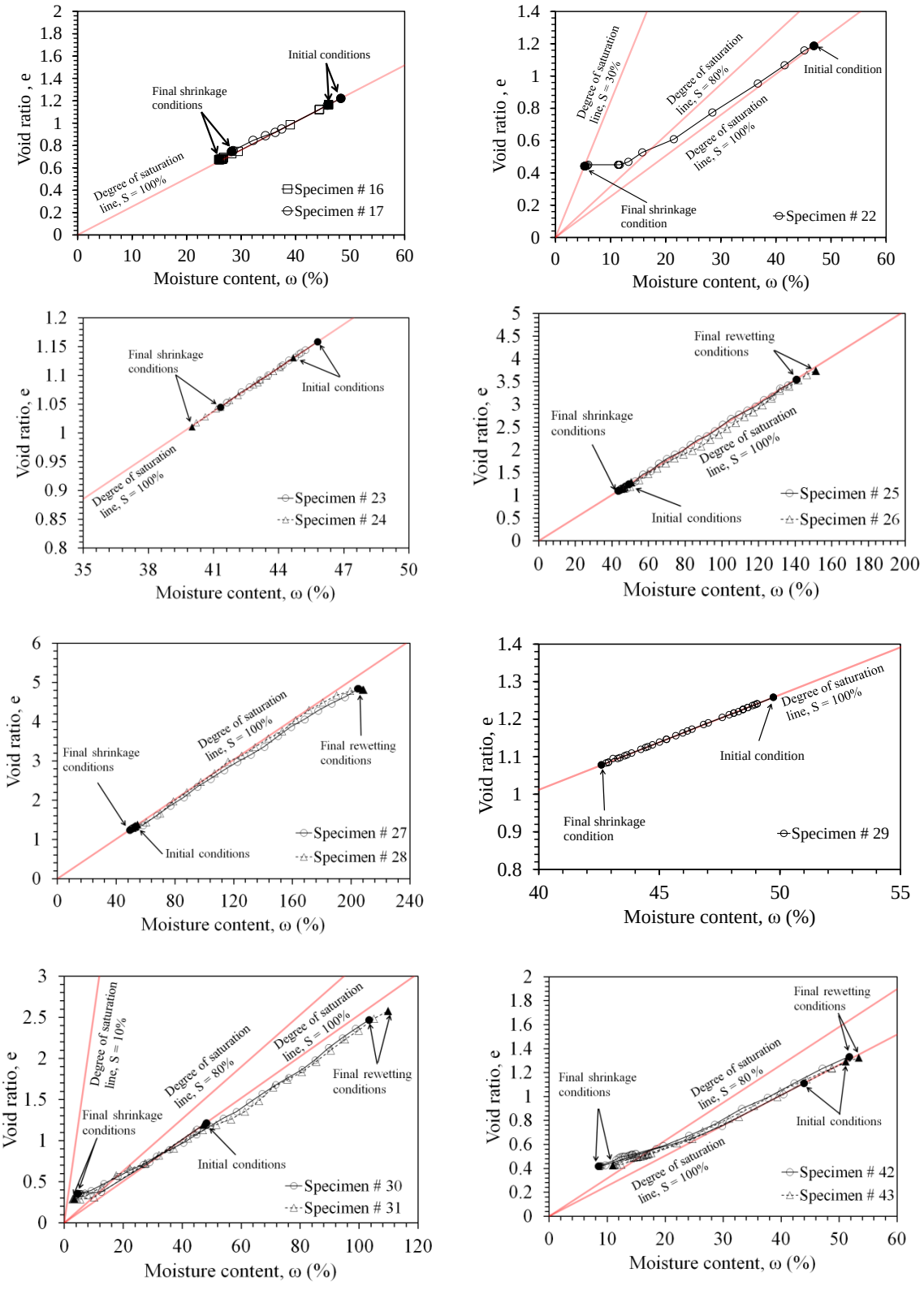

Figure F.1.1. (continued)

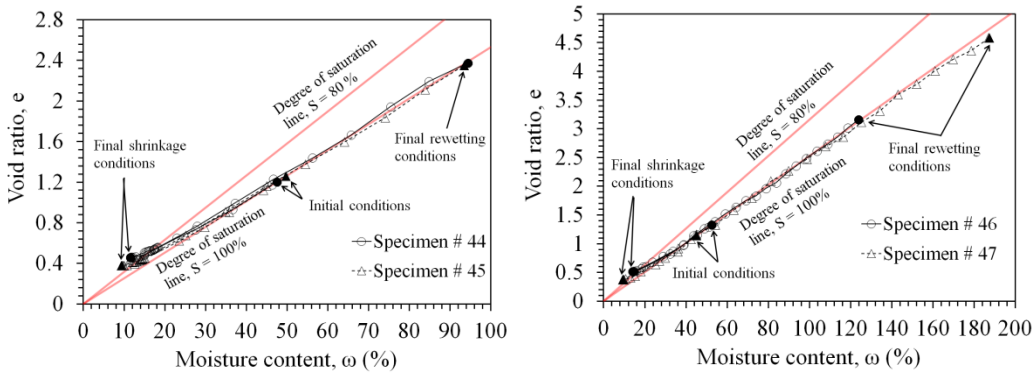

Figure F.1.1. (continued)

F.2 Analysis of the CVOT Results

In this section, the rest of the analysis of the CVOT results is presented herein as shown in Figures F.2.1., F.2.2., F.2.3., and F.2.4., respectively.

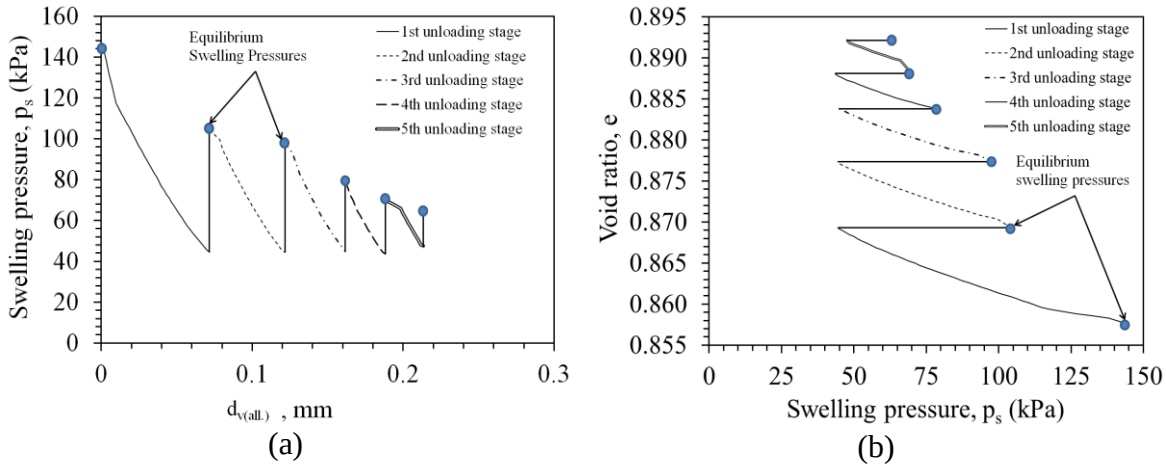

Figure F.2.1 The decrement of p_s as a function of (a) $d_{v(all.)}$, and (b) void ratio for specimen #SP2.

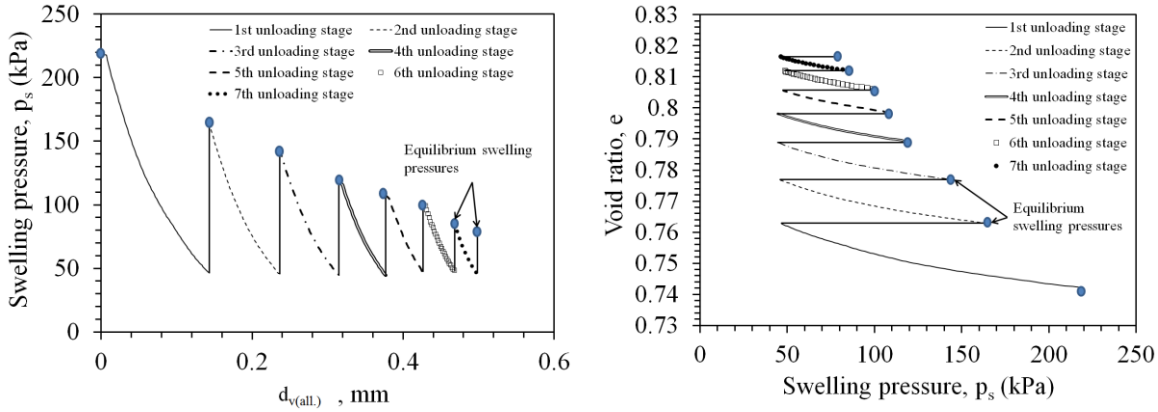

(a) (b)

Figure F.2.2 The decrement of p_s as a function of (a) $d_{v(all.)}$, and (b) void ratio for specimen #SP3.

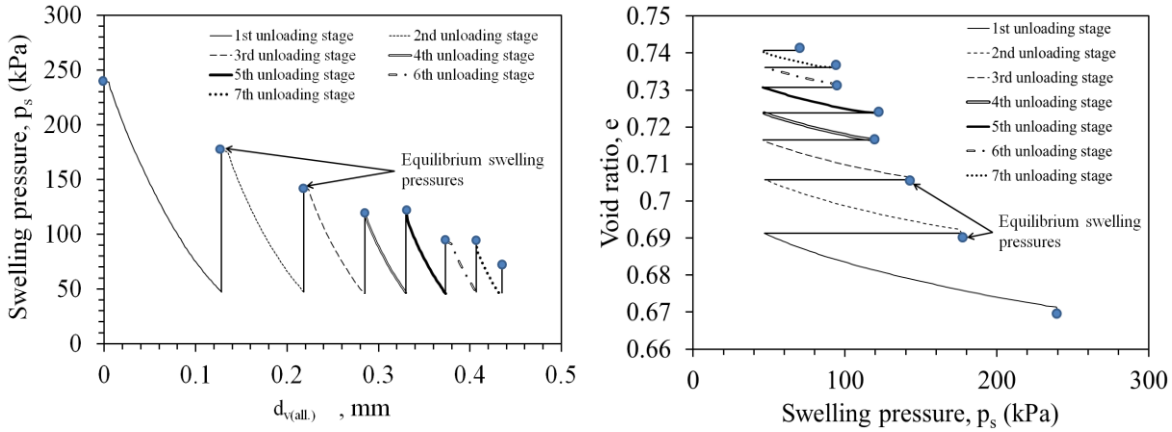

(a) (b)

Figure F.2.3 The decrement of p_s as a function of (a) $d_{v(all.)}$, and (b) void ratio for specimen #SP4.

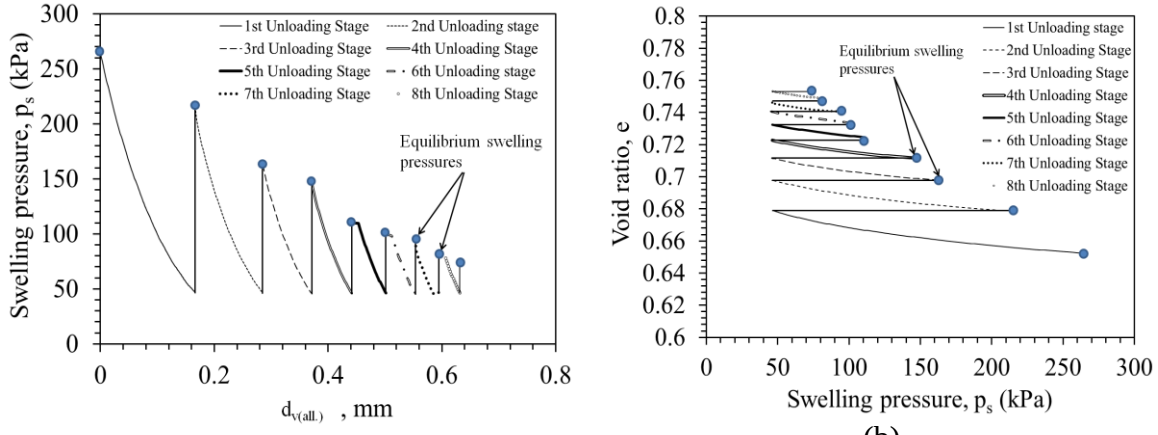

(a) (b)

Figure F.2.4 The decrement of p_s as a function of (a) $d_{v(all.)}$, and (b) void ratio for specimen #SP5.

F.3 Analysis of the Rate of the Swelling Pressure Results (CVOT)

The square root of time method is used to determine $\sqrt{t_{90}}$ in order to calculate the hydraulic diffusivity *D* as shown in Figures F.3.1. to F.3.6. In Figure F.3.1, the curve waves are replaced by the dashed line in order to smooth the curve for determining $\sqrt{t_{90}}$.

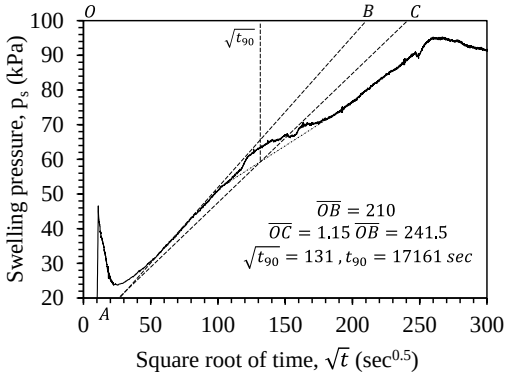

Figure F.3.1. The square root of time method for specimen #SP1.

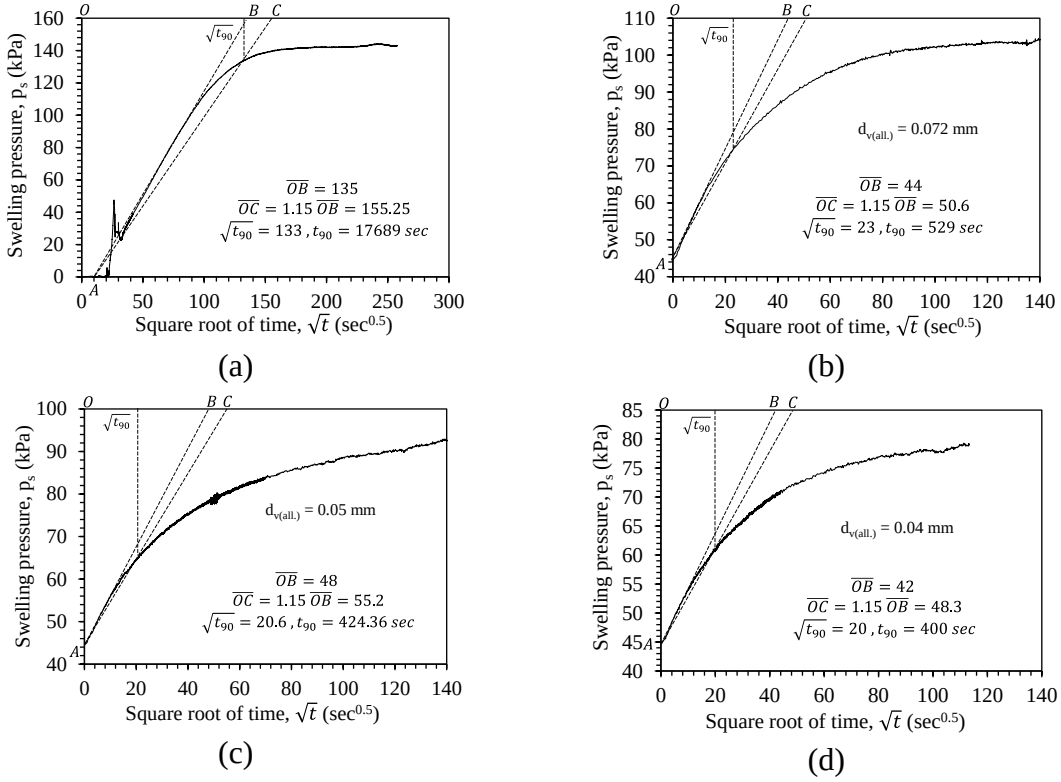

Figure F.3.2. The square root of time method for specimen #SP2 including (a) the actualp_s and unloading stages (b) #1, (c) #2, and (d) #3.

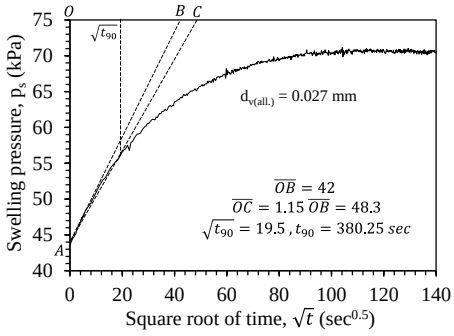

(e)

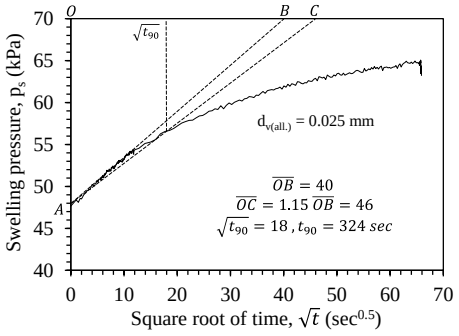

(f)

Figure F.3.2. (continued, unloading stages (e) #4 and (f) #5).

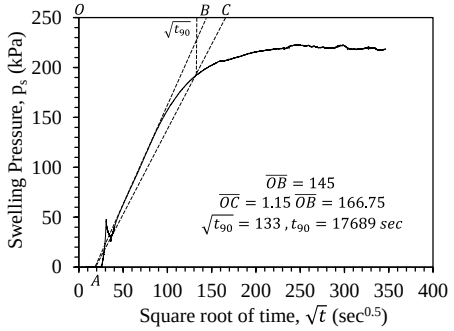

(a)

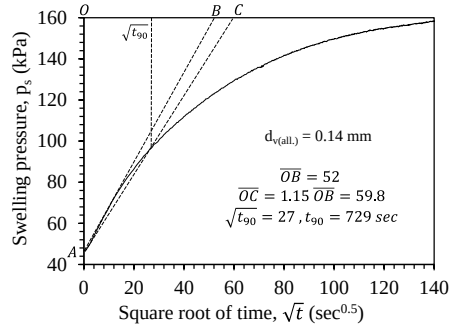

(b)

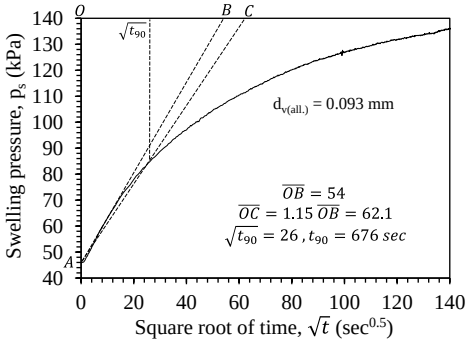

(c)

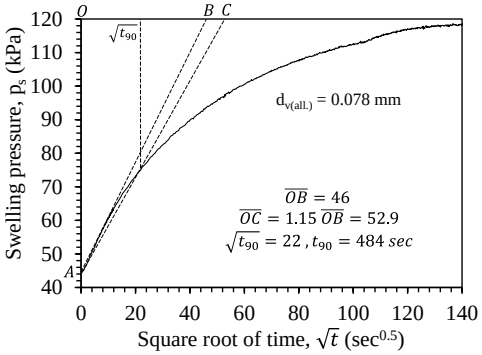

(d)

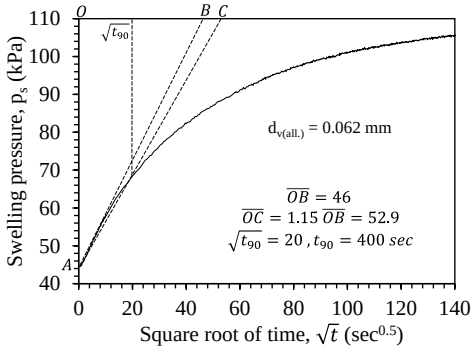

(e)

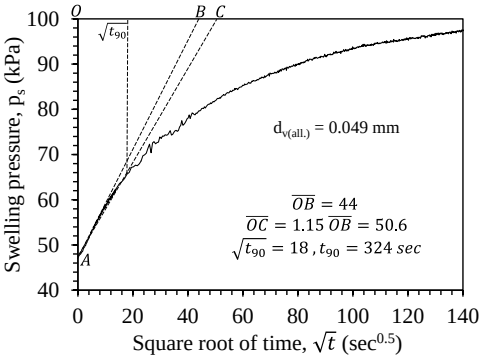

(f)

Figure F.3.3. The square root of time method for specimen #SP3 including (a) the actual p_s and unloading stages (b) #1, (c) #2, (d) #3, (e) #4, and (f) #5.

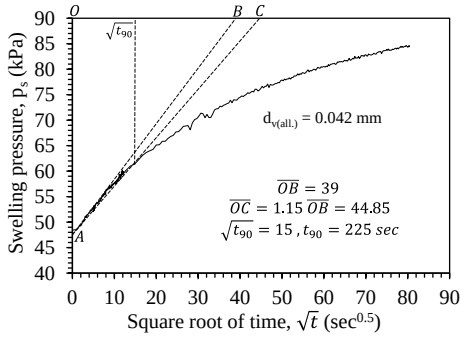

(g)

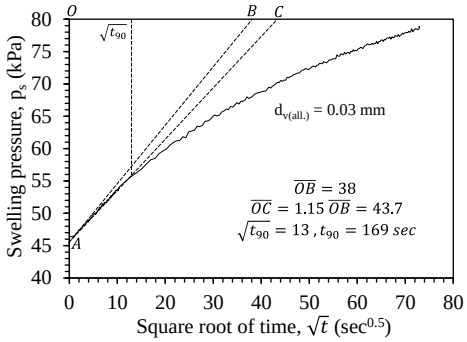

(h)

Figure F.3.3. (continued, unloading stages (g) #6 and (h) #7).

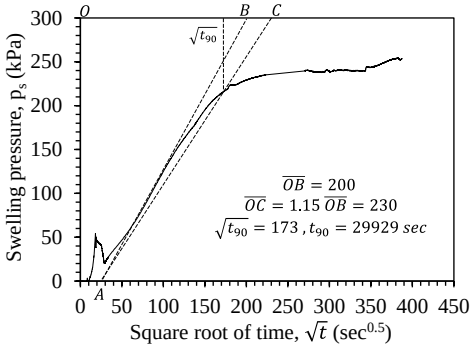

(a)

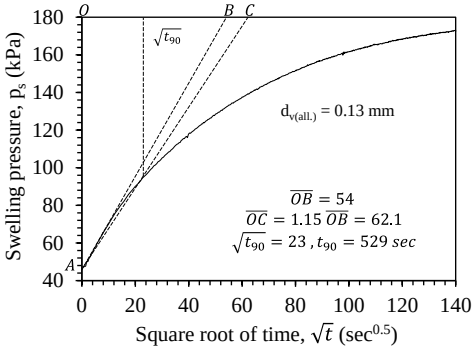

(b)

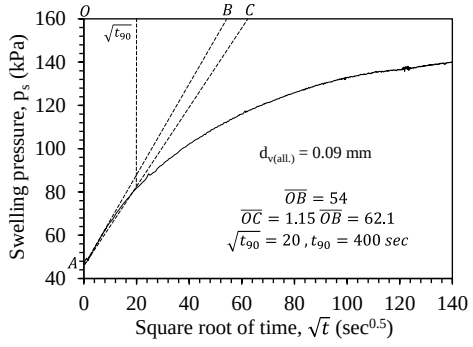

(c)

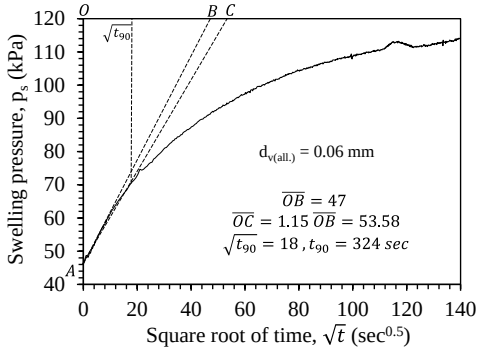

(d)

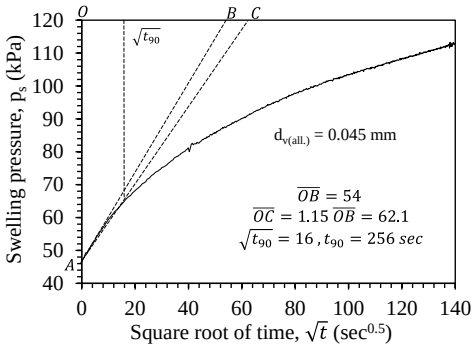

(e)

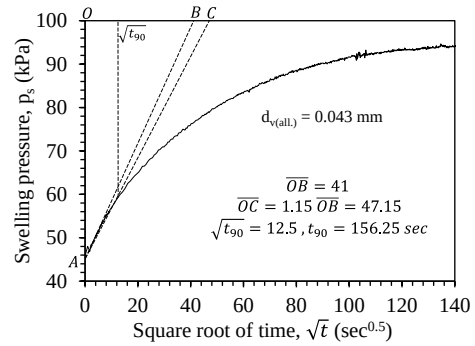

(f)

Figure F.3.4. The square root of time method for specimen #SP4 including (a) the actual p_s and unloading stages (b) #1, (c) #2, (d) #3, (e) #4, and (f) #5.

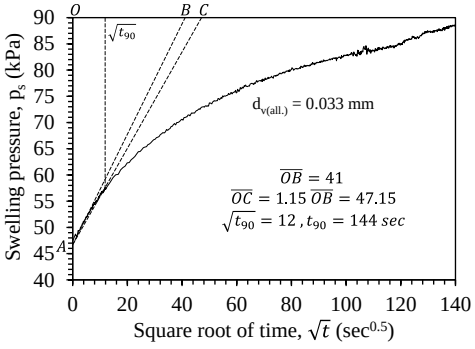

(g)

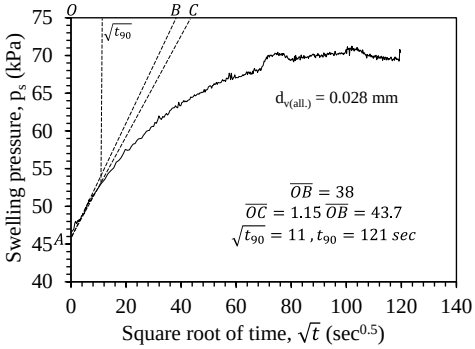

(h)

Figure F.3.4. (continued, unloading stages (g) #6 and (h) #7).

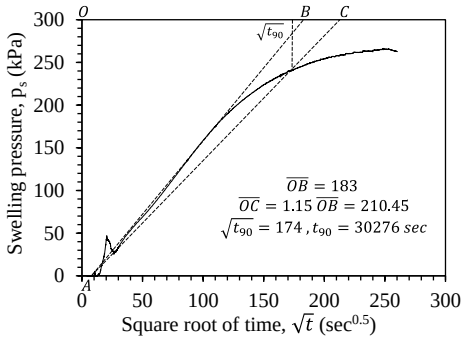

(a)

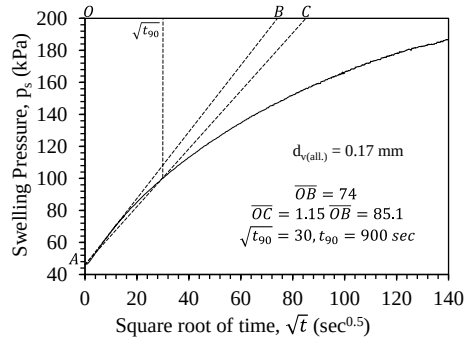

(b)

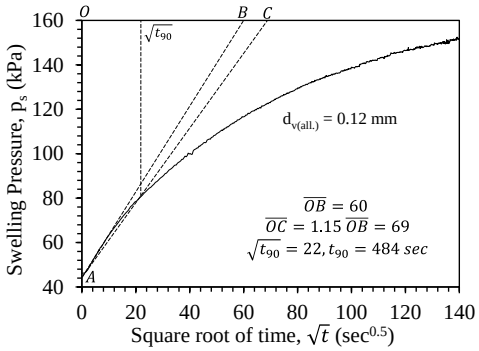

(c)

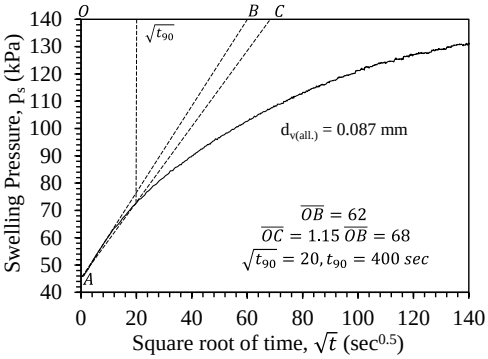

(d)

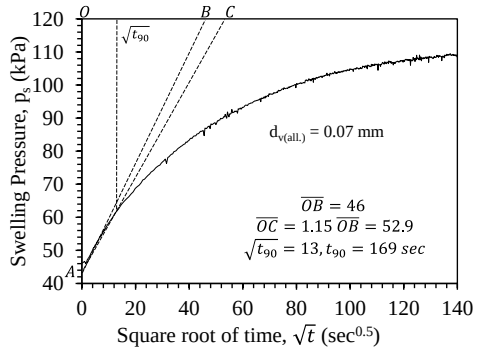

(e)

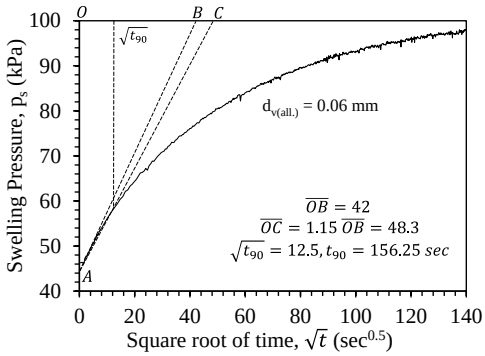

(f)

Figure F.3.5. The square root of time method for specimen #SP5 including (a) the actual p_s and unloading stages (b) #1, (c) #2, (d) #3, (e) #4, and (f) #5.

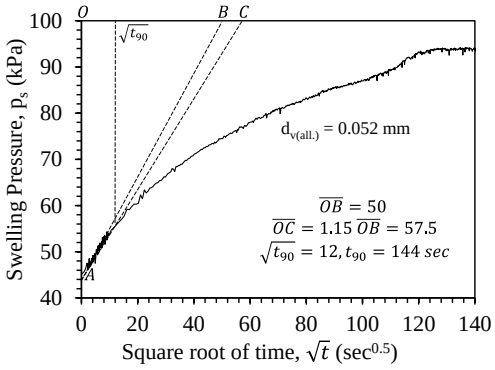

(g)

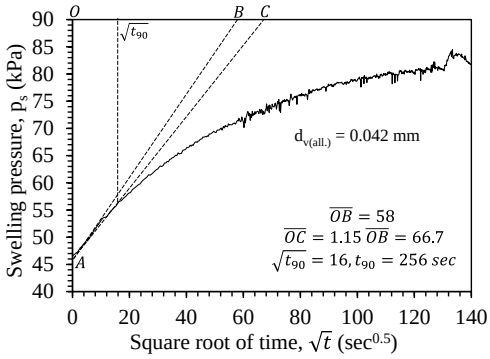

(h)

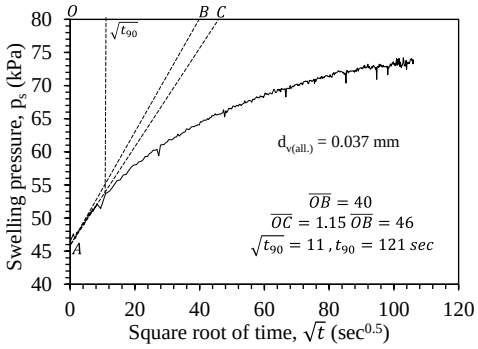

(i)

Figure F.3.5. (continued, unloading stages (g) #6, (h) #7, and (i) #8).

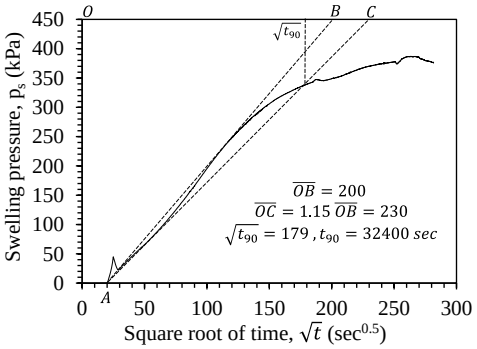

(a)

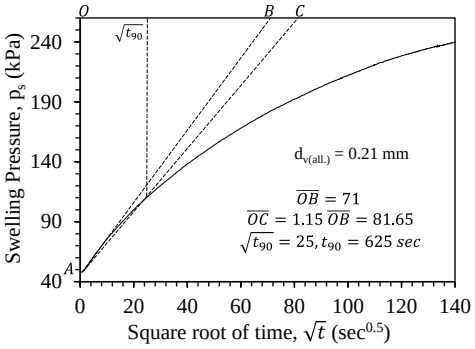

(b)

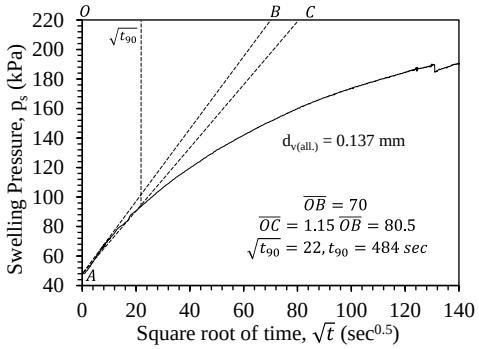

(d)

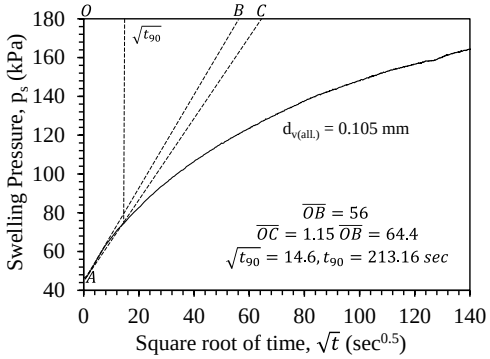

(e)

Figure F.3.6. The square root of time method for specimen #SP6 including (a) the actual p_s and unloading stages (b) #1, (c) #2, and (d) #3.

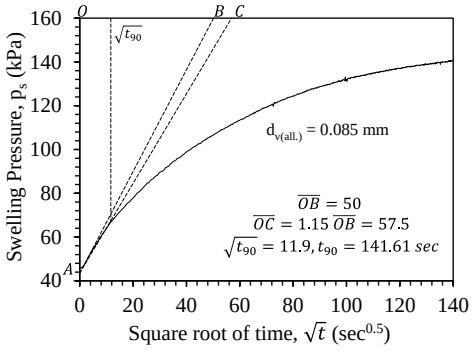

(e)

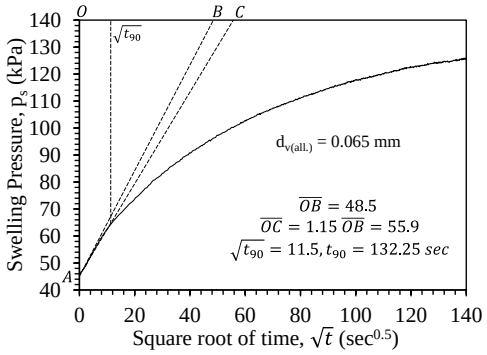

(f)

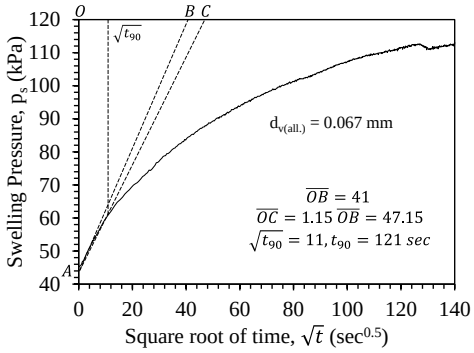

(g)

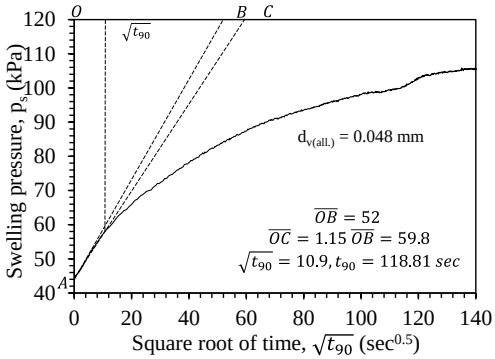

(h)

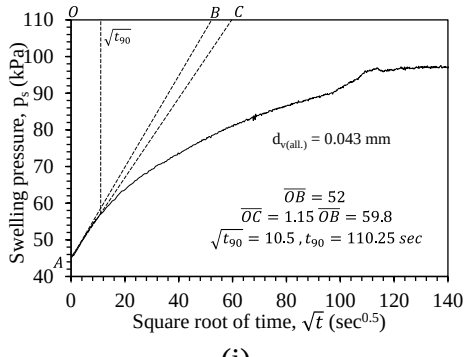

(i)

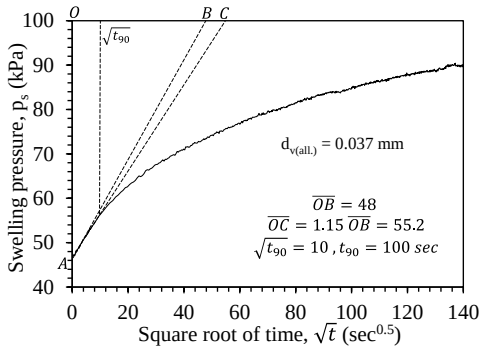

(j)

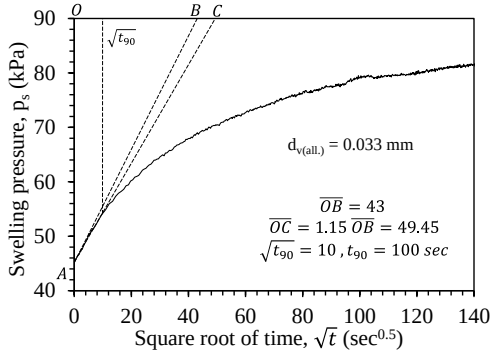

(k)

Figure F.3.6. (continued, unloading stages (e) #4, (f) #5, (g) #6, (h) #7, (i) #8, (j) #9, and (k) #10).

F.4 Analysis of the Rate of the Vertical Swelling Results (1DST)

The square root of time method is used to determine $\sqrt{t_{90}}$ in order to calculate the hydraulic diffusivity D as shown in Figures F.4.1.

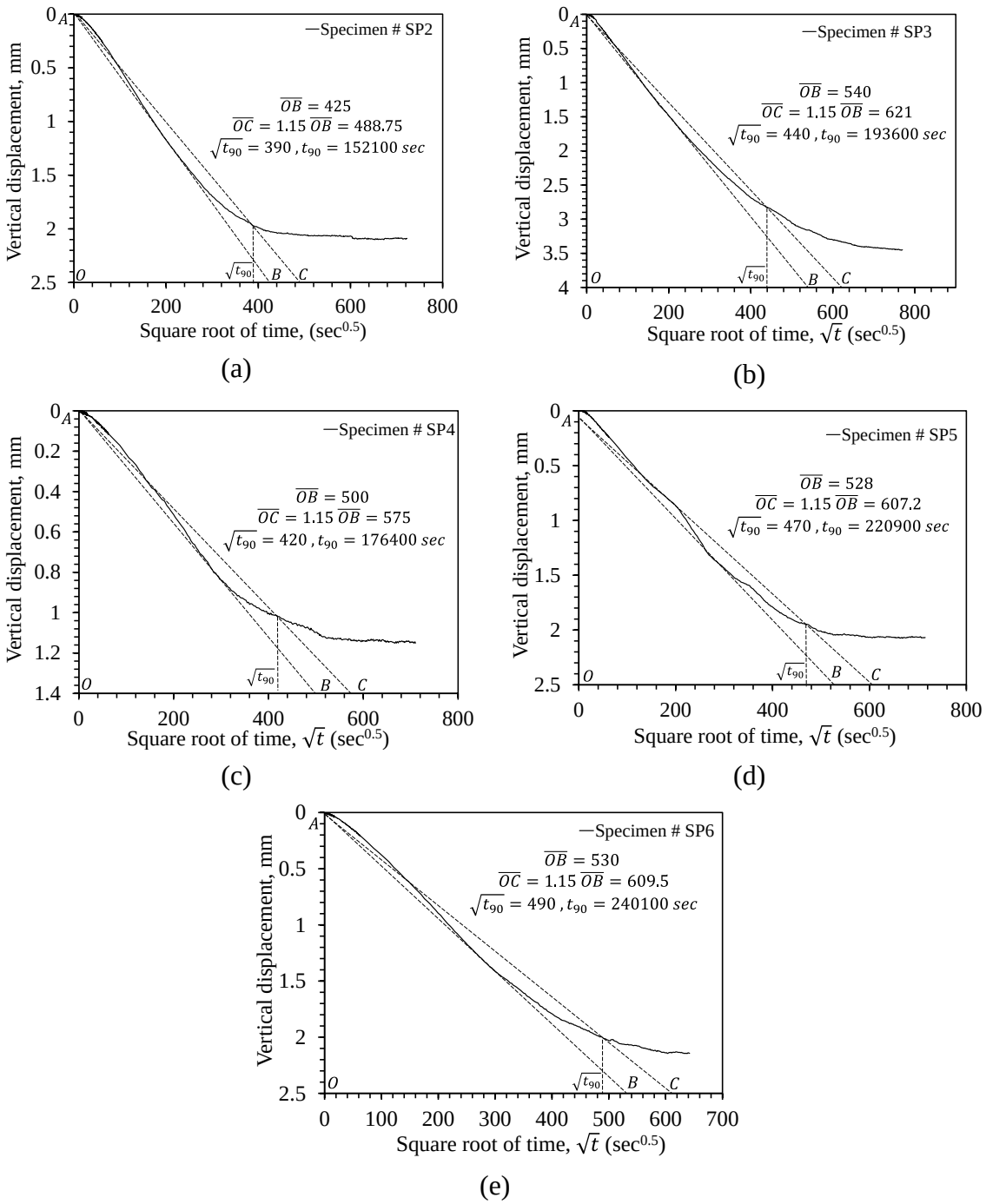

Figure F.4.1. The square root of time method for specimens (a) #SP2, (b) #SP3, (d) #SP4, (e) #SP5, and (f) #SP6.

F.5 Analysis of the m_v for the CVOTs and the 1DST

The analysis of the m_v development as a function of the equilibrium p_s is shown in Figure F.5.1.

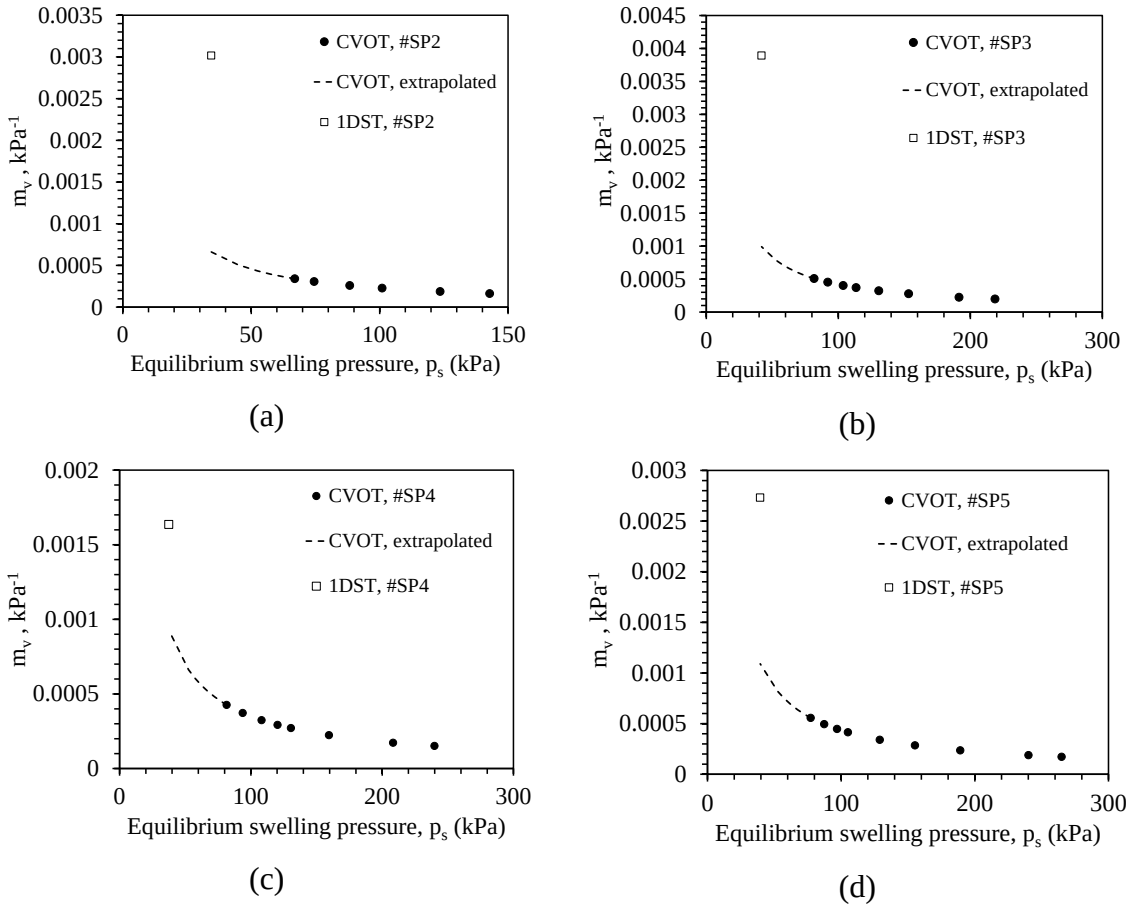

Figure F.5.1 The development of m_v as a function of the equilibrium p_s.